Flood, R.D., Piper, D.J.W., Klaus, A., et al., 1995
Proceedings of the Ocean Drilling Program, Initial Reports, Vol. 155

16. SITE 940[1]

Shipboard Scientific Party[2]

HOLE 940A

Date occupied: 3 May 1994

Date departed: 3 May 1994

Time on hole: 2 days, 18 hr, 45 min

Position: 5°8.596′N, 47°31.728′W

Bottom felt (drill pipe measurement from rig floor, m): 3202.7

Distance between rig floor and sea level (m): 11.30

Water depth (drill pipe measurement from sea level, m): 3191.4

Penetration (m): 248.60

Number of cores (including cores having no recovery): 27

Total length of cored section (m): 248.60

Total core recovered (m): 209.12

Core recovery (%): 84

Oldest sediment cored:
Depth (mbsf): 248.60
Nature: Silty clay
Earliest age: Pleistocene

Principal results: Site 940 (proposed Site AF-6) is located on the flank of the eastern levee of Amazon Channel about 3 km from the levee crest. Changes in reflection character in seismic profiles mark growth phases in the levee that may correlate with the avulsion of the Amazon-Brown Channel from the earlier Aqua Channel 5 km north of the site. The site was chosen to understand the processes associated with levee growth and to provide a biostratigraphic section of the Amazon-Aqua levee. The site was selected from a *Conrad* seismic profile (C2514; 1716 hr on 15 Dec. 1984) and was confirmed by a *JOIDES Resolution* pre-site survey.

Hole 940A was cored by APC to 69.3 mbsf, then by XCB to 248.6 mbsf, with total hole recovery of 209.12 m (84.1%). A temperature measurement was made at the mud line and at 50 mbsf (ADARA) and shows a geothermal gradient of 29°C/km. There was gas expansion in many cores. Methane was found throughout the hole, but higher hydrocarbons were not detected. The Quad-combination and FMS logs were run from 233 to 75 mbsf. A borehole deviation of 5°–7° south was detected with the FMS log.

Two lithologic units are recognized:

Unit I (0–0.24 mbsf) is a Holocene bioturbated foraminifer-nannofossil clay. Carbonate content decreases downhole, from 29% at 0.11 mbsf.

Unit II (0.24–248.60 mbsf) consists of mud with interbedded laminae and beds of silt and very fine sand. The mud has about 3% carbonate content. The unit is subdivided into nine subunits. Core-seismic correlation suggests that the upper two subunits were deposited after the avulsion of the Amazon from the Brown Channel farther downstream. Subunit IIA (0.24–9.50 mbsf) comprises color-banded and bioturbated mud. Subunit IIB (9.50–31.81 mbsf) is composed of mud with thin to thick beds of silt and fine sand, which increase in frequency and thickness toward the base of the subunit. Three thin intervals of contorted sediment are interpreted as slumps.

The section of the levee that was deposited when the Brown Channel was active downstream is correlated with Subunits IIC–IIE and the upper part of Subunit IIF. Subunit IIC (31.81–34.39 mbsf) consists of slightly bioturbated, color-banded mud. Subunit IID (34.39–55.71 mbsf) consists of mud with common laminae and beds of silt and fine sand, with the greatest abundance of sand at about 50 mbsf. Subunit IIE (55.71–60.01 mbsf) consists of moderately bioturbated mud with silt laminae that have been tilted and deformed and is interpreted as a slump. Subunit IIF (60.01–142.6 mbsf) consists of mud with laminae and thin beds of silt. The frequency of these beds fluctuates, but silt is more abundant near the base of the unit. Intervals of upward-decreasing gamma-ray response from 72 to 76 and 77 to 85 mbsf and of upward-increasing gamma-ray response from 85 to 91 mbsf do not correlate with any visible changes in sediment type.

Seismic profiles suggest that Unit II below 90 mbsf was deposited when the Aqua Channel was active. An upward increase in gamma-ray response from 92 to 115 mbsf corresponds to a fining-upward sequence in the lower part of Subunit IIF. Log data suggest abundant silt or sand in unrecovered intervals at 112–114 and 130–132 mbsf, the latter overlain by a 5-m-thick fining-upward sequence. Subunit IIG (142.6–210.57 mbsf) consists of mud with common laminae and beds of silt and sand. The top of the subunit is marked by a slump similar to that in Subunit IIE and is characterized by an abrupt increase in gamma-ray and resistivity response in log data. The slump overlies a fining-upward sequence from 140 to 160 mbsf. Recovery was poor through several intervals in this subunit. Subunit IIH (210.57–236.14 mbsf) comprises mud with laminae and beds of silt and common beds of sand up to 10 cm thick. Logs show substantial borehole washout at 218–230 mbsf. Subunit IIJ (236.14–248.60 mbsf) consists of mud with laminae of silt. Core-seismic correlation suggests that the hole was terminated just above the base of the Aqua levee.

Foraminifers are relatively abundant throughout the hole. The base of the Holocene was defined between 2.1 and 2.5 mbsf. *P. obliquiloculata* is absent below the Holocene section, indicating that the entire hole is younger than 40 ka. Cerrado-type vegetation is well represented in the palynomorph assemblage from Unit II, with *Byrsonima*, Compositae, and Graminae.

No magnetic excursion was detected at this site. Variation in magnetic inclination, interpreted as secular variation, is observed from 5 to 30 mbsf and from 42 to 55 mbsf. Remanence intensity can be tentatively correlated with Site 939 and suggests that 16 and 47 mbsf at Hole 940A correlate with 7 and 42 mbsf at Hole 939B.

In Unit II, carbonate content ranges from 1% to 3% and organic carbon from 0.8% to 1.2%. Pore-water samples show that sulfate reduction is not complete until 20–29 mbsf, the deepest encountered on Leg 155, and the peaks in phosphate (29 mbsf) and iron (91 mbsf) concentration are also deep. These observations suggest slower rates of organic-carbon remineralization than at other sites during Leg 155, probably as a result of the high depositional rate.

Sites 940, 939, 944, and 946 provide a detailed stratigraphy near the crests of the youngest levees (Amazon, Brown, and Aqua) on the upper,

[1]Flood, R.D., Piper, D.J.W., Klaus, A., et al., 1995. *Proc. ODP, Init. Repts.*, 155: College Station, TX (Ocean Drilling Program).

[2]Shipboard Scientific Party is as given in the list of participants in the contents.

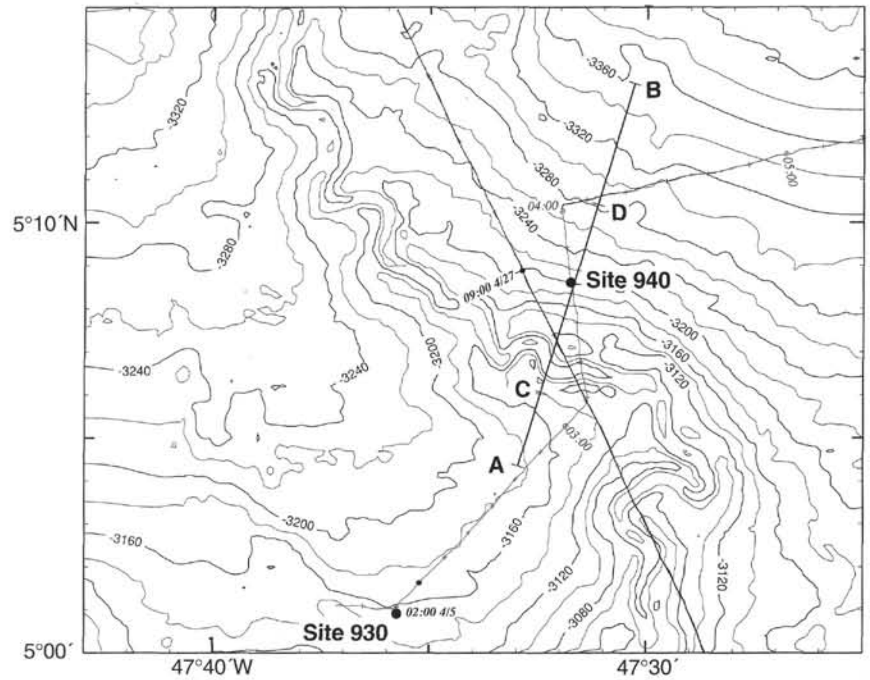

Figure 1. Location of Site 940 showing *Conrad* C2514 ship track on which Site 940 is located. A–B is the seismic profile in Figure 2; C–D is the 3.5-kHz profile in Figure 3. Other track lines are *JOIDES Resolution* seismic profiles collected during Leg 155. Bathymetric contours in meters.

middle, and lower fan. Site 940 has confirmed that the proportion of silt and sand to mud that are deposited fluctuates considerably within a single levee, but that each levee growth phase is represented by an overall fining-upward sequence. The relatively common foraminifers and the detailed paleomagnetic record at both Sites 939 and 940 indicate that shore-based study should provide a detailed correlation and chronology of the two sites. This will allow a detailed interpretation of the processes leading to variations in levee deposition, both down-fan and in a single hole.

SETTING AND OBJECTIVES

Introduction

Site 940 (proposed Site AF-6) is a single hole on the flank of the Amazon Channel in the uppermost middle fan to study the evolution of the Amazon levee in a water depth of 3195 mbsl. The hole penetrates several reflecting horizons on the Amazon levee and underlying sedimentary layers associated with earlier levee sequences.

Setting

Site 940 is located on the eastern (right) flank of the Amazon Channel about 3 km from and about 100 m below the highest local levee crest (Figs. 1 and 2). The levee at this location has several internal reflections that appear to mark growth phases, and sediment associated with the Orange Channel-levee System appears to underlie the entire levee. A deeper potential objective was the Unit R Debris Flow. Site 940 is located 2 km up-channel from the site of the Aqua avulsion and 60 km up-channel of the Brown avulsion point. The internal reflections within the levee may be related to those avulsion events (Pirmez, 1994). Site 940 is one of a series of sites located along the Amazon/Brown/Aqua Channel-levee systems. Other Amazon/Brown/Aqua sites include (from shallow to deep) 939, 930, 940 (this site), 935, 934, 936, 943, 944, 945, and 946.

The site was selected from a *Conrad* seismic profile (C2514; 1716UTC on 15 Dec. 1984; Fig. 2) and was chosen to sample sediment types associated with seismic reflections where they are best imaged. The 3.5-kHz profile at this site shows many weak layers in the upper 30 ms overlying a stronger but more diffuse layer (Fig. 3). Our pre-site 3.5-kHz and water-gun survey verified the reflection sequence at the proposed site. 0341UTC on 5 April 1994 on our *JOIDES Resolution* profile is at the same location as the proposed site.

Objectives

The principal objectives at Site 940 were:

1. To determine the nature of levee sediment on the uppermost middle fan through a complete levee sequence.
2. To characterize the nature of turbidity flow events through the Amazon Channel via analysis of levee-sediment characteristics.
3. To determine the nature of sediment associated with reflector horizons within the levee.
4. To obtain a high-resolution paleoclimatic record from planktonic foraminifers and organic material incorporated in the sediment.

OPERATIONS

Transit: Site 939 to Site 940 (AF-6)

The 24-nmi transit from Site 939 to Site 940 took 2.7 hr. A seismic survey had been conducted earlier in the leg. At 0114 hr 3 May, we deployed a beacon at 5°86´N, 47°31.73´W.

Hole 940A

We assembled a BHA similar to that used at Site 939, except we used an 11-7/16-in. four-cone roller bit (Security H86F) with upward discharge jets. This bit was used in an attempt to reduce XCB core disturbance (biscuiting). We positioned the bit at 3196.0 mbrf and spudded Hole 940A at 0913 hr 3 May. The distance from sea level to rig floor, which depends on the ship's draft, was 11.26 m for Hole 940A. Core 1H recovered 2.85 m (Table 1), and the mud line was defined to be at 3202.7 mbrf. Cores 1H through 8H were taken from 3202.7 to 3272.0 mbrf (0–69.3 mbsf) and recovered 69.95 m

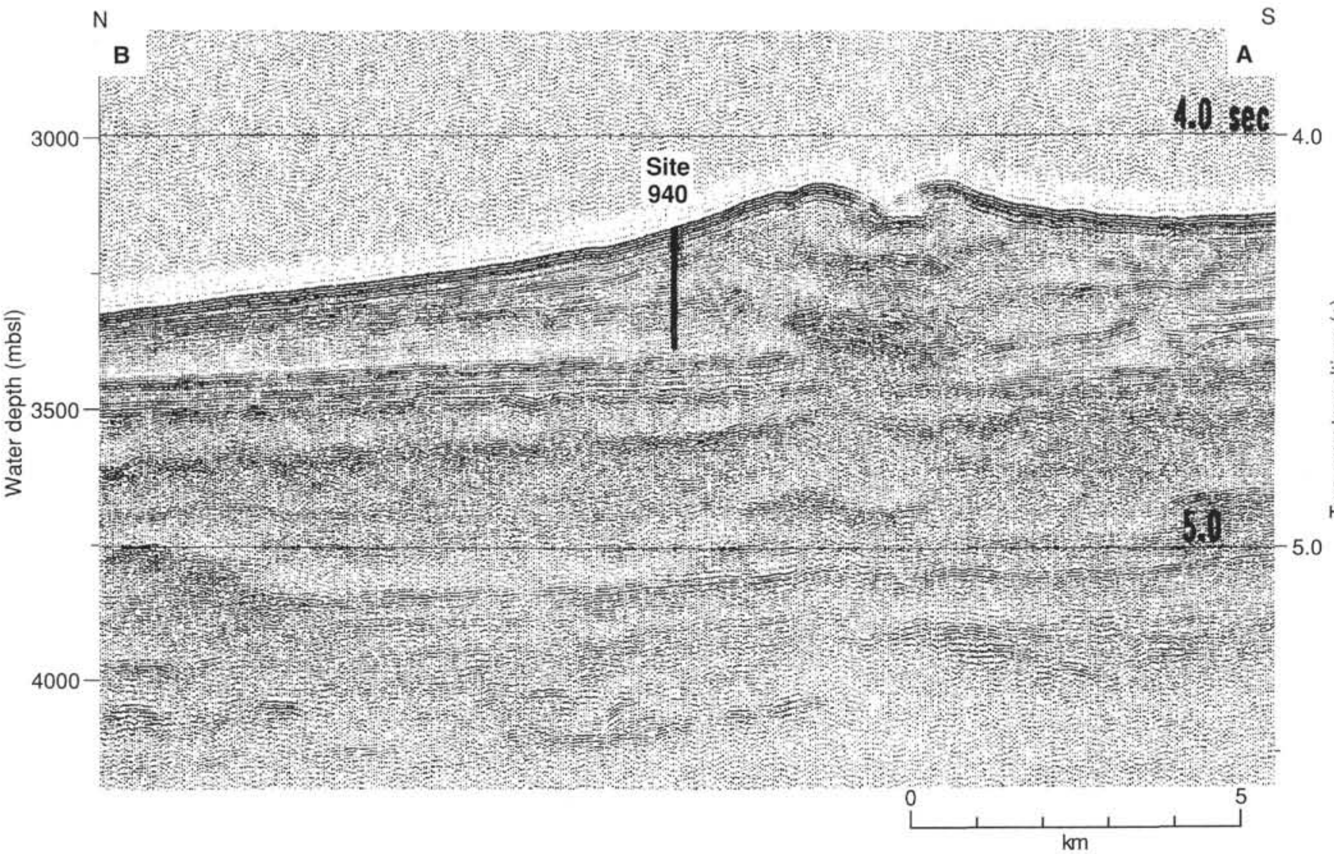

Figure 2. Seismic profile (water gun) through Site 940 (A–B in Fig. 1) (*Conrad* C2514, 1630–1800 UTC 15 Dec. 1984).

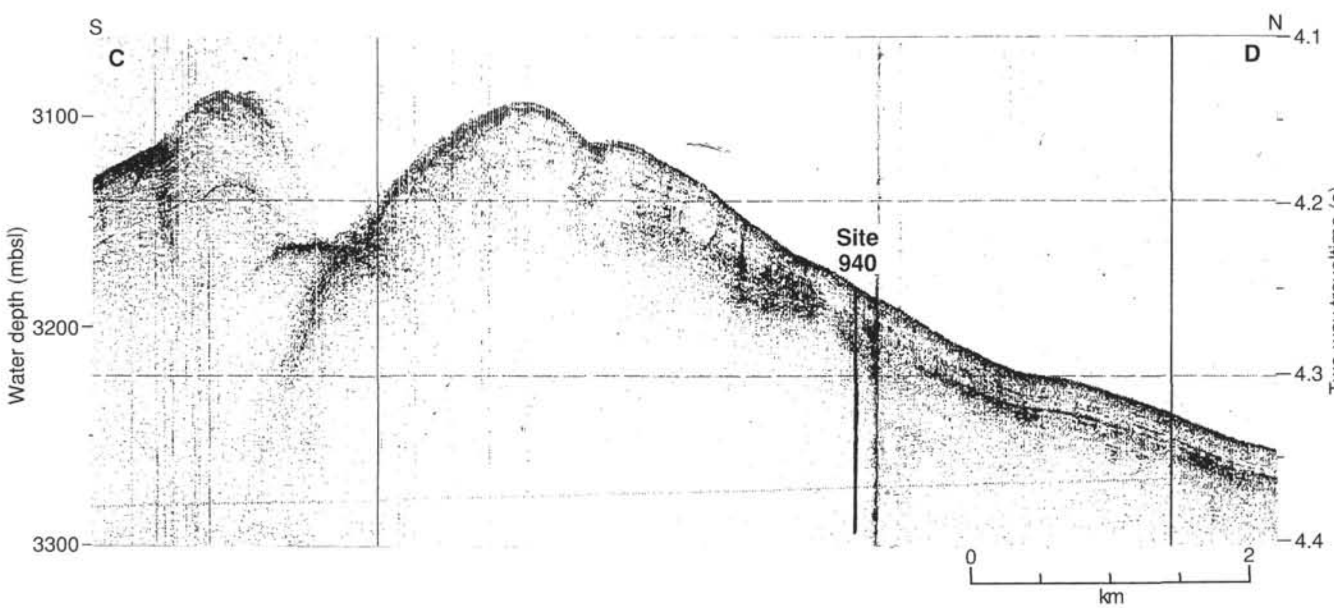

Figure 3. A 3.5-kHz profile through Site 940 (C–D in Fig. 1) (*Conrad* C2514, 1650–1730 UTC 15 Dec. 1984).

(100.9%). We oriented Cores 3H through 8H with the Tensor tool. An ADARA heat-flow measurement was taken during Core 6H.

XCB Cores 9X through 27X were taken from 3272.0 to 3451.3 mbrf (69.3–248.6 mbsf), coring 179.3 m and recovering 138.61 m (77.3%). A WSTP temperature measurement was attempted prior to Core 14X at 113.6 mbsf. The overall APC/XCB recovery was 83.9%. Parts of Cores 5H, 7H, 8H, 14X, and 23X were disturbed as a result of either gas-induced extrusion of core from the liner onto the rig floor or collapsed core liners.

The four-cone roller bit with upward discharge jets appeared to reduce core biscuiting. The biscuits were larger, and recovery appeared to be better. However, the rate of penetration was slower, and the hole

Table 1. Site 940 coring summary.

Core	Date (1994)	Time (UTC)	Depth (mbsf)	Length cored (m)	Length recovered (m)	Recovery (%)
155-940A-						
1H	May 3	1335	0.0–2.8	2.8	2.85	102.0
2H	May 3	1425	2.8–12.3	9.5	9.87	104.0
3H	May 3	1520	12.3–21.8	9.5	9.12	96.0
4H	May 3	1605	21.8–31.3	9.5	10.01	105.3
5H	May 3	1655	31.3–40.8	9.5	9.46	99.6
6H	May 3	1800	40.8–50.3	9.5	10.45	110.0
7H	May 3	1845	50.3–59.8	9.5	9.12	96.0
8H	May 3	1940	59.8–69.3	9.5	9.07	95.5
9X	May 3	2040	69.3–77.0	7.7	7.95	103.0
10X	May 3	2140	77.0–84.7	7.7	7.82	101.0
11X	May 3	2255	84.7–94.3	9.6	8.90	92.7
12X	May 4	0020	94.3–103.9	9.6	8.07	84.0
13X	May 4	0140	103.9–113.6	9.7	7.17	73.9
14X	May 4	0435	113.6–123.3	9.7	7.29	75.1
15X	May 4	0555	123.3–133.0	9.7	6.89	71.0
16X	May 4	0715	133.0–142.6	9.6	9.83	102.0
17X	May 4	0830	142.6–152.2	9.6	7.25	75.5
18X	May 4	1010	152.2–161.9	9.7	8.67	89.4
19X	May 4	1145	161.9–171.5	9.6	5.98	62.3
20X	May 4	1320	171.5–181.1	9.6	0.91	9.5
21X	May 4	1515	181.1–190.8	9.7	6.06	62.5
22X	May 4	1715	190.8–200.4	9.6	8.18	85.2
23X	May 4	1900	200.4–210.0	9.6	9.47	98.6
24X	May 4	2040	210.0–219.7	9.7	8.10	83.5
25X	May 4	2215	219.7–229.3	9.6	4.73	49.3
26X	May 5	0005	229.3–239.0	9.7	6.97	71.8
27X	May 5	0155	239.0–248.6	9.6	8.93	93.0
Coring totals				248.6	209.1	84.1

Note: An expanded version of this coring summary table that includes lengths and depths of sections, location of whole-round samples, and comments on sampling disturbance is included on the CD-ROM in the back pocket of this volume.

diameter was considerably larger (about 15 in. [38 cm]), reducing the quality of some of the logs, particularly the FMS. We decided to use the polycrystalline diamond compact (PDC) bit for the rest of the leg.

In preparation for logging, we circulated 20 barrels and then 30 barrels of sepiolite mud, and pulled the pipe up to 63 mbsf with negligible overpull. We then lowered the pipe to the bottom of the hole; no sediment fill was encountered. The go-devil was pumped through the LFV to allow logging tools to pass through the bit, and the pipe was pulled back up to 90.5 mbsf to log. At the end of each logging run, the bit was pulled up to 63 mbsf to log the upper part of the hole. The Quad-combination tool took 4.1 hr, and then the FMS run took 3.4 hr. The hole diameter ranged from 14 to 15.75 in. The bit cleared the seafloor at 1420 hr, and cleared the rotary table at 2000 hr 5 May; the beacon was recovered.

LITHOSTRATIGRAPHY

Introduction

Site 940, on the eastern levee of the Amazon Channel, penetrated 248.6 mbsf through the Amazon, Brown, and Aqua Channel-levee systems (Figs. 4 and 5). Core recovery was 84.1%, and lithologic interpretation of the relatively short intervals of poor recovery (especially between 161.9 and 181.1 mbsf; Cores 940A-19X through -21X) was aided by downhole logging data. Expansion of methane gas disrupted the primary sedimentary structures in some silt and sand beds, and produced void spaces within some core sections (see "Lithostratigraphy" section in the "Explanatory Notes" chapter, this volume).

Description of Lithostratigraphic Units

Unit I

Interval: 155-940A-1H-1, 0–24 cm
Age: Holocene
Depth: 0 to 0.24 mbsf

Unit I consists of 0.24 m of moderately bioturbated foraminifer-nannofossil clay, which grades in color from brownish yellow (10YR 6/6; 0–0.06 mbsf) to light olive brown (2.5Y 5/4; 0.06–0.24 mbsf) (Figs. 4 and 5). This unit contains four thin, indurated, diagenetic, iron-rich, olive brown (2.5Y 4/4) clay horizons, each less than 3 cm thick, at 0.06, 0.10, 0.15, and 0.20 mbsf. Similar horizons and "crusts" were analyzed previously and correlated throughout the Amazon Fan and adjacent Guiana Basin (Damuth, 1977; see "Introduction" chapter, this volume) and occur at most other Leg 155 sites. The carbonate content of Unit I is approximately 30% (see "Organic Geochemistry" section, this chapter).

Unit II

Interval: 155-940A-1H-1, 24 cm, through -27X-CC
Age: late Pleistocene
Depth: 0.24 to 248.60 mbsf

Unit II consists of 248.36 m of olive gray (5Y 4/2) to very dark gray (5Y 3/1) terrigenous clay, silty clay, silt, very fine sand, and fine sand. The unit extends from the base of Unit I to the bottom of the hole at 248.60 mbsf. A large proportion of the sediment is stained to varying degrees by diagenetic hydrotroilite, which imparts a black (N2/0) color to the sediment in the form of irregular patches and/or color bands and laminae (see "Introduction" chapter, this volume). The carbonate content of Unit II is low, with an average value of approximately 2%. Unit II has been subdivided into nine subunits based on the occurrence and frequency of silty clay, silt laminae, and thin beds of sand (Figs. 4 and 5).

Subunit IIA

Subunit IIA extends from 0.24 to 9.50 mbsf (Section 940A-1H-1 at 24 cm, through -2H-5 at 70 cm), and consists of dark gray (5Y 4/1), moderately bioturbated, silty clay with black (N2/0) color mottling throughout.

Subunit IIB

Subunit IIB extends from 9.50 to 31.48 mbsf (from Section 940A-2H-5 at 70 cm, through -4H-7 at 68 cm) and is characterized by dark gray (5Y 4/1), olive gray (5Y 4/1), and dark olive gray (5Y 3/2) terrigenous silty clay, which contains silt laminae and thin silt beds less than 2 cm thick. The boundary between Subunits IIA and IIB is placed at the uppermost occurrence of silt laminae. There are moderate levels of bioturbation and mottling from Section 940A-2H-5 at 70 cm, through -3H-3. The frequency of laminae and thin beds of silt increases with depth, ranging from a minimum of three per meter in Section 940A-3H-3 to a maximum of 30 per meter in Section 940A-4H-6. Three intervals of contorted sediment, interpreted as slumps, occur from 14.23 to 14.25 mbsf, 18.25 to 18.70 mbsf, and 21.80 to 23.60 mbsf (Fig. 6).

Subunit IIC

Subunit IIC extends from 31.48 to 34.39 mbsf (Section 940A-4H-CC through -5H-3 at 29 cm) and consists of very dark gray (5Y 3/1), slightly bioturbated, color-banded silty clay. The dark parts of the color bands are black (N2/0).

Subunit IID

This subunit is 21.32 m thick and extends from 34.39 to 55.71 mbsf (Section 940A-5H-3 at 29 cm through -7H-5 at 37 cm). The sediment is dark olive gray (5Y 3/2) and very dark gray (5Y 3/1) terrigenous silty clay with silt laminae and 1- to 3-cm-thick beds composed of silt and fine sand. In some cases, the silt laminae are color banded and graded; black (N2/O) coarse-grained silts alternate with lighter colored, dark olive gray, fine-grained silt beds. Discontinuous laminae of fine sand are common (Fig. 7). Some beds are parallel- or cross-laminated. The frequency of the laminae and beds increases

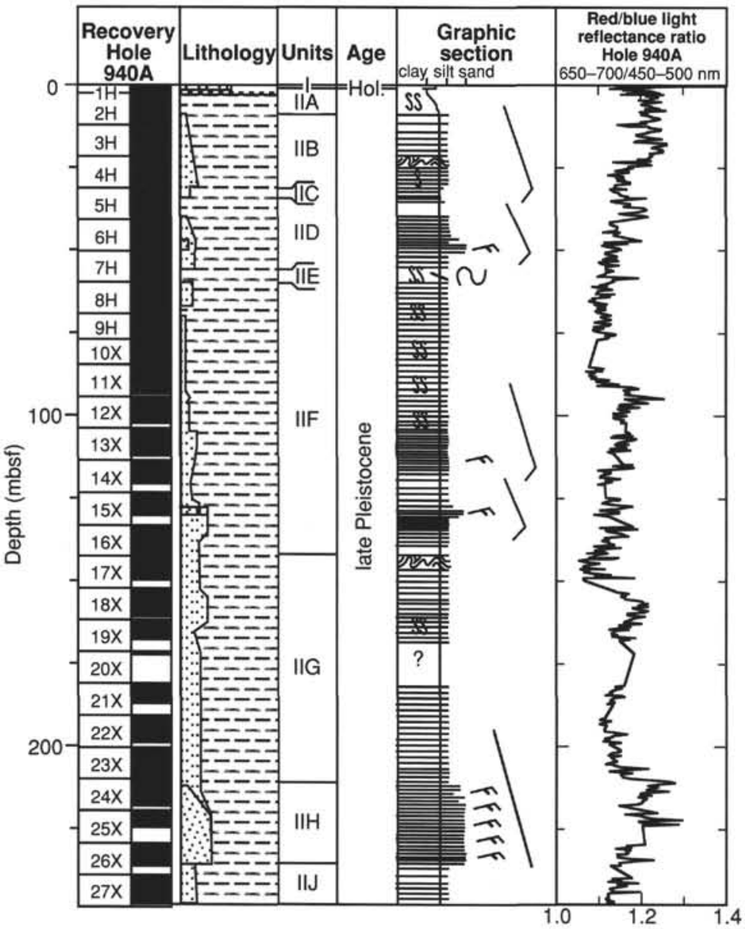

Figure 4. Composite stratigraphic section for Site 940 showing core recovery, simplified summary of lithology, depth of unit boundaries, age, a graphic section with generalized grain-size and bedding characteristics, and downhole variations in light-reflectance values. The lithologic symbols are explained in Figure 1 of the "Explanatory Notes" chapter, this volume.

from one to two per meter at the top of the subunit, to a maximum of approximately 60 per meter between 45.30 and 48.30 mbsf (Sections 940A-6H-4 and -6H-5), and then decreases to approximately four per meter at the base of Subunit IID.

Subunit IIE

Subunit IIE extends from 55.71 mbsf to 60.01 mbsf (Section 940A-7H-5 at 37 cm through -8H-1 at 21 cm) and consists of 4.30 m of very dark gray (5Y 3/1) deformed silty clay that contains truncated laminae and wisps of silt. A dip of approximately 45° is inferred from the orientation of the silt. Deformed burrow traces indicate moderate levels of bioturbation throughout the subunit. This subunit is interpreted as a slump.

Subunit IIF

The uppermost boundary of Subunit IIF is placed at the first silt laminae below Subunit IIE at 60.01 mbsf, with the base at 142.60 mbsf (Section 940A-8H-1 at 21 cm to -17X-1 at 0 cm). The subunit consists of 82.59 m of very dark gray (5Y 3/1) terrigenous silty clay, together with silt laminae, and 1- to 3-cm-thick silt beds. The frequency of laminae and beds fluctuates through the subunit, from a minimum of two per meter in the uppermost 30 m, to a maximum of 17 per meter between 105 and 111 mbsf (Fig. 5). Some of the silt laminae and beds contain parallel- or cross-lamination (Fig. 8). Subunit IIF is moderately bioturbated from its uppermost boundary to approximately 100 mbsf; from 100 to 123 mbsf, the subunit is slightly bioturbated. Between 61 and 120 mbsf, faint black (N2/0) color banding and mottling occur.

Subunit IIG

Subunit IIG (142.60 mbsf to 210.57 mbsf; Section 940A-17X-1 through -24X-1 at 57 cm) consists of 67.97 m of very dark gray (5Y 3/1) silty clay with silt laminae and less than 4-cm-thick beds of silt and very fine sand. Downhole logs were used to interpret intervals of poor core recovery. The uppermost boundary of Subunit IIG is placed at the top of an interval of contorted sediment that is about 5 m thick and includes discontinuous stringers of silt within a "wood-grain" fabric (see "Lithostratigraphy" section in the "Explanatory Notes" chapter, this volume). This interval is interpreted as a slump.

Subunit IIG is otherwise similar in composition to Subunit IIF except for the lower frequency of laminae and beds (six to 11 per meter; Fig. 5). Some of the thin beds and laminae are cross-laminated, especially from 195 to 205 mbsf. Downhole logs indicate that unrecovered intervals of this subunit consist of lithologies similar to those described from the recovered intervals. Some distorted bedding with chevron patterns in split cores is interpreted to be the result of tilting of "biscuits" formed through rotary drilling (Fig. 9).

Subunit IIH

This subunit extends from 210.57 to 236.14 mbsf (Section 940A-24X-1 at 57 cm through -26X-5 at 84 cm) and consists of 25.57 m of very dark gray (5Y 3/1) silty clay with silt laminae and less than 10-cm-thick beds of very fine and fine sand. The top of the subunit is placed at the first occurrence of sand below Subunit IIG at 210.57 mbsf. Silt laminae decrease in frequency down the subunit and are absent below 216 mbsf. Sand beds increase in abundance from 216 mbsf to the bottom of the subunit. The interval 220 to 236 mbsf con-

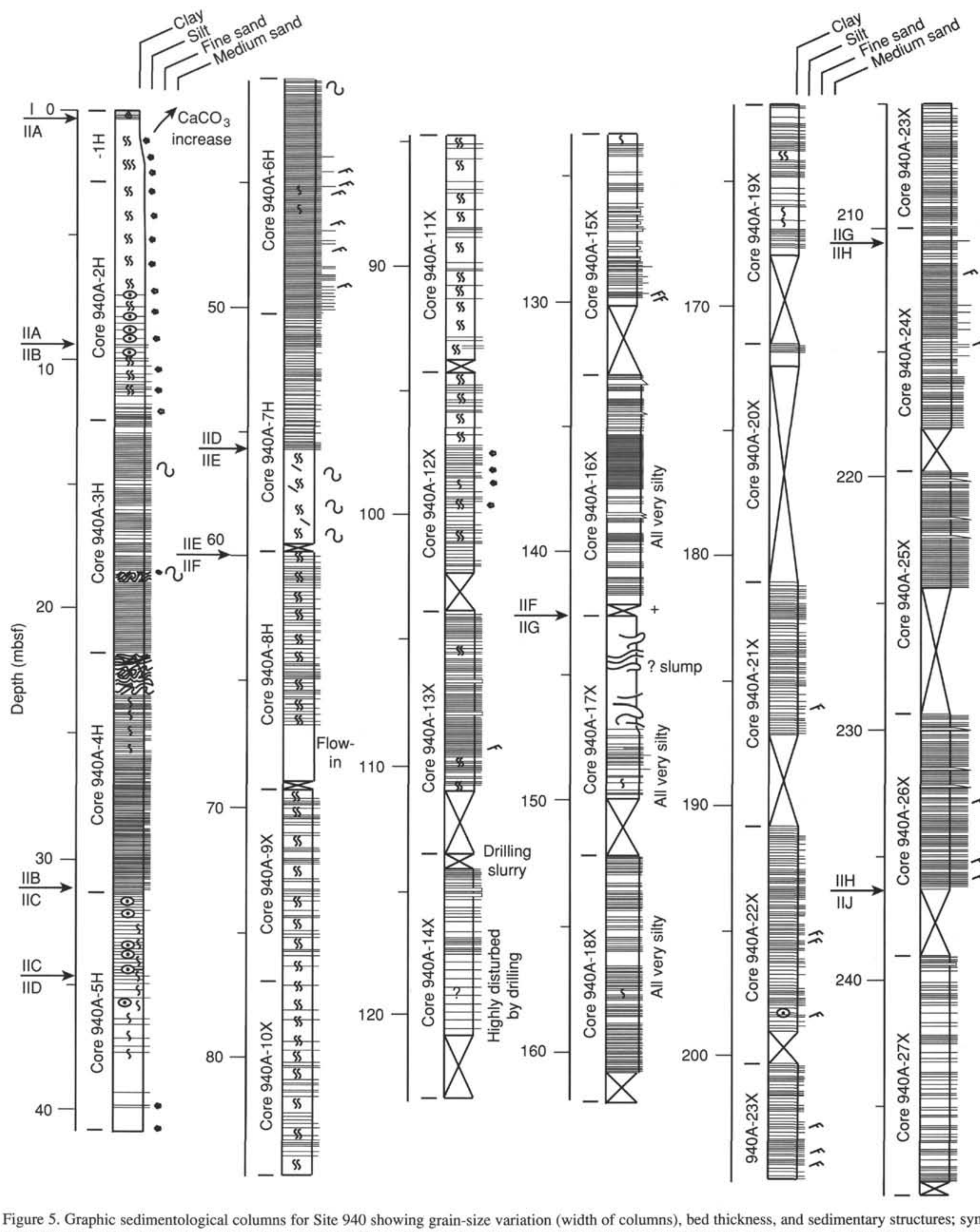

Figure 5. Graphic sedimentological columns for Site 940 showing grain-size variation (width of columns), bed thickness, and sedimentary structures; symbols and preparation of these columns are explained in the "Lithostratigraphy" section of the "Explanatory Notes" chapter, this volume. Arrows indicate the positions of unit and subunit boundaries. The upper part of the column is shown in the longitudinal profile of the foldout (back pocket, this volume) to show the down-fan changes in levee deposits. Void subtraction, but no compression, was applied to cores for which the ODP official recovery was less than 100%, although many of these cores also showed evidence of pervasive gas expansion. In one case (Core 155-940A-16X, + sign), subtraction of the larger voids resulted in a decrease in core length to less than the cored interval, even though ODP reports >100% recovery for this core (see recovery data, "Operations" section, this chapter).

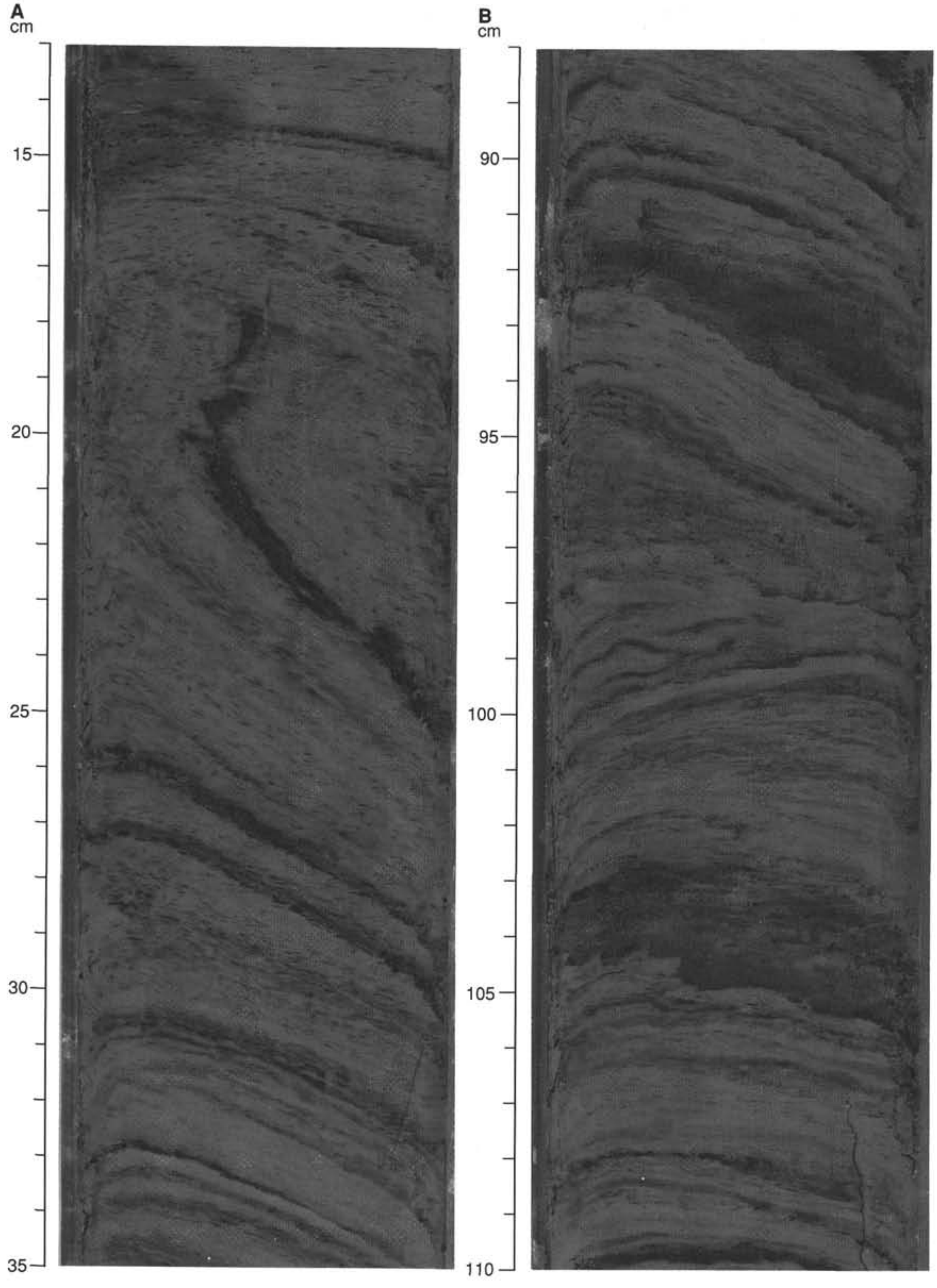

Figure 6. Two examples of contorted bedding, interpreted as a slump, from Subunit IIB. The black hydrotroilite staining of the coarser grained silt beds highlights the contortion. **A.** 155-940A-4H-1, 13–35 cm. **B.** 155-940A-4H-1, 88–110 cm.

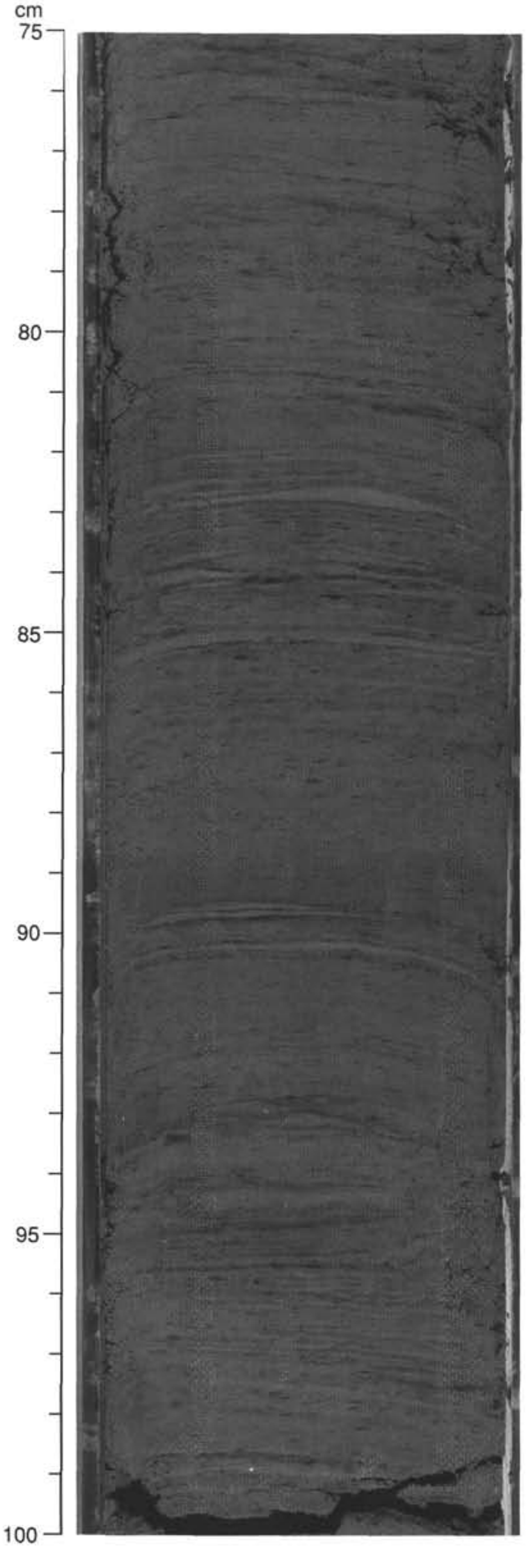

Figure 7. Thin and discontinuous silt and silty clay laminae from Subunit IID (155-940A-6H-4, 75–100 cm).

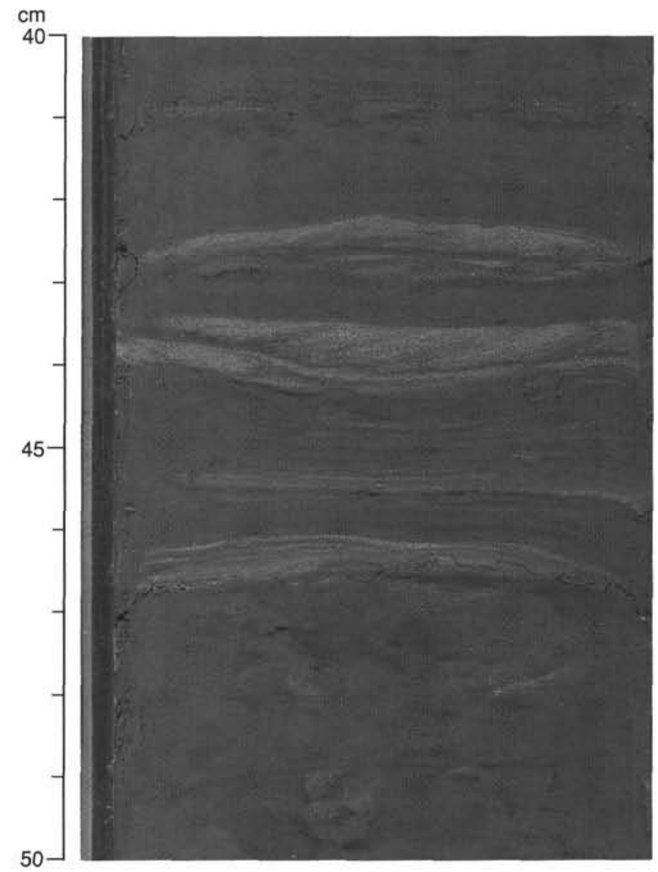

Figure 8. Parallel- and cross-laminated silt laminae and thin silt beds in Subunit IIF (155-940A-15X-5, 40–50 cm).

tains approximately 12 thin beds of fine sand per meter. These beds form approximately 50% of this subunit and are commonly cross laminated (Figs. 5 and 10). A thin section from a sand bed (Sample 940A-25X-2, 118–120 cm) consists of poorly sorted very fine sand with subangular grains composed of quartz (35%), rock fragments (20%), feldspar (15%), mica (13%), amphibole (12%), and plant fragments (5%). Many quartz grains are coated with iron oxide.

Subunit IIJ

Subunit IIJ extends from 236.14 mbsf to the bottom of the hole at 248.6 mbsf (Section 940A-26X-5 at 84 cm through -27X-CC). The uppermost boundary of this subunit is placed at the first occurrence of silt laminae below Subunit IIH. The sediment consists of very dark gray (5Y 3/1) silty clay that contains deformed silt beds and truncated laminae (Fig. 11). The primary structures have been destroyed by XCB coring.

Mineralogy

Mineralogy was determined by X-ray-diffraction analysis of 26 bulk samples of silt and silty clay, together with routine semiquantitative smear-slide identification. The common minerals inferred from XRD data are quartz, plagioclase, augite, and the clay minerals smectite, illite (+ mica), and kaolinite (Table 2). Most samples also contain K-feldspar. Fewer than half of the samples contain calcic amphibole (probably hornblende or a related mineral). Relative to quartz, the abundances of feldspars and ferromagnesian minerals show little stratigraphic variation (Fig. 12A). The phyllosilicate mineral group with the highest relative peak intensity is illite + mica (Fig. 12B).

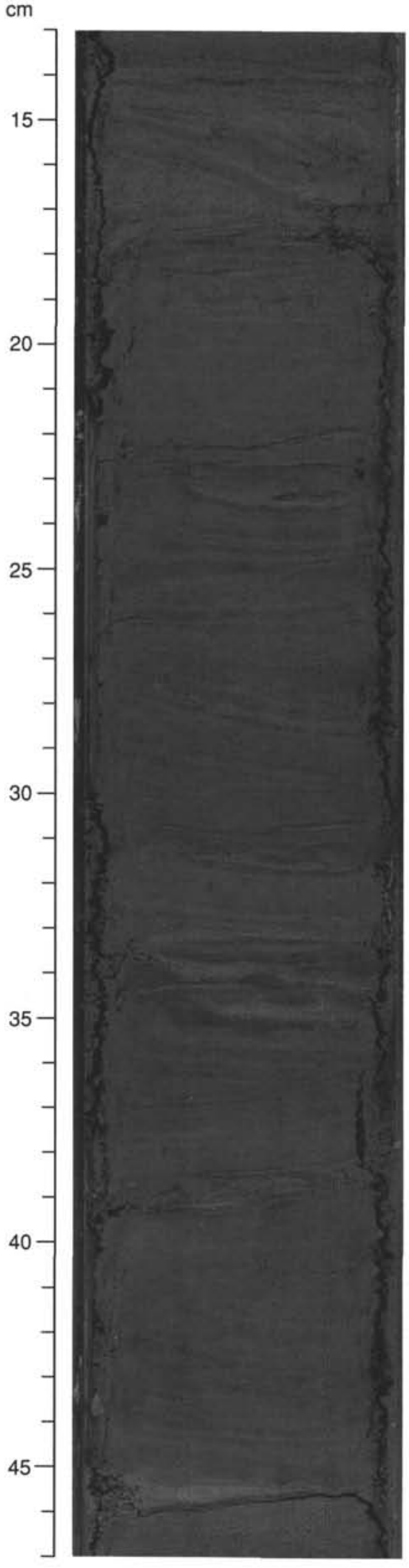

Figure 9. Inferred drilling disturbance in Subunit IIG. "Chevrons" of contorted sediment occur throughout. The rotary disturbance has obscured the primary fabric of the silt beds and produced discontinuous silt laminae (155-940A-22X-4, 13–47 cm).

Spectrophotometry

Reflectance of visible light was low throughout the sediment column. For all wavelength bands from 400 to 700 nm, reflectance values range between 10% and 28% in Unit II. In contrast, values reach 33% in the red spectrum at the top of Unit I. The ratio between red (650–700 nm) and blue (450–500 nm) spectral reflectance averages 1.18 (Fig. 4). The highest red/blue ratio of 1.6 corresponds to the brown calcareous clay of Unit I, indicating the enhancement of red reflectance caused by iron oxyhydroxides. In Unit II, the changes in reflectance of individual wavelength bands, in particular in the red/blue spectrum ratio, are dominated by a high-frequency variability. This trend results from black color banding or mottling, gas partings, and layers of silt and sand. No significant correlation was identified between the reflectance record and the lithologic units, presumably because the amount of iron sulfide in the sediment (color banding and mottling) varies, in most cases, independently of silt and sand layers.

Discussion

Site 940 recovered a sequence of sediment from the levee of the Amazon Channel (i.e., Channel 1) that was deposited during the Amazon, Brown, and Aqua phases of its activity. The site provided a unique opportunity to test existing channel-levee evolution theories that, to date, have been based solely upon the interpretation of seismic data and short piston cores (e.g., Manley and Flood, 1988; Pirmez, 1994). Most of the sequence recovered at Site 940 (Unit II) consists of silty clay with laminae and beds of silt and sand whose frequency and occurrence fluctuate throughout the unit (Fig. 5). Three depositional "packages" are apparent in Unit II and are described from the base of the hole upward.

1. The oldest "package" comprises Subunits IIJ, IIH, and IIG. The base of the "package" (Subunit IIJ) consists of an interval of thin silt laminae and beds intercalated within a silty clay. This interval is followed by an interval of abundant sand turbidites (>10 per meter) (Subunit IIH). This interval is overlain by fairly uniform silt with little sand (Subunit IIG). This "package" is inferred to represent a time of levee progradation and aggradation. A similar fining- and thinning-upward sequence (with no analog for the basal part of Subunit IIJ at Site 940) was recovered at Site 935, where it was inferred to represent deposits of the Aqua Channel-levee System.
2. The second "package" consists of Subunit IIF and contains two cycles or "pulses" of abundant (>10 events per meter) silty turbidites (at approximately 104–111 and 133–140 mbsf). These cycles or "pulses" alternate with less abundant (<5 events per meter) silty turbidites intercalated within hemipelagic silty clay, which is moderately bioturbated and color banded (Fig. 5). This sequence apparently represents periods of relatively "rapid" levee growth separated by periods of slower growth. The base of this "package" corresponds to the inferred base of the Brown Channel-levee System (Fig. 28).
3. The third "package" includes Subunits IIB through IIE, which are characterized by two cycles of abundant turbidites (30/m in Subunit IIB to 60/m in Subunit IID). The turbidites alternate with a few intervals consisting of moderately bioturbated and color-banded silty clay. This "package" is distinguished from the underlying "package" in that the frequency of turbidites is significantly higher in Subunits IIB and IID than in Subunit IIF, and there are thicker intervals of bioturbated and color-banded sediment in Subunit IIF.

Seismic data indicate that Subunits IIA through IID make up the Amazon Channel-levee System. However, the lack of a distinctive lithologic boundary in the interval between 50 and 70 mbsf makes separation of the Brown and Amazon systems difficult. In addition, a

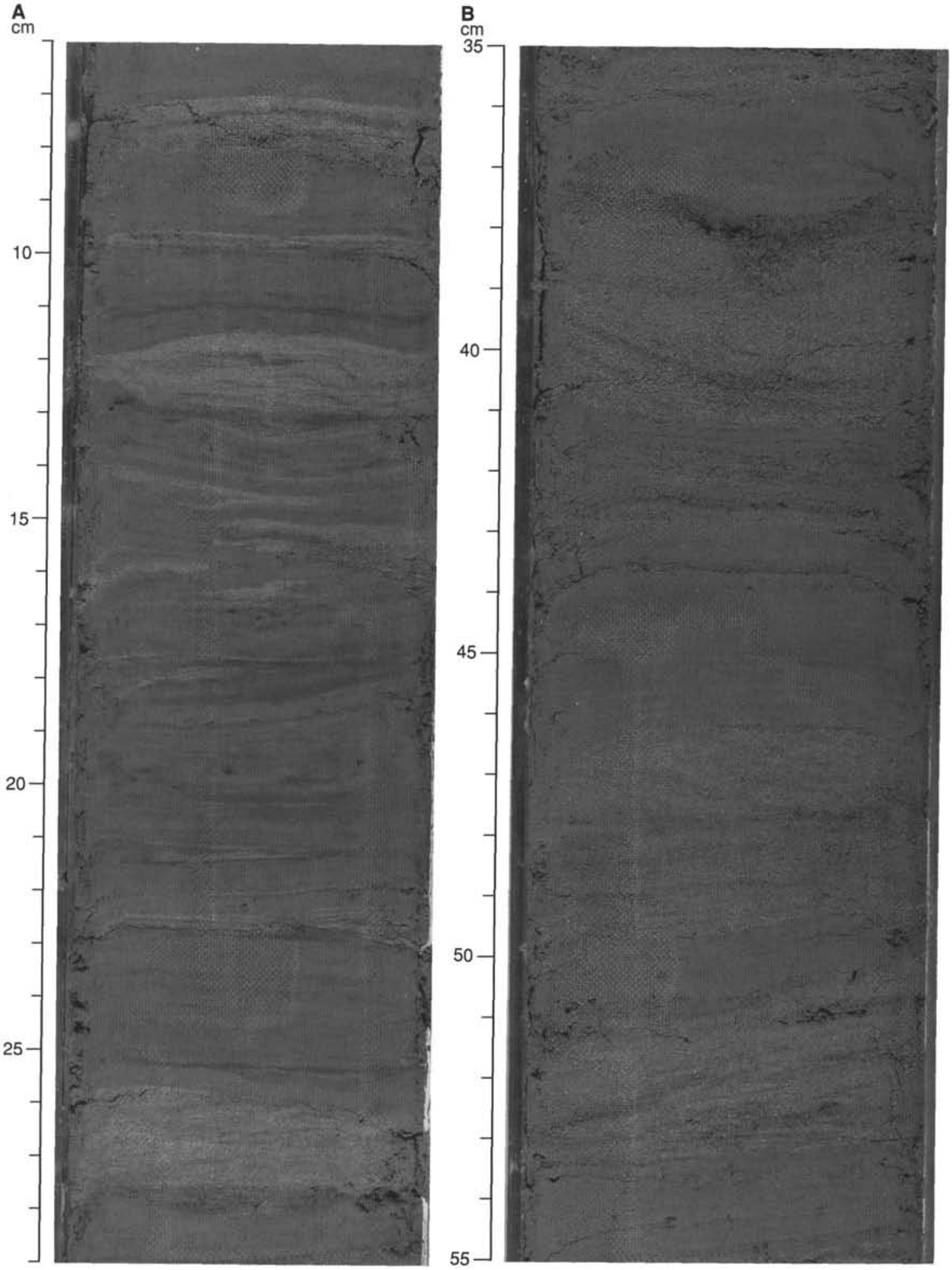

Figure 10. Silt laminae and beds in Subunit IIH. **A.** Interval 155-940A-24X-6, 6–29 cm, illustrating the lithology above 220 mbsf, where silt laminae are predominant. **B.** Interval 155-940A-26X-5, 35–55 cm, illustrating the abundance of sand beds below 220 mbsf.

strong seismic reflection marking the initiation of the Amazon System is not observed within the 50- to 70-mbsf interval (see "Core-Seismic Integration" section, this chapter).

Subunit IIA and Unit I are common to all Leg 155 sites and consist of hemipelagic calcareous clay and silty clay that are inferred to reflect the decrease in terrigenous input to the fan in response to sea-level rise during the late Pleistocene–Holocene.

BIOSTRATIGRAPHY

Calcareous Nannofossils

Calcareous nannofossils recovered at Site 940 are all from nannofossil Zone CN15b (Table 3). An abundant, well-preserved, and low-diversity nannofossil assemblage is present in the nannofossil and

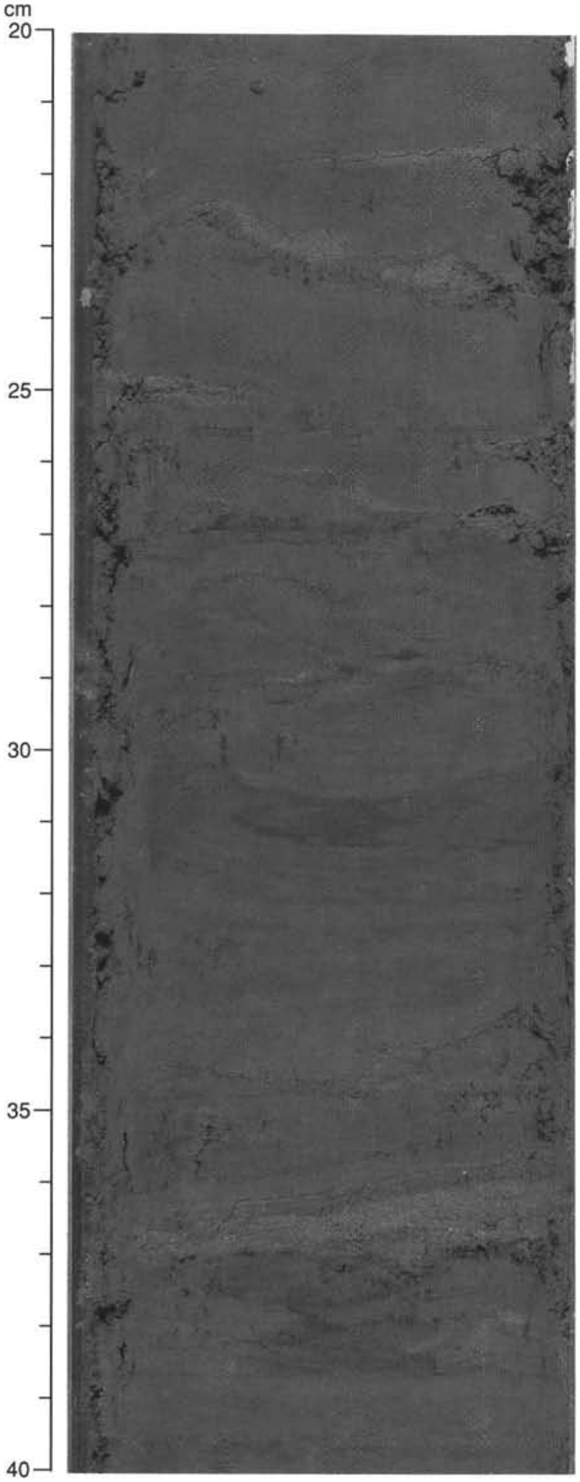

Figure 11. Wispy and discontinuous silt laminae and silty clay from Subunit IIJ. Much of the primary fabric in this subunit has been destroyed by rotary drilling (155-940A-27X-2, 20–40 cm).

foraminifer clay in the mud-line sample. As this sample resembles nannofossil assemblages found deeper in the Holocene sections of previous sites, it indicates that the uppermost part of the Holocene is missing, or was not recovered, in Hole 940A. The abundance of nannofossils is high throughout Unit I, in contrast to the downhole decrease in abundance observed at previous sites.

Nannofossils are absent or occur in low abundance in Unit II 2.5 to 247.9 mbsf (Samples 940A-1H-2, 100–105 cm, through -27X-CC, 43–44 cm). All assemblages have a low diversity and are dominated by *Gephyrocapsa oceanica* and the cold-water species *Coccolithus pelagicus*. Two intervals are barren of nannofossils: the lower part of Subunit IID to the upper part of Subunit IIF 51.2–77.25 mbsf (Samples 940A-6H-CC, 55–56 cm, through -9X-CC, 23–24 cm) and the lower part of Subunit IIH to the middle part of Subunit IIJ 209.9 to 224.4 mbsf (Samples 940A-23X-CC, 33–34 cm, through -25X-CC, 14–15 cm). No nannofossils were observed in the lighter colored sediment examined at the very top of some turbidites (Samples 940A-3H-3, 28.5 cm, compared to -3H-3, 29 cm). The occurrence of *E. huxleyi* places the glacial-age sediment of Unit II in Zone CN15b.

Planktonic Foraminifers

Foraminifers are relatively abundant throughout Hole 940A. The boundary between Ericson Zones Z and Y (disappearance of *G. tumida*) is between Samples 940A-1H-2, 62–67 cm (2.12 mbsf), and -1H-2, 100–105 cm (2.50 mbsf; Fig. 13; Table 4). The low abundance of *G. tumida* found in Sample 940A-1H-CC, 1–9 cm (2.75 mbsf), has been discounted for the purposes of defining the Z/Y boundary, because of possible downhole core-catcher contamination. The interval between the Z/Y boundary and 248 mbsf (Sample 940A-27H-CC, 29–43 cm), which corresponds to Unit II (Fig. 13), has been defined as the Y Zone on the basis of the absence of *G. menardii* and *G. tumida*. This interval can also be constrained in age to less than 40 ka by the absence of *P. obliquiloculata*.

Benthic Foraminifers

Benthic foraminifers are rare or absent throughout the hole. In Subunits IIB and IIF bathyal benthic foraminifers occur in low abundances (Samples 940A-4H-CC, 17–32 cm [31 mbsf], and -10X-CC, 17–31 cm [84 mbsf]). Abyssal benthic foraminifers are absent in Hole 940A.

Siliceous Microfossils

Rare marine diatoms including small specimens of *Actinocyclus ellipticus* are present in the mud-line sample of Site 940. The pre-Holocene section of Hole 940A is barren of diatoms (Table 4). A few radiolarian fragments were observed in the mud-line sample of Hole 940A. Siliceous sponge spicules are present in low abundance in Unit I, Subunits IIC and IIH.

Palynology

Fourteen samples were examined from Hole 940A (Table 5). The samples had low to moderate abundance and poor to moderate preservation. Pollen and spore assemblages were obtained from clays, silty clays, and silts (Unit II) between 2.84 and 224.42 mbsf (Fig. 13). This late Pleistocene (Y Zone) assemblage has low to moderate abundance and contains *Byrsonima, Salix,* Compositae, Cyperaceae, Gramineae, tricolporate, and tricolpate (TC) types, with Cyatheaceae and monolete spores present. *Byrsonima* spp., Compositae, and Gramineae are commonly found in cerrado-type vegetation with *Salix* spp., which is an important pioneer species along river courses. Wood particles were observed in all sample slides in low to moderate abundance (Table 5). Macroscopic wood fragments (>63 µm) were observed in four core-catcher samples at 59.27, 93.45, 110.97, and 247.78 mbsf. Dinoflagellates are present in very low abundance at 93.59 and 187.15 mbsf.

Stratigraphic Summary

Site 940 is a high-sedimentation-rate site, where planktonic foraminifers indicate an age younger than 40 ka. Unit I contains nannofossil and planktonic foraminifer assemblages indicative of the Holocene. The nannofossil assemblages are well preserved and rep-

Table 2. Relative peak intensities of main minerals in representative lithologies at Site 940.

Core, section, interval (cm)	Lithology	Depth (mbsf)	Relative intensity of primary peaks								
			Smectite	Mica + Illite	Kaolinite	Quartz	Plagioclase	K-feldspar	Feldspar	Augite	Hornblende
155-940A-											
1H-1, 131–132	Silty clay	1.31	8.2	11.5	7.6	100.0	7.4	9.5	16.9	5.0	*
2H-3, 140–141	Silty clay	7.20	14.5	18.8	10.0	100.0	12.6	4.9	17.5	3.0	*
3H-5, 56–57	Silt	18.86	11.4	17.1	11.9	100.0	11.4	5.8	17.2	3.4	*
4H-5, 90–91	Silt	28.70	18.6	19.3	8.6	100.0	8.3	4.3	12.6	2.7	*
5H-4, 75–76	Silty clay	35.89	7.5	19.8	13.6	100.0	5.7	*	5.7	10.2	*
6H-3, 84–85	Silt	44.64	14.4	16.8	8.4	100.0	9.0	*	9.0	2.5	*
7H-2, 39–40	Silt	51.46	5.6	13.4	4.8	100.0	11.3	5.1	16.4	1.4	*
8H-2, 123–124	Silty clay	62.53	12.5	24.2	11.4	100.0	8.2	*	8.2	2.7	*
9X-4, 138–139	Silt	75.18	4.8	16.0	7.7	100.0	8.3	2.6	10.9	1.6	*
10X-3, 39–40	Silt	80.39	2.6	8.9	4.3	100.0	10.4	3.6	14.0	1.2	1.4
11X-6, 54–55	Silt	92.71	3.1	7.8	4.8	100.0	7.9	3.3	11.2	1.3	*
12X-2, 11–12	Silt	95.91	2.8	12.5	5.5	100.0	6.8	4.9	11.7	1.4	1.0
13X-4, 107–108	Silt	109.35	3.5	8.0	4.1	100.0	7.4	3.5	10.9	1.0	1.2
14X-5, 48–49	Silt	119.53	2.6	14.4	7.5	100.0	8.1	3.9	12.0	1.6	*
15X-1, 27–28	Silt	123.57	7.6	19.3	11.0	100.0	9.4	9.4	18.8	2.8	*
16X-2, 76–77	Silt	135.26	4.7	10.8	6.2	100.0	12.0	5.4	17.4	1.2	*
17X-4, 16–17	Silty clay	147.26	17.0	26.1	15.0	100.0	13.4	9.8	23.2	3.2	*
18X-5, 84–85	Silt	158.04	2.9	6.2	3.7	100.0	12.5	4.2	16.7	0.9	*
19X-1, 56–57	Silt	162.46	13.9	26.0	12.6	100.0	15.4	4.8	20.2	1.6	2.7
21X-4, 48–49	Silt	186.08	7.8	17.6	7.5	100.0	7.8	5.4	13.2	1.7	*
22X-2, 90–91	Silt	193.20	10.4	21.7	10.1	100.0	11.7	3.9	15.6	1.8	3.7
23X-6, 124–125	Silt	208.77	7.1	13.2	8.4	100.0	10.5	5.2	15.7	0.9	0.9
24X-3, 97–98	Silt	213.97	5.6	19.1	8.7	100.0	8.4	4.3	12.7	1.9	4.6
25X-3, 53–54	Silt	223.06	7.4	20.2	11.2	100.0	12.2	4.5	16.7	2.4	2.6
26X-3, 49–50	Silt	232.79	3.7	7.6	4.6	100.0	9.8	7.6	17.4	1.3	0.9
27X-4, 25–26	Silt	243.75	2.4	5.5	3.1	100.0	9.2	*	9.2	1.0	0.6

Notes: See "Lithostratigraphy" section in the "Explanatory Notes" chapter, this volume, for XRD methods. * = non-detection.

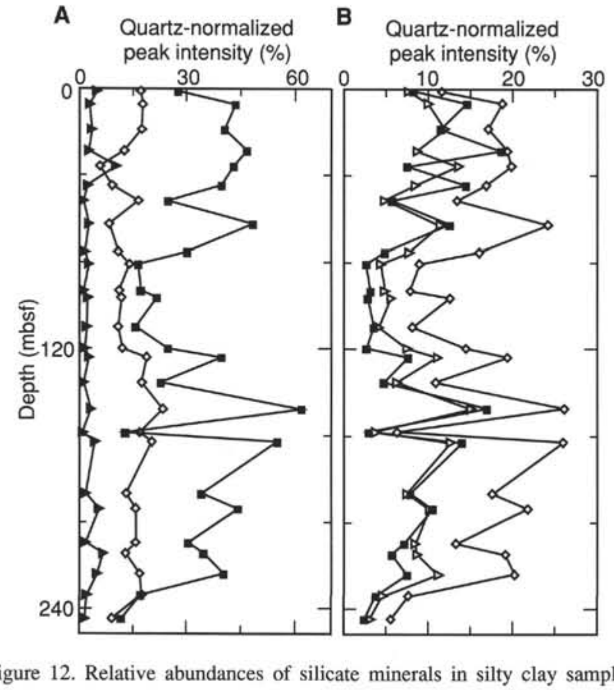

Figure 12. Relative abundances of silicate minerals in silty clay samples, based on XRD analysis (Table 2). **A.** Plot against depth of the quartz-normalized peak intensities of the major mineral groups (quartz peak intensity set at 100%). Squares = clay minerals + mica; diamonds = feldspar; triangles = augite + hornblende. **B.** Plot against depth of the quartz-normalized peak intensities of clay minerals and micas. Squares = smectite; diamonds = mica + illite; triangles = kaolinite.

resent nannofossil Zone CN15b. Ericson zones were assigned to sediment in Hole 940A. The boundary between Ericson Zones Z and Y (disappearance of *G. tumida*) is between 2.12 and 2.50 mbsf. The interval between the Z/Y boundary and 248 mbsf, which corresponds to Unit II, has been defined as the Y Zone (<40 ka) on the basis of the absence of *G. menardii*, *G. tumida*, and *P. obliquiloculata*. Palynomorphs have low to moderate abundance in the Y Zone sediment (Unit II).

PALEOMAGNETISM

Remanence Studies

Archive-half sections from all APC cores and from 18 of the 19 XCB cores were measured on the pass-through cryogenic magnetometer. Only Core 940A-20X, which consisted of one short section, was not measured. Cores 940A-4H through -8H were oriented with the Tensor tool.

In general, the declinations from Hole 940A showed considerable scatter due to core disturbance, or showed appreciable rotation, or twisting, downward within each core.

Short wavelength inclination oscillations are better defined than long wavelength oscillations in Hole 940A (Fig. 14). Their wavelengths are 0.9 to 1.2 m in the interval from 5 to 30 mbsf, and ~0.5 m in the interval from 42 to 55 mbsf. The change in the wavelengths between 30 and 42 mbsf may suggest a slowing of the sedimentation rate by about a factor of two between these zones.

Remanence intensities after AF demagnetization to 20 mT show considerable variation in Hole 940A, with the highest values occurring in the top 60 m of the hole (Fig. 15).

A comparison of the remanence intensity, after AF demagnetization to 20 mT, between Hole 940A and the top 50 mbsf in Hole 935A suggests a correlation between three intensity peaks (Fig. 15). In Hole 940A, peaks "1" and "2" fall within the Amazon Channel-levee deposits, while peak "3" is near the top of the Aqua Channel-levee deposits (Fig. 29). In Hole 935A, peak "3" also falls near the top of the Aqua Channel-levee deposits (see Fig. 35, "Site 935" chapter, this volume). Peaks "1" and "2" in Hole 940A may also correlate with similar peaks in the remanence intensity observed at Hole 939B (see Cisowski, this volume).

No geomagnetic excursions were observed in the APC cores. The general persistence of a drill stem overprint in the XCB cores prohibited the identification of anomalous geomagnetic behavior in the lower portions of Hole 940A.

Magnetic Susceptibility

Whole-core and discrete-sample magnetic susceptibilities were measured on all cores from Hole 940A (Fig. 16). The highest whole-

Table 3. Calcareous nannofossil and siliceous microfossil abundance data for Hole 940A.

Core, section, interval (cm)	Top interval (mbsf)	Bottom interval (mbsf)	Calcareous nannofossils			Diatoms				Ericson Zone (inferred from foraminifers)	Age (inferred from foraminifers)
			Abundance	Preservation	Zone	Marine	Fresh water	Sponge spicules	Radiolarians		
155-940A-											
1H-Ml, 0	0.00		a	g	CN15b	vr	b	f	b	Z	Holocene
1H-1, 0–1	0.00	0.01	a	g						Z	Holocene
1H-1, 7–8	0.07	0.08	a	g						Z	Holocene
1H-1, 13–15	0.13	0.15	c	g						Z	Holocene
1H-1, 21–22	0.21	0.22	a	g						Z	Holocene
1H-1, 29–30	0.29	0.30	c	g						Z	Holocene
1H-1, 50–52	0.50	0.52	c	g						Z	Holocene
1H-1, 54–55	0.54	0.55	c	g						Z	Holocene
1H-1, 100–105	1.00	1.05	f	m						Z	Holocene
1H-2, 100–105	2.50	2.55	tr	—						Y	late Pleist.
1H-CC, 9–10	2.84	2.85	r	m		b	b	f	b	Y	late Pleist.
2H-CC, 22–23	12.66	12.67	vr	—		b	b	b	b	Y	late Pleist.
3H-3, 28.5	15.58		vr	—		b	b	b	b	Y	late Pleist.
3H-3, 29	15.59		tr	—		b	b	b	b	Y	late Pleist.
3H-CC, 11–12	21.41	21.42	b	—		b	b	b	b	Y	late Pleist.
4H-CC, 32–33	31.80	31.81	vr	—		b	b	r	b	Y	late Pleist.
5H-CC, 55–56	40.25	40.26	tr	—		b	b	b	b	Y	late Pleist.
6H-CC, 55–56	51.24	51.25	b	—		b	b	b	b	Y	late Pleist.
7H-CC, 70–71	59.41	59.42	b	—		b	b	b	b	Y	late Pleist.
8H-CC, 34–35	68.86	68.87	b	—		b	b	b	b	Y	late Pleist.
9X-CC, 23–24	77.24	77.25	b	—		b	b	b	b	Y	late Pleist.
10X-CC, 31–32	84.81	84.82	tr	—		b	b	b	b	Y	late Pleist.
11X-CC, 35–36	93.59	93.60	tr	—		b	b	b	b	Y	late Pleist.
12X-CC, 28–29	102.36	102.37	vr	—		b	b	b	b	Y	late Pleist.
13X-CC, 23–24	111.06	111.07	tr	—		b	b	b	b	Y	late Pleist.
14X-CC, 33–34	120.88	120.89	vr	—		b	b	b	b	Y	late Pleist.
15X-CC, 22–23	130.18	130.19	vr	—		b	b	b	b	Y	late Pleist.
16X-CC, 23–24	142.82	142.83	vr	—		b	b	b	b	Y	late Pleist.
17X-CC, 51–52	149.84	149.85	tr	—		b	b	b	b	Y	late Pleist.
18X-CC, 49–50	160.86	160.87	tr	—		b	b	b	b	Y	late Pleist.
19X-CC, 34–35	167.87	167.88	vr	—		b	b	b	b	Y	late Pleist.
20X-CC, 14–15	172.40	172.41	vr	—		b	b	r	b	Y	late Pleist.
21X-CC, 14–15	187.15	187.16	tr	—		b	b	b	b	Y	late Pleist.
22X-CC, 14–15	198.97	198.98	tr	—		b	b	b	b	Y	late Pleist.
23X-CC, 33–34	209.86	209.87	b	—		b	b	b	b	Y	late Pleist.
24X-CC, 32–33	218.09	218.10	b	—		b	b	b	b	Y	late Pleist.
25X-CC, 14–15	224.42	224.43	b	—		b	b	b	b	Y	late Pleist.
26X-CC, 12–13	236.26	236.27	tr	—		b	b	b	b	Y	late Pleist.
27X-CC, 43–44	247.92	247.93	b	—		b	b	b	b	Y	late Pleist.

core and discrete-sample susceptibility values occur within Subunit IIH, and the lowest values are found in Unit I. In general, these values do not change significantly across subunit boundaries.

ORGANIC GEOCHEMISTRY

Volatile Hydrocarbons

Headspace methane concentrations are moderately high throughout Hole 940A. They range from 6500 to 37,000 ppm (172.26–29.30 mbsf), with a mean of about 9000 ppm (Table 6; Fig. 17). Vacutainer methane values are higher than those of headspace concentrations (Fig. 17), ranging from 38,500 to 633,500 ppm in Hole 940A. The maximum concentration (633,500 ppm) was detected at 29.50 mbsf, corresponding to the highest headspace methane concentration. Higher molecular weight hydrocarbons were not measured, indicating a predominantly biogenic methane source at Site 940.

Carbon, Nitrogen, and Sulfur Concentrations

The content of carbonate, calculated as $CaCO_3$, decreases from 29.0% at 0.11 mbsf to 1.0% at 1.75 mbsf and then ranges mainly from 1% to ~3% downhole (Table 7; Fig. 18). TOC is low (0.4% and 0.49%) in the two shallowest samples (0.11, 0.60 mbsf), then varies mainly between 0.8% and 1.2% downhole. A few lower concentrations (<0.5%) are observed in silt and sand layers (at 11.29, 46.24, 51.29, 126.86, 135.25, and 195.47 mbsf).

In general, the TN profile is similar to that of TOC, with lower values in silt and sand layers. Most TN concentrations in Hole 940A range from 0.07% to 0.11%, with lower values (≤0.04%) in sand and silt beds. [C/N]a ratios are uniform and range mainly from 6 to 13. A high value of 20 is observed in a silt layer at 11.29 mbsf.

Total sulfur concentrations are low and generally range between 0% and 0.15%. A few higher concentrations (1.35%, 0.9%, and 1.34%) are observed at the upper 35 mbsf (8.18, 17.18, and 31.52 mbsf, respectively). Most likely, this is a zone where more reactive organic matter is oxidized by sulfate reduction to yield sediment enriched in iron sulfides.

INORGANIC GEOCHEMISTRY

Interstitial Water Analysis

Analyses of interstitial waters were performed on 12 sediment samples at Hole 940A. Samples were taken approximately every 10 m for the upper 30 mbsf and approximately every 30 m thereafter to a depth of 244.90 mbsf (Table 8; Fig. 19).

Salinities of the water samples range from 32.5 to 35.0 (Fig. 19A). Over the interval 1.45–29.25 mbsf, salinity decreases from 35.0 to 34.0. Between 29.25 and 32.55 mbsf, there is a sharp drop to 32.5; this correlates with a decline in longitudinal resistivity in the sediment at approximately 30 mbsf (see "Physical Properties" section, this chapter). The decrease in salinity is caused by decreases in alkalinity, sulfate, calcium, and magnesium between 29.25 and 32.55 mbsf (see below). Below 32.55 mbsf, salinity varies between 32.5 and 33.5.

Chloride concentrations range from 552 to 565 mM. Concentrations increase asymptotically from 552 mM at 1.45 mbsf to 565 mM at 145.50 mbsf (Fig. 19B). Below 145.50 mbsf, chloride values remain between 564 and 565 mM.

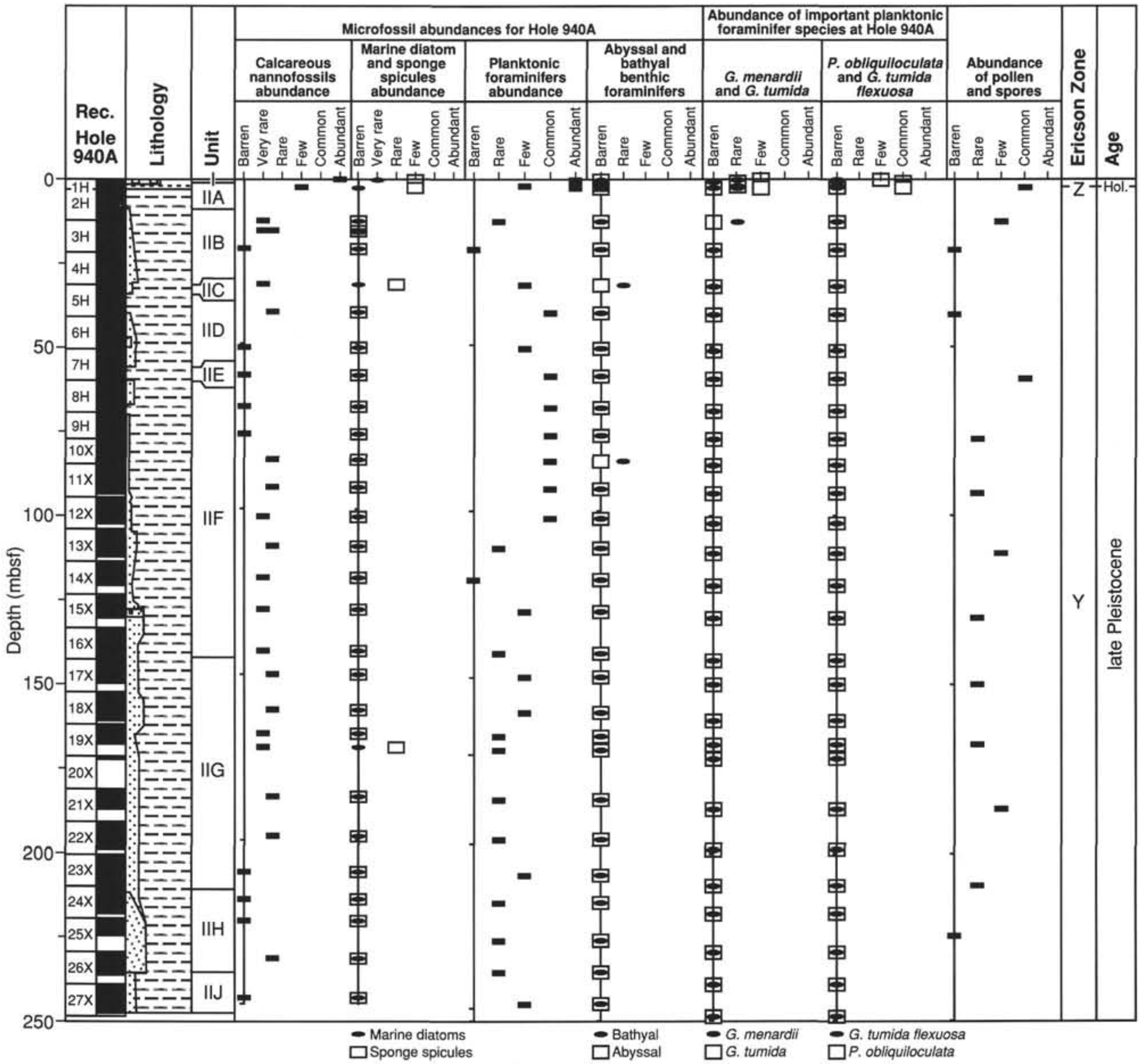

Figure 13. Biostratigraphic summary for Site 940.

Pore-water pH values are about 7.5 throughout the hole (Fig. 19C). There is a small increase to 7.6 at 30 mbsf, and a small decrease to 7.26 at 64.20 mbsf.

Alkalinity values increase steadily from 14.51 mM at 1.45 mbsf to 35.82 mM at 29.25 mbsf (Fig. 19D). Alkalinity then drops sharply to 21.62 mM at 32.25 mbsf and to 6.11 mM at 64.20 mbsf. Below 64.20 mbsf, alkalinity values are relatively uniform, ranging from 10.18 to 12.22 mM.

Magnesium and calcium concentrations decrease in the upper 32.25 mbsf, from 48.0 mM magnesium and 8.9 mM calcium at 1.45 mbsf to 41.3 mM magnesium and 4.8 mM calcium at 32.25 mbsf (Fig. 19E and 19F). Below 32.25 mbsf, the values show little variation.

Pore-water sulfate concentrations decrease from 19.2 mM at 1.45 mbsf to zero at 29.25 mbsf (Fig. 19G). This is the greatest depth of total sulfate depletion thus far encountered during Leg 155. Below 29.25 mbsf, sulfate concentrations generally remain at or near zero for most of the remainder of the hole. As at several previous sites, however, a few nonzero values also were measured: 1.9 mM at 32.25 mbsf, and up to 5.3 mM in the three lowermost samples. Because high methane concentrations were measured at these same depths, the measurable sulfate probably represents a sampling artifact.

Ammonium concentrations increase steadily with depth from 0.6 mM at 1.45 mbsf to 7.0 mM at 90.57 mbsf (Fig. 19H). Below 90.57 mbsf, the ammonium concentration varies irregularly between 5.5 and 7.5 mM.

Pore-water phosphate concentrations increase in the uppermost part of the hole, from 78.2 µM at 1.45 mbsf to 131.6 µM at 29.25 mbsf (Fig. 19I). The concentrations then decrease quickly to 2.3 µM at 64.20 mbsf, and remain below 10 µM throughout the remainder of the hole. The peak in phosphate concentration is tens of meters deeper here than at most previous sites. Together with the greater depth of

Table 4. Foraminifer abundance data for Hole 940A.

Core, section, interval (cm)	Top interval (mbsf)	Bottom interval (mbsf)	*Globorotalia menardii*	*Globorotalia tumida*	*Globorotalia tumida flexuosa*	*Pulleniatina obliquiloculata*	*Globigerinoides ruber* (white)	*Globigerinoides ruber* (pink)	*Globorotalia hexagonus*	*Neogloboquadrina dutertrei*	*Globorotalia trilobus trilobus*	*Globorotalia inflata*	*Globorotalia truncatulinoides*	*Globigerina bulloides*	*Globigerinoides trilobus sacculifer*	*Globorotalia fimbriata*	*Bolliella adamsi*	*Hastigerinella digitata*	*Globigerina calida calida*	*Globorotalia crassaformis hessi*	*Globorotalia crassaformis viola*	*Globorotalia tosaensis*	*Globorotalia crassaformis crassaformis*	Other planktonic foraminifers	Vivianite nodules	Overall foraminifer abundance	Preservation	Abundance of bathyal benthic foraminifers	Abundance of abyssal benthic foraminifers	Comments	Ericson Zone	Age
155-940A-																																
1H-1, 50–52	0.50	0.52	R	F	B	F	C	R	B	C	C	B	R	B	F	B	B	B	R	B	B	B	B	B	B	A	G	B	B		Z	Holocene
1H-1, 100–105	1.00	1.05	B	R	B	C	F	R	B	F	C	B	F	B	F	B	B	B	B	B	B	B	B	B	B	A	G	B	B		Z	Holocene
1H-2, 62–67	2.12	2.17	R	R	B	C	R	F	B	F	C	B	F	B	R	B	B	B	B	B	B	B	B	B	B	F	G	B	B	BN	Z	Holocene
1H-2, 100–105	2.50	2.55	B	B	B	B	C	R	B	F	F	B	F	B	C	B	B	B	B	B	B	B	B	B	B	A	G	B	B	BN	Y	late Pleist.
1H-CC, 1–9	2.75	2.84	R	F	B	C	C	B	B	C	C	B	F	C	F	B	B	B	B	R	B	B	B	B	R	A	B	B	B	RN,BN,SP	Y	late Pleist.
2H-CC, 8–22	12.52	12.66	R	B	B	B	R	B	B	R	R	B	R	B	B	B	B	B	B	B	B	B	B	B	R	R	M	B	B	IS,PT,RN,BN	Y	late Pleist.
3H-CC, 0–12	21.30	21.41	B	B	B	B	B	B	B	B	B	B	B	B	R	B	B	B	B	B	B	B	B	B	R	B	M	B	B	PT,BN,RN,IS	Y	late Pleist.
4H-CC, 17–32	31.66	31.80	B	B	B	B	F	R	B	C	F	B	B	B	C	B	B	B	B	B	B	B	B	B	R	F	M	R	B	BN,IS	Y	late Pleist.
5H-CC, 41–55	40.11	40.25	B	B	B	B	F	B	B	F	C	R	B	B	C	B	B	B	B	R	B	B	B	B	C	C	G	B	B	M,RN,IS,PT	Y	late Pleist.
6H-CC, 41–55	51.10	51.24	B	B	B	B	R	R	B	C	C	B	B	B	C	B	B	B	B	B	B	B	B	B	C	F	G	B	B	PT,M	Y	late Pleist.
7H-CC, 56–70	59.27	59.41	B	B	B	B	C	R	B	C	A	B	B	B	A	B	B	B	B	R	B	B	B	F	C	C	G	B	B	IS,M,FO	Y	late Pleist.
8H-CC, 20–34	68.72	68.86	B	B	B	B	F	R	R	C	C	B	B	B	C	B	B	B	B	B	B	B	B	B	C	C	G	B	B	SP,RN,IS	Y	late Pleist.
9X-CC, 9–23	77.15	77.24	B	B	B	B	C	F	B	C	C	B	B	B	C	B	B	B	B	B	B	B	B	B	A	C	G	B	B	IS,M	Y	late Pleist.
10X-CC, 17–31	84.67	84.81	B	B	B	B	F	B	R	C	C	B	F	B	C	B	B	B	B	B	B	B	B	B	C	C	G	R	B	M,IS	Y	late Pleist.
11X-CC, 21–35	93.45	93.59	B	B	B	B	F	R	B	C	C	B	F	B	C	B	B	B	B	B	B	B	B	B	A	C	G	B	B	SP,FO,IS	Y	late Pleist.
12X-CC, 14–28	102.22	102.36	B	B	B	B	F	B	B	C	C	B	B	B	C	B	B	B	B	R	B	B	B	B	C	C	G	B	B	IS,M	Y	late Pleist.
13X-CC, 14–23	110.97	111.06	B	B	B	B	R	R	B	R	R	B	B	B	F	B	B	B	B	B	B	B	B	B	F	R	M	B	B	M,FO,IS,RN	Y	late Pleist.
14X-CC, 19–33	120.74	120.88	B	B	B	B	B	B	B	B	R	B	B	B	B	B	B	B	B	B	B	B	B	B	C	B	M	B	B	M	Y	late Pleist.
15X-CC, 8–22	130.04	130.18	B	B	B	B	F	B	B	C	C	B	B	B	F	B	B	B	B	B	B	B	B	R	A	F	G	B	B	M	Y	late Pleist.
16X-CC, 9–23	142.68	142.82	B	B	B	B	R	B	B	R	F	B	B	B	F	B	B	B	B	B	B	B	B	B	F	R	G	B	B	M	Y	late Pleist.
17X-CC, 37–51	149.70	149.84	B	B	B	B	R	B	B	R	F	B	F	B	R	B	B	B	B	B	B	B	B	B	C	F	G	B	B	M,FO,RN	Y	late Pleist.
18X-CC, 35–49	160.72	160.86	B	B	B	B	R	R	B	C	C	R	F	B	F	B	B	B	B	B	B	B	B	B	C	F	M	B	B	M,SF,IS	Y	late Pleist.
19X-CC, 0–15	167.63	167.87	B	B	B	B	F	R	B	C	C	B	F	B	C	B	B	B	B	B	B	B	B	B	A	R	M	B	B		Y	late Pleist.
20X-CC, 0–15	172.26	172.40	B	B	B	B	C	R	B	F	C	B	F	B	C	B	B	B	B	R	B	B	B	F	A	R	M	B	B	M	Y	late Pleist.
21X-CC, 0–15	187.01	187.15	B	B	B	B	F	R	B	C	C	B	C	B	C	B	B	B	B	B	B	B	B	B	A	R	G	B	B	M	Y	late Pleist.
22X-CC, 0–15	198.83	198.97	B	B	B	B	F	R	B	C	C	B	F	B	A	B	B	B	B	B	B	B	B	B	A	R	G	B	B	M	Y	late Pleist.
23X-CC, 19–33	209.72	209.86	B	B	B	B	C	R	B	C	C	B	C	B	C	B	B	B	B	R	B	B	B	R	A	F	G	B	B	M	Y	late Pleist.
24X-CC, 18–32	217.95	218.09	B	B	B	B	C	R	B	C	C	B	C	B	C	B	B	B	B	B	B	B	B	B	A	R	G	B	B	M,FO	Y	late Pleist.
25X-CC, 0–14	224.28	224.42	B	B	B	B	C	B	B	C	C	B	C	B	C	B	B	B	B	B	B	B	B	B	F	R	G	B	B	M	Y	late Pleist.
26X-CC, 0–12	236.14	236.26	B	B	B	B	F	R	B	C	C	B	C	B	C	B	B	B	B	B	B	B	B	B	F	R	G	B	B	M	Y	late Pleist.
27X-CC, 29–43	247.78	247.92	B	B	B	B	F	B	B	F	C	B	F	B	C	B	B	B	B	B	B	B	B	B	C	F	G	B	B	M,FO	Y	late Pleist.

Notes: Key to Comments section: Sediment composition: PT = pteropods, S = sand, M = mica, BN = black nodules, RN = red nodules, AM = authigenic minerals; indicators of reworking: SF = shell fragments, FO = fine organics, W = wood fragments, SP = sponge spicules or spines, IS = iron-stained foraminifers. Note also the occurrence of bathyal benthic foraminifers.

Table 5. Spores and pollen data for Hole 940A.

Core, section, interval (cm)	Top interval (mbsf)	Bottom interval (mbsf)	Pollen and spores: Abundance	Preservation	Major types recorded	Dinocysts	Wood/ carbonized particles	Ericson Zone (inferred from forams)	Age (inferred from forams)
155-940A-									
1H-CC, 9–10	2.84	2.85	c	m	Gramineae, TCP, monolete spore, *Byrsonima*	b	c	Y	late Pleist.
2H-CC, 22–23	12.66	12.67	f	m	Myrtaceae, monolete spore, *Salix*	b	f	Y	late Pleist.
3H-CC, 11–12	21.41	21.42	b			b	f	Y	late Pleist.
5H-CC, 55–56	40.25	40.26	b			b	f	Y	late Pleist.
7H-CC, 70–71	59.41	59.42	c	m	TCP, Cyatheaceae, monolete spore, *Byrsonima*	b	f	Y	late Pleist.
9X-CC, 23–24	77.24	77.25	r	p	TCP, monolete spore	b	f	Y	late Pleist.
11X-CC, 35–36	93.59	93.60	r	p	TC, Cyatheaceae	r	c	Y	late Pleist.
13X-CC, 23–24	111.06	111.07	f	m	Cyperaceae, TCP, Cyatheaceae	b	c	Y	late Pleist.
15X-CC, 22–23	130.18	130.19	r	p	Monolete (echinate) spore	b	f	Y	late Pleist.
17X-CC, 51–52	149.84	149.85	r	m	Cyatheaceae, monolete spore	b	f	Y	late Pleist.
19X-CC, 34–35	167.87	167.88	r	m	Compositae, Gramineae	b	f	Y	late Pleist.
21X-CC, 14–15	187.15	187.16	f	m	Gramineae, monolete spore	r	f	Y	late Pleist.
23X-CC, 33–34	209.86	209.87	r	m	Cyatheaceae	b	f	Y	late Pleist.
25X-CC, 14–15	224.42	224.43	b			b	r	Y	late Pleist.

Notes: TCP = tricolporate pollen; TC = tricolpate pollen.

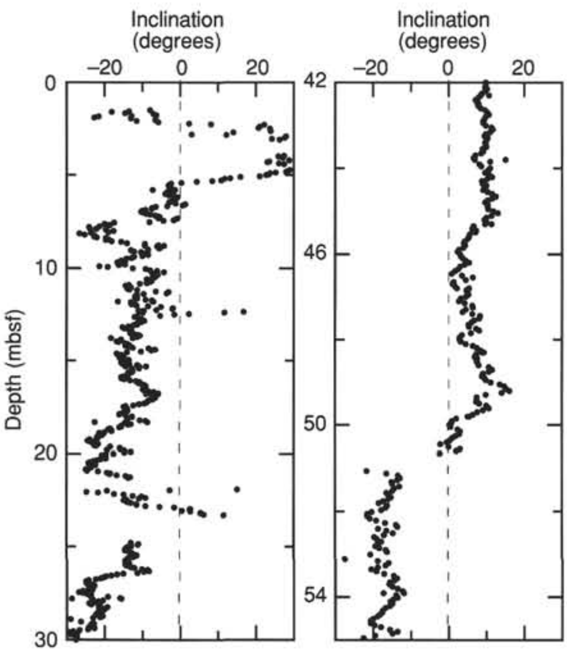

Figure 14. Inclinations for the intervals 0–30 mbsf and 42–55 mbsf of archive-half cores from Hole 940A. AF demagnetization level was 20 mT.

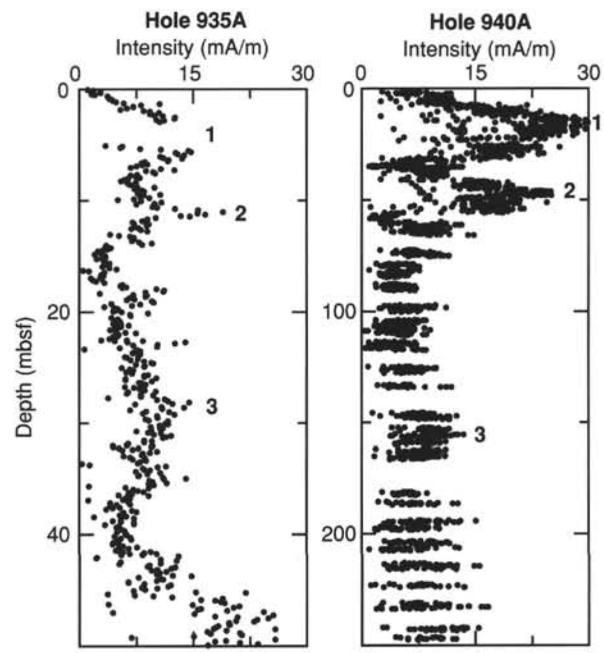

Figure 15. Comparison of remanence intensities, after AF demagnetization to 20 mT, of Holes 935A and 940A. Correlatable intensity peaks are numbered 1–3.

total sulfate reduction, this observation suggests slower rates of organic carbon remineralization at this site, at least in the upper 30 mbsf, than at any previous Leg 155 sites.

Dissolved silica concentrations range from 272 to 446 µM (Fig. 19J). There is no clear trend downhole.

Pore-water potassium concentrations decrease over the upper 65 m of the hole, from 11.6 mM at 1.45 mbsf to 7.1 mM at 64.20 mbsf (Fig. 19K). Below 64.20 mbsf, the values are more uniform, varying between 6.5 and 7.6 mM downhole.

Dissolved sodium concentrations increase slightly in the uppermost part of the hole, from 479 mM at 1.45 mbsf to 487 mM at 19.75 mbsf (Fig. 19L). The concentration then decreases to 463 mM at 64.20 mbsf. Below that depth, the concentration varies between 467 and 480 mM and tends to increase downhole.

Dissolved iron concentrations are between 29.3 and 46.5 µM in the upper 32.55 mbsf (Fig. 19M). The concentrations increase to 95.8–109.7 µM between 64.20 and 90.57 mbsf, and then decrease again to about 20 µM over the interval 116.50–145.50 mbsf. Below 145.50 mbsf, the concentrations vary between 34.2 and 117 µM.

Manganese concentrations decrease from 10 µM in the upper 10 mbsf to 5.6 µM at 32.55 mbsf. Below this depth, the concentrations remain low, varying between 6.4 and 2.8 µM.

Sediment Geochemistry

Ten mud samples from the Amazon, Brown, and Aqua levees of the Upper Levee Complex were analyzed for major- and trace-element geochemistry (Tables 9 and 10). Geochemical compositions are similar to muds from previous sites, although the range in SiO_2 is greater than for most sites. SiO_2 varies from 61 to 67 wt%; Al_2O_3, between 18 and 22 wt%; and CaO, between 0.6 and 1.0 wt%, indicating a dominantly silicate mineralogy. Slight but systematic variations with depth are observed. SiO_2, Na_2O, CaO, and Sr increase in abundance downcore, whereas Al_2O_3 and Fe_2O_3 tend to decrease. K_2O/Al_2O_3 and Na_2O/Al_2O_3 also increase downhole. These trends may reflect a downcore increase in the silt-to-clay ratio in the muds, which is related to a fining-upward sequence in the levee sediment.

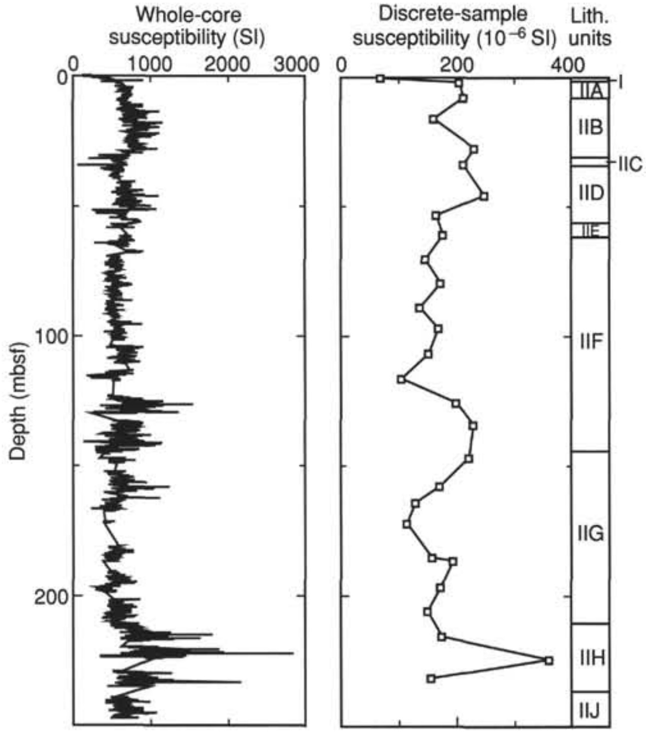

Figure 16. Whole-core and discrete-sample magnetic susceptibilities for Hole 940A.

PHYSICAL PROPERTIES

Index Properties

Index properties were measured on intact, predominantly clayey, sediment intervals of lithologic Unit II in Hole 940A (Table 11). Within the terrigenous silty clay of Unit II, water content decreases uniformly with depth from 57% near the seafloor to 23% at the base of Hole 940A (Fig. 20). A corresponding decrease in porosity from 78% to 44% also occurs over this interval. Water content decreases rapidly downhole to 34% at 25 mbsf. Between 25 and 39 mbsf, water content remains at approximately 34% with little change. Below 39 mbsf, water content decreases downhole with increasing scatter. Below 70 mbsf, the water content profile has two slight changes in trend, at gaps in core recovery at 120 and 180 mbsf. These trends may reflect differences in lithology, sediment fabric, or sedimentation rates. Selected samples taken from sand and sandy silt beds, particularly near the base of the hole, have water contents slightly less than the normal trend.

Grain density averages 2.75 g/cm^3 with most of the values between 2.7 and 2.8 g/cm^3 (Table 11). Grain density changes slightly downhole (Fig. 20) with an increase from 2.68 to 2.76 g/cm^3 at the top of the hole to about 2.72–2.82 g/cm^3 around 75 mbsf. Below 75 mbsf, it decreases to a minimum of 2.68–2.74 g/cm^3 at about 155 mbsf before increasing again. From 180 mbsf to the base of the hole, grain density decreases again from about 2.78 g/cm^3 to 2.68–2.72 g/cm^3. There is little difference between grain densities of sandy sediment and the adjacent clays (Fig. 20).

Downhole variation of wet-bulk density essentially matches the variation in water content (Fig. 20). From the top to the base of Hole 940A, wet-bulk density increases from approximately 1.5 to 2.0 g/cm^3. There are a few values at about 60 mbsf that are above the general trend and correlate with slump sediment of lithologic Subunit IIE and the underlying sediment at the top of Subunit IIF. The higher densities may also indicate a reduction in sedimentation rates at the top of Subunit IIF. The sandy sediment near the base of the hole has wet-bulk densities above the general trend.

Comparison of the discrete-sample wet-bulk densities with the GRAPE bulk density profile provides a qualitative measure of the expansion experienced by the cores. Unlike at previous Leg 155 sites, there are several intervals of good agreement between profiles. They agree well in the upper 25 m, between 40 and 45 mbsf, 133 and 140 mbsf, and 211 and 217 mbsf (Fig. 20). Outside these intervals, GRAPE densities vary between 0.1 and 0.4 g/cm^3 less than the discrete sample values.

Compressional-wave Velocity

Compressional-wave velocity measurements made with the PWL were restricted by gas expansion to the interval 0–24.7 mbsf in Hole 940A. The average transverse velocities range between 1460 and

Table 6. Gas concentrations in sediments from Site 940.

Core, section, interval (cm)	Depth (mbsf)	Sed. temp.* (°C)	Methane HS (ppm)	Methane VAC (ppm)
155-940A-				
2H-6, 0–5	10.30	2	3	261,057
3H-6, 0–5	19.80	3	3	179,369
4H-4, 0–5	29.30	3	36,974	633,510
5H-1, 115–120	32.45	3	8,384	47,330
6H-7, 0–5	49.80	4	7,343	105,723
7H-3, 0–5	52.41	4	9,036	
8H-6, 0–5	67.32	4	8,655	
9X-3, 0–5	72.30	4	8,827	477,836
10X-4, 0–5	83.00	5	7,584	38,506
11X-5, 0–5	90.67	5	10,937	122,518
12X-4, 0–5	100.30	5	10,008	66,979
13X-4, 0–5	108.28	5	9,096	
14X-2, 0–5	116.60	6	8,296	
15X-3, 0–5	127.80	6	9,419	
16X-5, 0–5	140.50	6	8,675	
17X-3, 0–5	145.60	7	7,926	
18X-3, 0–5	155.20	7	8,564	
19X-3, 0–5	164.90	7	8,354	
20X-1, 0–5	172.26	8	6,467	
21X-3, 0–5	184.10	8	9,554	
22X-2, 0–5	192.30	8	9,807	
23X-3, 0–5	203.03	8	10,091	
24X-5, 0–5	216.00	9	9,247	
25X-2, 0–5	221.20	9	10,767	
26X-3, 0–5	232.30	9	8,864	
27X-4, 0–5	243.50	10	13,650	

Notes: HS = headspace; VAC = vacutainer. Geothermal gradient = 29°C/km. Bottom-water temperature = 2°C. *See "In-situ Temperature Measurements" section, this chapter.

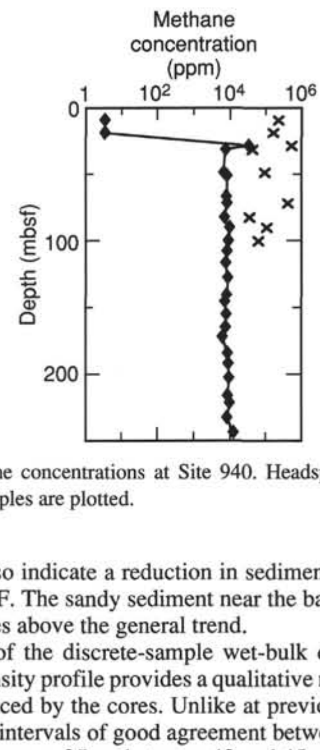

Figure 17. Methane concentrations at Site 940. Headspace (diamond) and vacutainer (×) samples are plotted.

Table 7. Elemental and organic carbon compositions of sediments from Site 940.

Core, section, interval (cm)	Depth (mbsf)	IC (%)	$CaCO_3$* (%)	TC (%)	TOC (%)	TN (%)	TS (%)	[C/N]a
155-940A-								
1H-1, 11–12	0.11	3.48	29.0	3.91	0.43	0.07	0.03	7
1H-1, 60–61	0.60	1.46	12.2	1.95	0.49	0.06	0.00	9
1H-2, 25–26	1.75	0.12	1.0	0.92	0.80	0.08	0.18	11
2H-4, 88–89	8.18	0.31	2.6	1.05	0.74	0.07	1.35	13
2H-4, 92–93	8.22	0.21	1.7	1.13	0.92	0.08	0.18	13
2H-6, 99–100	11.29	0.14	1.2	0.58	0.44	0.03	0.39	20
2H-6, 122–123	11.52	0.32	2.7	1.23	0.91	0.08	0.11	13
3H-4, 39–40	17.18	0.32	2.7	1.11	0.79	0.07	0.90	13
3H-6, 22–23	20.02	0.25	2.1	1.42	1.17	0.09	0.17	15
4H-4, 15–16	26.45	0.24	2.0	0.92	0.68	0.07	0.33	12
4H-4, 21–23	26.51	0.25	2.1	1.23	0.98	0.10	0.00	12
5H-1, 22–23	31.52	0.24	2.0	1.14	0.90	0.09	1.34	12
5H-1, 25–26	31.55	0.30	2.5	1.32	1.02	0.10	0.15	12
5H-5, 13–14	36.07	0.22	1.8	1.13	0.91	0.10	0.07	11
6H-4, 94–95	46.24	0.15	1.2	0.37	0.22	0.03	0.06	9
6H-4, 101–102	46.31	0.26	2.2	1.18	0.92	0.09	0.08	11
7H-2, 22–23	51.29	0.08	0.7	0.16	0.08	0.02	0.00	6
7H-4, 110–111	55.01	0.32	2.7	1.27	0.95	0.10	0.06	11
8H-3, 120–121	64.00	0.30	2.5	1.07	0.77	0.10	0.06	9
8H-6, 48–49	67.80	0.27	2.2	1.11	0.84	0.10	0.07	10
9X-3, 85–86	73.15	0.32	2.7	1.17	0.85	0.09	0.05	11
9X-5, 27–28	75.57	0.27	2.2	1.04	0.77	0.09	0.04	10
10X-4, 47–48	81.97	0.28	2.3	1.30	1.02	0.10	0.05	12
10X-5, 139–140	84.39	0.36	3.0	1.33	0.97	0.10	0.04	11
11X-2, 50–51	86.70	0.33	2.7	1.25	0.92	0.11	0.05	10
11X-5, 35–36	91.02	0.35	2.9	1.42	1.07	0.11	0.04	11
11X-6, 44–45	92.61	0.34	2.8	1.36	1.02	0.11	0.15	11
12X-2, 91–92	96.71	0.40	3.3	1.42	1.02	0.12	0.08	10
12X-4, 78–79	99.58	0.34	2.8	1.31	0.97	0.10	0.02	11
13X-2, 59–60	105.95	0.32	2.7	1.17	0.85	0.09	0.02	12
13X-5, 25–26	110.03	0.35	2.9	1.21	0.86	0.10	0.03	10
14X-3, 55–56	117.15	0.34	2.8	1.15	0.81	0.08	0.03	12
15X-3, 56–57	126.86	0.11	0.9	0.40	0.29	0.03	0.00	11
15X-3, 60–61	126.90	0.43	3.6	1.45	1.02	0.11	0.00	11
16X-2, 75–76	135.25	0.20	1.7	0.56	0.36	0.04	0.00	10
16X-4, 66–67	138.16	0.11	0.9	1.16	1.05	0.09	0.00	13
17X-4, 25–26	147.35	0.35	2.9	1.10	0.75	0.08	0.03	11
17X-4, 47–48	147.57	0.26	2.2	1.11	0.85	0.10	0.00	10
18X-2, 126–128	154.96	0.30	2.5	1.38	1.08	0.11	0.07	11
18X-4, 35–36	157.05	0.26	2.2	1.17	0.91	0.10	0.08	10
18X-4, 126–127	157.96	0.41	3.4	1.38	0.97	0.11	0.03	11
19X-3, 22–23	165.12	0.30	2.5	1.29	0.99	0.09	0.02	12
21X-3, 60–61	184.70	0.22	1.8	0.93	0.71	0.07	0.03	13
21X-3, 65–66	184.75	0.29	2.4	1.11	0.82	0.09	0.03	11
21X-4, 40–42	186.00	0.25	2.1	1.23	0.98	0.10	0.01	11
22X-4, 17–18	195.47	0.10	0.8	0.33	0.23	0.04	0.00	7
22X-4, 44–45	195.74	0.24	2.0	1.20	0.96	0.10	0.05	11
23X-4, 66–67	205.19	0.24	2.0	0.96	0.72	0.09	0.00	9
23X-7, 20–21	209.23	0.24	2.0	0.97	0.73	0.07	0.02	12
24X-4, 11–12	214.61	0.50	4.2	1.36	0.86	0.09	0.01	11
25X-3, 81–82	223.34	0.32	2.7	1.19	0.87	0.08	0.05	13
26X-4, 116–117	234.96	0.24	2.0	1.26	1.02	0.10	0.01	12
27X-4, 75–76	244.25	0.26	2.2	1.10	0.84	0.07	0.04	14
27X-5, 29–30	245.29	0.36	3.0	1.13	0.77	0.09	0.00	10

Note: * = calculated assuming all IC is calcite.

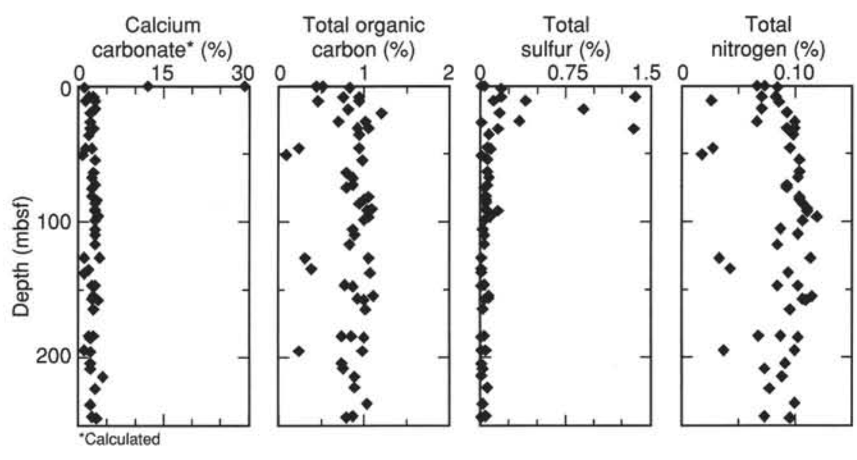

Figure 18. Concentration profiles of carbonate calculated as calcium carbonate, total organic carbon, total sulfur, and total nitrogen in Hole 940A.

Table 8. Interstitial water chemistry, Site 940.

Core, section, interval (cm)	Depth (mbsf)	Salinity	pH	Alkalinity (mM)	Cl^- (mM)	Mg^{2+} (mM)	Ca^{2+} (mM)	K^+ (mM)	HPO_4^{2-} (µM)	SO_4^{2-} (mM)	NH_4^+ (mM)	H_4SiO_4 (µM)	Na^+ (mM)	Fe^{2+} (µM)	Mn^{2+} (µM)
155-940A-															
1H-1, 145–150	1.45	35.0	7.47	14.51	552	48.0	8.9	11.6	78.2	19.2	0.6	357	479	30.2	10.2
2H-5, 145–150	10.25	35.0	7.40	20.11	554	46.9	8.5	10.1	91.9	15.0	1.5	434	482	40.2	10.0
3H-5, 145–150	19.75	34.5	7.50	25.30	556	45.0	7.7	9.4	122.8	11.4	2.2	427	487	29.3	8.4
4H-5, 145–150	29.25	34.0	7.60	32.82	557	42.2	5.6	8.3	131.6	0.2	4.4	405	482	42.8	6.4
5H-1, 125–130	32.55	32.5	7.62	21.62	557	41.3	4.8	7.9	71.8	1.9	4.5	446	478	46.5	5.6
8H-3, 140–150	64.20	32.5	7.26	6.11	560	41.6	4.4	7.1	2.3	0.8	5.9	320	463	95.8	4.8
11X-4, 140–150	90.57	33.0	7.36	10.18	562	41.1	3.5	6.5	5.0	0.7	7.0	403	471	109.7	4.0
14X-2, 140–150	116.50	33.0	7.50	11.28	563	39.0	3.4	7.1	4.0	0.5	7.1	272	477	17.1	2.8
17X-2, 140–150	145.50	33.0	7.44	10.99	565	40.0	3.8	6.6	4.0	0.5	7.5	388	475	23.8	4.0
21X-2, 140–150	184.00	33.0	7.52	12.22	564	40.3	4.1	6.8	9.0	1.2	5.6	396	478	63.9	4.0
24X-4, 140–150	215.90	33.5	7.57	11.21	565	41.4	4.7	7.6	7.5	5.3	7.4	284	479	34.2	3.6
27X-4, 140–150	244.90	33.0	7.36	11.48	564	40.2	4.6	7.5	9.0	3.5	5.5	394	480	111.7	5.2

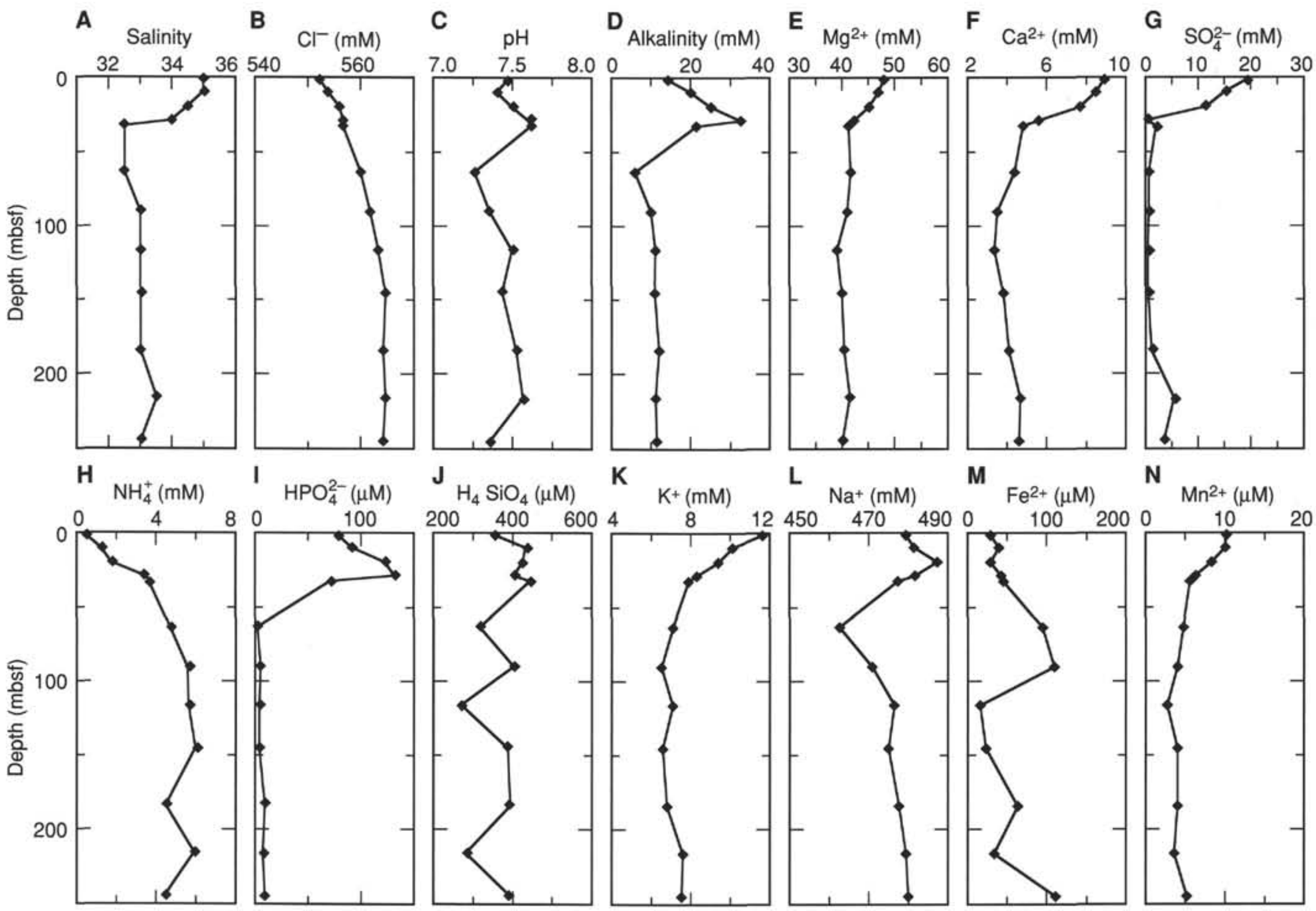

Figure 19. Downhole variation in pore-water chemistry. **A.** Salinity. **B.** Chloride. **C.** pH. **D.** Alkalinity. **E.** Magnesium. **F.** Calcium. **G.** Sulfate. **H.** Ammonium. **I.** Phosphate. **J.** Silica. **K.** Potassium. **L.** Sodium. **M.** Iron. **N.** Manganese.

1520 m/s. Longitudinal and transverse velocity measurements were made with the DSV between 2.40 and 24.18 mbsf (Table 12). Longitudinal velocities range from 1495 to 1570 m/s, and transverse velocities range from 1480 to 1580 m/s, generally showing isotropic behavior. There is good agreement between the PWL and DSV results (Fig. 21).

Shear Strength

Measurements of undrained shear strength were made using the motorized shear vane on all cores from Hole 940A (Table 13). Below 65 mbsf, compressive strengths were determined using a pocket penetrometer.

Hole 940A (Fig. 22) exhibits a general increase in shear strength downhole, and the profile can be divided into four parts. There is a relatively uniform increase in undrained shear strength from 6 kPa just below the seafloor to 32 kPa at 24 mbsf. Between 24 and 32 mbsf there is an overall reduction in shear strength of about a third, from 32 to 20 kPa. Below 32 mbsf, strengths increase in the range 17 to 52 kPa to 58 mbsf. From 60 mbsf to the base of the hole there is a general increase in shear strength but also a wide scatter of values. Correlation of shear strength estimated from compressive strength and that determined by the lab vane is generally poor between 85 and 120 mbsf and between 180 and the base of the hole (Fig. 22). Values estimated from the compressive strength generally exceed those measured by the lab vane.

Table 9. Major element composition (wt%) of sediment samples, Site 940.

Core, section, interval (cm)	Depth (mbsf)	Lithology	SiO_2	TiO_2	Al_2O_3	Fe_2O_3	MnO	MgO	CaO	Na_2O	K_2O	P_2O_5	Total	LOI
155-940A-														
2H-6, 111–114	11.41	Mud	62.72	1.04	21.39	7.57	0.13	2.01	0.73	1.31	2.94	0.18	100.03	8.02
7H-4, 112–115	55.03	Mud	62.34	1.05	21.66	8.03	0.14	2.08	0.74	1.46	2.91	0.19	100.59	7.70
9X-5, 31–36	75.61	Mud	61.11	1.08	22.46	7.82	0.12	2.09	0.64	1.44	3.12	0.18	100.06	9.37
11X-5, 36–38	91.03	Mud	62.64	1.05	21.36	7.81	0.11	2.06	0.73	1.54	3.00	0.22	100.51	9.34
13X-5, 19–22	109.97	Mud	62.69	1.03	20.80	7.49	0.12	2.09	0.79	1.57	2.99	0.20	99.78	8.24
16X-4, 68–71	138.18	Mud	65.25	1.02	19.25	7.02	0.11	1.92	0.82	1.47	2.81	0.22	99.88	8.49
17X-4, 48–54	147.58	Mud	64.21	1.05	19.78	7.16	0.12	1.98	0.80	1.40	2.87	0.18	99.56	8.03
21X-4, 40–45	186.00	Mud	63.76	1.08	20.55	7.28	0.11	2.06	0.86	1.44	2.98	0.20	100.33	7.94
25X-3, 77–80	223.30	Mud	66.73	0.99	18.18	6.44	0.10	1.90	0.96	1.61	2.81	0.18	99.90	6.67
27X-5, 25–28	245.25	Mud	65.15	1.02	19.22	6.74	0.10	1.94	0.89	1.51	2.92	0.17	99.65	6.53

Notes: Total iron is reported as Fe_2O_3. LOI = loss on ignition.

Table 10. Trace element composition (ppm) of sediment samples, Site 940.

Core, section, interval (cm)	Depth (mbsf)	Lithology	Ba	Ce	Cr	Cu	Nb	Ni	Rb	Sr	V	Y	Zn	Zr
155-940A-														
2H-6, 111–114	11.41	Mud	453	103	63	30	20	32	126	139	83	39	121	227
7H-4, 112–115	55.03	Mud	477	109	66	32	21	35	126	144	85	40	121	231
9X-5, 31–36	75.61	Mud	509	105	66	33	21	35	137	139	79	37	126	213
11X-5, 36–38	91.03	Mud	491	109	64	32	21	35	129	146	84	39	121	231
13X-5, 19–22	109.97	Mud	483	107	64	31	20	34	129	148	76	39	121	228
16X-4, 68–71	138.18	Mud	467	96	58	27	20	30	121	148	70	40	111	262
17X-4, 48–54	147.58	Mud	487	103	62	30	21	32	125	150	78	40	117	262
21X-4, 40–45	186.00	Mud	504	104	63	32	21	32	130	154	82	39	119	251
25X-3, 77–80	223.30	Mud	495	91	56	26	20	29	120	165	71	39	106	283
27X-5, 25–28	245.25	Mud	491	95	60	28	20	30	128	160	82	38	114	276

The residual undrained shear strength also increases downhole (Table 13), but at a lower rate than the peak strength, resulting in a slight downhole decrease in the ratio of residual to peak undrained shear strength. At 60 mbsf, there is a break of uncertain origin in the strength ratio profile.

Resistivity

Longitudinal resistivity displays a general downhole increase (Table 14; Fig. 23) that reflects the downhole decrease in porosity. Resistivity increases from 0.20 Ωm near the seafloor to 0.43 Ωm at the base of Hole 940A. There is a distinct increase above the background trend between 24 and 32 mbsf. Below 24 mbsf, resistivity values increase by about a third above the general trend to reach a peak at 30 mbsf before decreasing to the normal trend at 32 mbsf. Such a change could be due to a significant increase in the tortuosity of the sediment, which would be expected to correlate with a decrease in porosity or a change in the electrical conductivity of the pore fluids. Porosity values are very nearly constant within this interval, and there is a significant salinity decrease (Fig. 19).

Comparison of longitudinal and transverse resistivities indicates that the sediment is slightly anisotropic (Fig. 23). There are slight variations with lithology, but they are not as distinct as those at previous Amazon Fan sites. Changes in the degree of scatter of anisotropy values occur at 120 and 180 mbsf, similar depths in the hole to those noted in the correlation of shear strength determined by lab vane and estimated from compression strength.

DOWNHOLE LOGGING

Logging Operations and Quality of Logs

After drilling and coring were completed, sepiolite mud mixed with seawater was circulated in the hole to remove debris from the borehole. The base of the bottom-hole assembly (BHA) was raised to 93 mbsf and subsequently returned to the total drilled depth (TD) drilled (248.6 mbsf) to ream borehole irregularities. No fill was encountered at TD. The base of the BHA again was raised to 93 mbsf, and the drill string assembled so that we could raise the BHA an additional 21 m during the upgoing logging runs.

The Quad-combination and Formation MicroScanner (FMS) tool strings reached a maximum depth of 234 mbsf and obtained useful logs between 233 and 75 mbsf (Table 15). The density (HLDT) tool caliper showed a large cavity near the base of the borehole, between 218 and 230 mbsf, where cores indicate a high proportion of silt and sand. The quality of the logging data in this interval has been degraded, and the density data are particularly affected because the tool did not remain in contact with the borehole wall. Otherwise, the HLDT caliper log shows that the borehole had a generally constant diameter of 14.5 to 15.5 in. (37–40 cm). This diameter was noticeably larger than in the previously logged holes at Sites 931, 933, 935, and 936, probably a result of the larger 11.44-in. (29-cm) diameter bit used at this site instead of the 10.125-in. (25.7-cm) PDC bit used at the rest of Leg 155 drill sites.

Most of the borehole was logged by only two or three of the FMS pads. Because the FMS tool was inclined in the deviated borehole, it is possible that the tilted tool's weight may have partially collapsed the "downside" caliper pad springs, resulting in poor contact with the "upside" pad with the borehole. Two FMS passes were made with different gain settings.

Results

The logged interval covered lithostratigraphic Subunits IIF, IIG, and IIH (Fig. 24). Within Subunit IIF, velocity and density increase almost linearly from 75 to 100 mbsf. The abnormally low density from 89 to 92 mbsf may have been caused by poor tool contact within this washed-out interval. Between 100 and 120 mbsf, velocity data display large oscillations, with a downhole linear increase similar to that in Subunit IIF, whereas density increases only slightly. Velocity, density, resistivity, and gamma-ray values are distinctly lower between 124 and 134 mbsf and may have been affected by an increase

Table 11. Index properties at Site 940.

Core, section, interval (cm)	Depth (mbsf)	Water content (%)	Wet-bulk density (g/cm^3)	Grain density (g/cm^3)	Dry-bulk density (g/cm^3)	Porosity (%)	Void ratio
155-940A-							
1H-1, 67–69	0.67	56.5	1.47	2.79	0.62	78.0	3.54
1H-2, 89–91	2.39	50.2	1.52	2.71	0.74	72.7	2.67
2H-1, 59–61	3.39	44.9	1.58	2.70	0.86	68.3	2.15
2H-2, 79–81	5.09	43.3	1.62	2.69	0.90	66.7	2.01
2H-3, 94–96	6.74	41.7	1.65	2.76	0.94	65.8	1.92
2H-4, 77–79	8.07	41.6	1.63	2.76	0.94	65.7	1.92
2H-5, 110–112	9.90	42.0	1.63	2.69	0.93	65.5	1.90
2H-6, 79–81	11.09	39.9	1.68	2.68	0.98	63.5	1.74
2H-7, 9–11	11.89	40.0	1.67	2.67	0.98	63.5	1.74
3H-1, 71–73	13.01	38.0	1.71	2.71	1.03	61.8	1.62
3H-2, 117–119	14.97	39.0	1.70	2.76	1.01	63.2	1.72
3H-3, 142–144	16.72	37.1	1.72	2.70	1.06	60.8	1.55
3H-4, 40–42	17.20	36.9	1.73	2.73	1.07	60.8	1.55
3H-5, 15–17	18.45	33.3	1.79	2.69	1.17	56.7	1.31
3H-6, 67–69	20.47	35.4	1.76	2.81	1.12	60.0	1.50
4H-1, 116–118	22.96	34.8	1.76	2.70	1.12	58.4	1.41
4H-2, 87–89	24.17	34.7	1.78	2.75	1.13	58.9	1.43
4H-3, 38–40	25.18	34.4	1.77	2.72	1.14	58.2	1.39
4H-4, 67–69	26.97	34.1	1.79	2.76	1.15	58.2	1.39
4H-5, 76–78	28.56	32.6	1.80	2.69	1.19	56.0	1.27
4H-6, 84–86	30.14	33.6	1.80	2.74	1.17	57.4	1.35
4H-7, 43–45	31.23	33.5	1.78	2.72	1.16	57.2	1.34
5H-1, 96–98	32.26	34.3	1.77	2.74	1.14	58.3	1.40
5H-2, 87–89	33.47	34.6	1.78	2.78	1.14	58.9	1.44
5H-3, 19–21	34.29	34.0	1.77	2.70	1.15	57.6	1.36
5H-4, 9–11	35.23	33.3	1.80	2.72	1.17	57.0	1.32
5H-5, 58–60	36.52	33.2	1.79	2.73	1.18	56.9	1.32
5H-6, 47–49	37.20	33.4	1.80	2.80	1.18	57.8	1.37
5H-7, 80–82	39.00	33.5	1.79	2.76	1.17	57.5	1.36
6H-1, 67–69	41.47	31.9	1.82	2.72	1.21	55.4	1.24
6H-2, 72–74	43.02	32.0	1.81	2.71	1.21	55.4	1.24
6H-3, 69–71	44.49	31.9	1.81	2.72	1.21	55.4	1.24
6H-4, 87–89	46.17	32.9	1.83	2.79	1.20	57.2	1.34
6H-5, 82–84	47.62	31.5	1.84	2.74	1.23	55.1	1.23
6H-6, 82–84	49.12	32.8	1.81	2.71	1.18	56.4	1.29
6H-7, 53–55	50.33	34.1	1.80	2.76	1.15	58.2	1.39
7H-2, 18–20	51.25	32.4	1.81	2.70	1.19	55.9	1.27
7H-3, 17–19	52.58	33.3	1.81	2.71	1.17	56.8	1.32
7H-4, 39–41	54.30	31.6	1.83	2.72	1.22	55.0	1.23
7H-5, 63–65	55.97	30.9	1.86	2.75	1.25	54.6	1.20
7H-6, 76–78	57.60	29.7	1.89	2.78	1.30	53.4	1.15
8H-1, 96–98	60.76	30.2	1.88	2.77	1.28	53.9	1.17
8H-2, 94–96	62.24	30.3	1.88	2.72	1.26	53.6	1.16
8H-3, 91–93	63.71	30.8	1.85	2.75	1.25	54.4	1.20
8H-4, 49–51	64.79	30.8	1.87	2.82	1.27	55.1	1.23
9X-1, 119–121	70.49	32.2	1.84	2.78	1.22	56.3	1.29
9X-2, 93–95	71.73	31.9	1.83	2.72	1.21	55.4	1.24
9X-3, 93–95	73.23	32.0	1.83	2.75	1.22	55.8	1.26
9X-4, 93–95	74.73	30.9	1.86	2.82	1.26	55.2	1.23
9X-5, 93–95	76.23	31.9	1.84	2.78	1.22	56.0	1.27
10X-1, 96–98	77.96	32.2	1.84	2.80	1.22	56.5	1.30
10X-2, 96–98	79.46	30.9	1.85	2.70	1.24	54.1	1.18
10X-3, 96–98	80.96	31.0	1.87	2.73	1.24	54.4	1.20
10X-4, 96–98	82.46	30.7	1.88	2.76	1.26	54.4	1.19
10X-5, 96–98	83.96	30.3	1.85	2.73	1.26	53.7	1.16
11X-1, 85–87	85.55	31.7	1.86	2.76	1.23	55.5	1.25
11X-2, 85–87	87.05	32.4	1.82	2.75	1.20	56.2	1.28
11X-3, 83–85	88.50	30.2	1.88	2.72	1.27	53.5	1.15
11X-4, 81–83	89.98	30.6	1.86	2.74	1.26	54.1	1.18
11X-5, 85–87	91.52	29.8	1.90	2.77	1.29	53.4	1.15
11X-6, 87–89	93.04	29.2	1.91	2.77	1.31	52.7	1.11
12X-1, 64–66	94.94	31.5	1.86	2.77	1.24	55.4	1.24
12X-2, 64–66	96.44	28.8	1.89	2.67	1.30	51.4	1.06
12X-3, 64–66	97.94	29.2	1.87	2.68	1.29	51.9	1.08
12X-4, 64–66	99.44	30.7	1.85	2.67	1.24	53.6	1.15
12X-5, 44–46	100.74	29.5	1.89	2.75	1.30	53.0	1.13
12X-6, 7–9	101.81	29.8	1.89	2.72	1.28	52.9	1.12
13X-1, 84–86	104.74	29.0	1.92	2.72	1.31	52.0	1.08
13X-2, 100–102	106.36	31.4	1.86	2.73	1.23	54.9	1.22
13X-3, 99–101	107.77	31.1	1.87	2.75	1.24	54.8	1.21
13X-4, 59–61	108.87	27.6	1.94	2.71	1.35	50.1	1.00
13X-5, 59–61	110.37	30.5	1.88	2.72	1.26	53.8	1.17
14X-1, 146–148	115.06	29.8	1.88	2.71	1.28	53.0	1.13
14X-2, 80–82	115.90	28.7	1.92	2.73	1.32	51.7	1.07
14X-3, 82–84	117.42	29.3	1.92	2.77	1.31	52.8	1.12
15X-1, 103–105	124.33	28.3	1.91	2.69	1.32	50.9	1.04
15X-2, 104–106	125.84	25.7	1.98	2.74	1.42	48.1	0.93
15X-3, 34–36	126.64	27.7	1.92	2.70	1.35	50.3	1.01
15X-4, 124–126	129.04	27.3	1.93	2.68	1.35	49.6	0.98
15X-5, 49–51	129.79	26.5	1.96	2.75	1.40	49.2	0.97
16X-1, 92–94	133.92	27.7	1.93	2.74	1.36	50.6	1.02
16X-2, 104–106	135.54	28.7	1.89	2.70	1.31	51.5	1.06
16X-3, 117–119	137.17	28.9	1.90	2.68	1.30	51.5	1.06
16X-4, 89–91	138.39	26.7	1.93	2.70	1.38	49.0	0.96
16X-5, 109–111	140.09	27.1	1.94	2.76	1.38	50.1	1.00
16X-6, 105–107	141.55	25.5	1.98	2.75	1.44	47.8	0.92
16X-7, 45–47	142.45	27.1	1.98	2.75	1.38	50.0	1.00

Table 11 (continued).

Core, section, interval (cm)	Depth (mbsf)	Water content (%)	Wet-bulk density (g/cm^3)	Grain density (g/cm^3)	Dry-bulk density (g/cm^3)	Porosity (%)	Void ratio
17X-1, 72–74	143.32	27.6	1.95	2.77	1.36	50.8	1.03
17X-2, 96–98	145.06	27.7	1.93	2.71	1.35	50.4	1.02
17X-3, 97–99	146.57	27.4	1.92	2.70	1.35	49.8	0.99
17X-4, 100–102	148.10	27.5	1.92	2.68	1.35	49.7	0.99
17X-5, 55–57	149.15	27.4	1.95	2.70	1.35	49.8	0.99
18X-1, 25–27	152.45	28.0	1.91	2.71	1.33	50.8	1.03
18X-2, 75–77	154.45	27.1	1.92	2.71	1.37	49.6	0.99
18X-3, 102–104	156.22	27.5	1.93	2.72	1.36	50.1	1.00
18X-4, 48–50	157.18	26.8	1.95	2.71	1.38	49.3	0.97
18X-5, 65–67	158.85	26.6	1.95	2.69	1.38	48.8	0.95
18X-6, 42–44	160.12	25.4	2.00	2.74	1.44	47.6	0.91
19X-1, 67–69	162.57	25.5	2.00	2.81	1.45	48.4	0.94
19X-2, 66–68	164.06	26.8	1.95	2.71	1.38	49.1	0.97
19X-3, 83–85	165.73	28.0	1.93	2.77	1.35	51.3	1.05
19X-4, 54–56	166.94	28.0	1.95	2.76	1.35	51.2	1.05
21X-1, 82–84	181.92	27.8	1.93	2.79	1.36	51.2	1.05
21X-2, 82–84	183.42	24.8	2.01	2.78	1.47	47.3	0.90
21X-3, 82–84	184.92	24.4	2.00	2.78	1.48	46.8	0.88
21X-4, 82–84	186.42	25.8	1.97	2.77	1.43	48.4	0.94
22X-1, 84–86	191.64	25.5	1.97	2.78	1.44	48.2	0.93
22X-2, 84–86	193.14	26.3	1.95	2.77	1.41	49.0	0.96
22X-3, 67–69	194.47	24.5	2.00	2.78	1.48	46.8	0.88
22X-4, 106–108	196.36	26.0	1.95	2.72	1.41	48.3	0.93
22X-5, 104–106	197.84	25.7	1.97	2.73	1.42	47.9	0.92
22X-6, 34–36	198.64	25.7	1.99	2.78	1.43	48.4	0.94
23X-2, 63–65	202.16	24.6	1.99	2.73	1.46	46.5	0.87
23X-3, 49–51	203.52	25.8	1.95	2.74	1.42	48.2	0.93
23X-4, 49–51	205.02	25.1	1.98	2.72	1.44	47.1	0.89
23X-5, 46–48	206.49	25.1	1.98	2.72	1.44	47.0	0.89
23X-6, 37–39	207.90	25.8	1.97	2.72	1.41	48.0	0.92
23X-7, 34–36	209.37	23.0	2.05	2.74	1.52	44.3	0.80
24X-1, 72–74	210.72	27.9	1.91	2.72	1.34	50.7	1.03
24X-2, 84–86	212.34	26.5	1.97	2.79	1.41	49.6	0.98
24X-3, 71–73	213.71	25.7	1.96	2.73	1.42	47.9	0.92
24X-4, 43–45	214.93	24.6	1.99	2.76	1.47	46.7	0.88
24X-5, 49–51	216.49	26.6	1.95	2.73	1.39	49.0	0.96
24X-5, 70–72	216.70	21.9	2.07	2.76	1.57	43.1	0.76
25X-1, 66–68	220.36	26.7	1.95	2.74	1.39	49.3	0.97
25X-2, 9–11	221.29	25.9	1.98	2.78	1.43	48.8	0.95
25X-3, 131–133	223.84	23.0	2.05	2.79	1.54	44.8	0.81
26X-1, 79–81	230.09	26.3	1.95	2.72	1.40	48.7	0.95
26X-1, 87–89	230.17	25.8	1.96	2.76	1.43	48.3	0.94
26X-2, 88–90	231.68	27.2	1.93	2.72	1.37	49.8	0.99
26X-3, 79–81	233.09	24.8	2.00	2.72	1.45	46.7	0.88
26X-4, 47–49	234.27	27.7	1.95	2.78	1.36	51.0	1.04
26X-5, 47–49	235.77	22.4	2.04	2.74	1.55	43.5	0.77
26X-5, 59–61	235.89	25.6	1.97	2.72	1.42	47.8	0.91
27X-1, 99–101	239.99	23.6	2.01	2.76	1.51	45.5	0.83
27X-2, 84–86	241.34	23.8	2.01	2.69	1.48	45.1	0.82
27X-3, 58–60	242.58	23.3	2.01	2.72	1.50	44.7	0.81
27X-4, 78–80	244.28	24.2	1.99	2.69	1.47	45.6	0.84
27X-5, 69–71	245.69	24.3	1.99	2.70	1.46	45.9	0.85
27X-6, 68–70	247.10	23.5	2.01	2.69	1.49	44.6	0.81
27X-CC, 2–4	247.51	22.9	2.02	2.68	1.51	43.8	0.78

in borehole diameter. Poor borehole conditions may also be related to the presence of more silty sand beds in this interval (Figs. 24 and 25A).

Density and velocity values indicate an overall increase downhole between 150 and 200 mbsf, with small-scale variations that may be related to cyclic depositional events characterized by changes in grain size and bed thickness. Below 200 mbsf, a gradual decrease downhole in gamma-ray, resistivity, velocity, and density values, with an accompanying increase in porosity, coincide with a downhole increase in sand at the base of Subunit IIG and the upper part of Subunit IIH. A highly porous and unconsolidated sandy formation is probably responsible for these trends and the associated borehole irregularities below ~210 mbsf.

Apparent Depositional Cycles from Logs

Subtle changes in gamma-ray counts and resistivity values apparently represent depositional cycles on the order of a few to tens of meters thick (Figs. 25A and 25B).Changes in gamma-ray and resistivity data appear to correspond primarily to downhole variations in clay content.

Resistivity is nearly constant between 75 and 110 mbsf (~1.4 Ωm; Fig. 25A). Two intervals of upward decreasing gamma ray can be identified between 72 and 85 mbsf, within Subunit IIF; these correspond to an overall increase in the frequency of silt beds. Below 85 mbsf, two intervals have an overall upward increase in gamma ray that corresponds to thinning-upward intervals in the cores. A zone of no core recovery between 112 and 115 mbsf exhibits a sharp decrease in gamma-ray and resistivity values and may indicate the presence of thicker silt and possibly sand beds.

The interval between 125 and 132 mbsf is characterized by low gamma-ray and resistivity values. An interval of no recovery from 130 to 132 mbsf was interpreted from the log character to be a relatively thick silt to sandy silt interval that marks a change from a fining-upward to a coarsening-upward interval near the base of Subunit IIF. An abrupt increase in gamma-ray and resistivity values below 140 mbsf corresponds to the upper part of a deformed, mud-rich interval that apparently marks the top of a fining-upward interval between 140 and 160 mbsf. The interval of poor core recovery between 168 and 181 mbsf has high resistivity, which, based on an analogy to the interval between 140 to 142 mbsf, has been interpreted to be rich in mud.

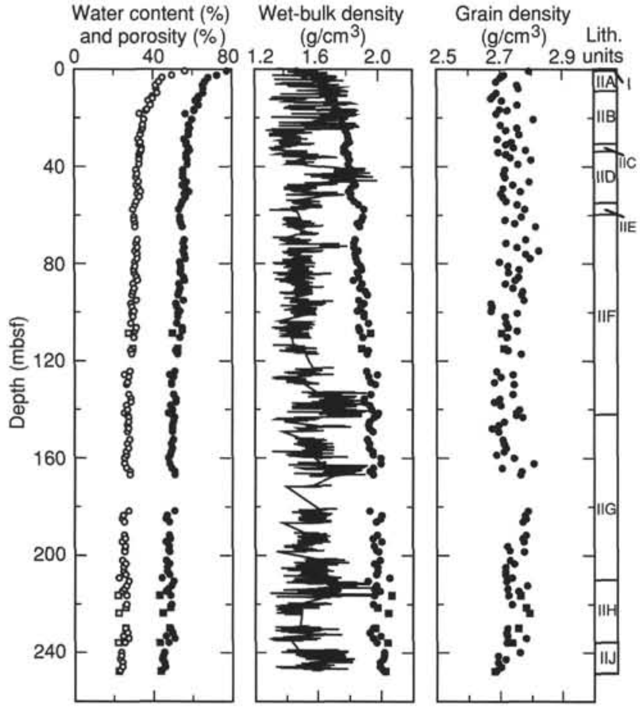

Figure 20. Water content (open symbols) and porosity (solid symbols), wet-bulk density, and grain density as determined for discrete samples and by the GRAPE (line) in Hole 940A. Circles = clayey sediment; squares = sand and sandy silt.

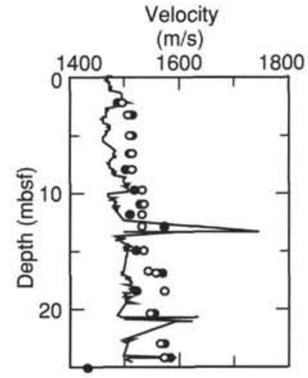

Figure 21. Uncorrected compressional-wave velocity determined by the PWL (line) and the DSV, longitudinal (open circles) and transverse (solid circles) in Hole 940A.

The abrupt decrease in resistivity below 209 mbsf corresponds to the boundary between Subunits IIG and IIH (Fig. 25B). Resistivity also abruptly decreases below 215 mbsf, where sand beds become more frequent. The downhole decrease in resistivity within Subunit IIH correlates with an overall fining-upward trend that was observed in the cores. Low recovery at 226 to 228 mbsf also corresponds to a low resistivity interval, suggesting the presence of silt and sand beds.

Borehole Characteristics from the FMS Tool String

The borehole deviates toward the south (180°) from 5° at the top to 7° near the base of the logged interval. The borehole was elliptical, with a ratio of 1.2 through most of the logged interval, except between 110 and 140 mbsf, where it was nearly circular, despite irregular, small, washed-out intervals (Fig. 26A). The orientation of the long axis of the ellipse was approximately 180°, similar to the direction of borehole deviation. It is thought that the long-axis caliper measurement is less than the actual borehole diameter, as the maximum diameter measured by the FMS caliper was only about 13 in. (33 cm). This is less than the maximum aperture of the tool (15 in. or 38 cm), and less than the borehole diameter measured by the HLDT caliper (up to 15.5 in. or 40 cm; Fig. 24). Because the HLDT caliper generally measures the largest dimension of the borehole, it is possible that ellipticity may have been as high as 1.3. The apparent borehole diameter was more even where measured by the long-axis caliper (C1 in the first run), in comparison to the short-axis caliper (C2) (Fig. 26A). The reason for this is unclear, but may be related to the calipers not extending completely.

Table 12. DSV compressional-wave velocity at Site 940.

Core, section, interval (cm)	Depth (mbsf)	Longitudinal velocity (m/s)	Transverse velocity (m/s)
155-940A-			
1H-2, 86–94	2.40	1495	1488
2H-1, 56–64	3.40	1507	1513
2H-2, 76–84	5.10	1510	1514
2H-3, 91–99	6.75	1513	1508
2H-4, 74–82	8.08	1515	1502
2H-5, 107–115	9.91	1530	1516
2H-6, 76–84	11.10	1535	1528
2H-7, 6–14	11.90	1530	1511
3H-1, 68–76	13.02	1530	1574
3H-2, 114–122	14.98	1535	1522
3H-3, 139–147	16.73	1543	
3H-4, 17–25	17.01	1556	1568
3H-5, 12–20	18.46	1574	1519
3H-6, 64–72	20.48	1546	1552
4H-1, 113–121	22.97	1566	1574
4H-2, 84–92	24.18	1571	1584
4H-3, 35–43	25.19	1433	1149

The orientation of the elliptical borehole at this site, in comparison to the fan morphology, indicates that the long axis of the ellipse (N0°–20°E) is aligned in the same direction as the local topographic gradient, which is about N20°E. This contrasts with other sites (e.g., Sites 935 and 936), where the long axis was perpendicular to the topographic gradient. However, the long axis at this site is oriented approximately parallel to the path of the older Aqua Channel. Detailed comparison of borehole shape and fan topography, may be useful for investigating horizontal stress variations on the fan.

Borehole Temperature

Borehole temperatures were measured with the TLT approximately 6 hr after seawater was circulated in the borehole. A downhole temperature increase was observed in both the upgoing and downgoing runs, from 3°C at the mud line (3.5°C for the upgoing run), to 4.5°C at 205 mbsf (Fig. 27). Below 205 mbsf, temperature decreased downhole to 4.3°C during the first run, then increased to 4.5°C while the tool remained at the bottom of the hole. The upgoing run shows the same general characteristics of the downgoing run, except that temperature remains nearly constant between TD and 180 mbsf and was about 0.5°C warmer for most of the upgoing run.

As in previous sites, the downhole temperature gradient indicated by the TLT (~6°C/km) is much lower than that suggested by the ADARA measurements (29°C/km at this site). Anomalously abrupt increases of up to ~0.2°C occur at 10–15 and 40–50 (inside drill pipe, both runs), 100–110 (upgoing run), 120 (upgoing run), 135–140 (both runs), and 170–180 mbsf (both runs). The consistent measurement of temperature anomalies at the same depth during both upgoing and downgoing runs suggests that it is unlikely that these were related to malfunctioning of the tool and may indicate a complex relationship between variations in formation temperature and circulation of seawater in the borehole.

Table 13. Strength measurements at Site 940.

Core, section, interval (cm)	Depth (mbsf)	Peak undrained shear strength (kPa)	Residual undrained shear strength (kPa)	Unconfined compressive strength* (kPa)
155-940A-				
1H-1, 68	0.68	6.1	4.5	
1H-2, 90	2.40	4.6	3.4	
2H-1, 60	3.40	6.9	4.7	
2H-2, 80	5.10	6.8	4.9	
2H-3, 95	6.75	7.7	5.0	
2H-4, 78	8.08	9.6	7.5	
2H-5, 111	9.91	10.2	7.9	
2H-6, 80	11.10	12.4	8.6	
2H-7, 10	11.90	14.2	9.2	
3H-1, 72	13.02	16.4	10.5	
3H-2, 118	14.98	23.0	13.0	
3H-3, 143	16.73	21.2	14.7	
3H-4, 41	17.21	22.3	15.0	
3H-5, 16	18.46	21.2	14.1	
3H-6, 68	20.48	22.6	14.6	
4H-1, 117	22.97	26.9	16.8	
4H-2, 88	24.18	31.7	20.2	
4H-3, 39	25.19	26.0	16.6	
4H-4, 68	26.98	27.2	14.9	
4H-5, 77	28.57	21.8	12.8	
4H-6, 85	30.15	22.6	13.6	
4H-7, 44	31.24	21.5	13.9	
5H-1, 97	32.27	19.8	13.6	
5H-2, 88	33.48	22.1	14.3	
5H-3, 20	34.30	23.8	15.8	
5H-4, 10	35.24	24.9	15.2	
5H-5, 59	36.53	27.2	17.6	
5H-6, 48	37.21	17.0	11.5	
5H-7, 81	39.01	20.7	14.0	
6H-1, 68	41.48	30.8	18.0	
6H-2, 73	43.03	28.3	18.0	
6H-3, 74	44.54	37.1	20.6	
6H-4, 88	46.18	31.7	17.4	
6H-5, 83	47.63	30.0	17.9	
6H-6, 83	49.13	20.7	10.8	
6H-7, 54	50.34	21.8	10.8	
7H-2, 19	51.26	38.1	24.9	112.8
7H-3, 18	52.59	46.8	26.2	122.6
7H-4, 40	54.31	52.5	30.1	117.7
7H-5, 64	55.98	51.9	30.0	127.5
7H-6, 77	57.61	41.7	23.8	107.9
8H-1, 97	60.77	32.4	20.9	103.0
8H-2, 97	62.27	28.3	19.0	93.2
8H-3, 92	63.72	33.4	23.2	93.2
8H-4, 50	64.80	37.0	24.8	112.8
9X-1, 120	70.50	20.6	15.6	54.0
9X-2, 94	71.74	26.7	18.7	73.6
9X-3, 94	73.24	31.9	22.3	93.2
9X-4, 94	74.74	34.5	23.5	93.2
9X-5, 94	76.24	23.7	17.1	68.7
10X-1, 97	77.97	32.9	22.1	78.5
10X-2, 97	80.97	29.8	21.8	107.9
10X-3, 97	82.47	33.9	22.5	83.4
10X-4, 97	83.97	24.2	18.0	122.6
10X-5, 97	83.97	49.4	29.9	132.4
11X-1, 86	85.56	28.3	20.5	73.6
11X-2, 86	87.06	24.7	18.3	73.6
11X-3, 84	88.51	32.9	23.1	93.2
11X-4, 82	89.99	44.7	28.6	147.2
11X-5, 86	91.53	48.9	30.6	132.4
11X-6, 88	93.05	42.7	27.6	127.5
12X-1, 65	94.95	26.7	19.7	63.8
12X-2, 65	96.45	39.1	24.7	147.2
12X-3, 65	97.95	42.7	30.9	122.6
12X-4, 65	99.45	41.1	27.3	107.9
12X-5, 45	100.75	52.5	31.4	137.3
12X-6, 8	101.82	50.9	29.2	142.2
13X-1, 85	104.75	33.4		132.4
13X-2, 101	106.28			68.7
13X-3, 100	107.78	25.7	18.6	78.5
13X-5, 60	110.38	39.1	25.7	127.5
14X-2, 81	115.91	31.9		103.0
14X-3, 83	117.43	40.1	27.6	122.6
15X-1, 104	124.34	44.2	27.3	98.1
15X-2, 105	125.85	52.5	33.4	98.1
15X-3, 35	126.65	35.5	23.6	98.1
15X-4, 125	129.05	35.5	24.2	88.3
15X-5, 50	129.80	66.3	36.5	196.2
16X-1, 93	133.93	37.5	24.6	98.1
16X-2, 105	135.55	35.0	25.7	73.6
16X-3, 118	137.18	30.3	20.0	68.7
16X-4, 90	138.40	41.7	27.2	117.7
16X-5, 110	140.10	26.2	14.6	73.6
16X-6, 106	141.56	39.1	24.8	107.9
16X-7, 46	142.46	47.3	29.6	127.5
17X-1, 73	143.33	36.0	24.2	83.4
17X-2, 97	145.07	55.5	31.4	103.0
17X-3, 98	146.58	65.3	34.3	132.4
17X-4, 101	148.11	39.6	23.9	88.3
17X-5, 56	149.16	61.7	31.9	127.5
18X-1, 26	152.46	54.5	27.6	107.9
18X-2, 76	154.46	51.9	30.0	117.7
18X-3, 103	156.23	55.5	27.9	103.0
18X-4, 49	157.19	62.2	37.3	147.2
18X-5, 66	158.86	49.9	32.8	112.8
18X-6, 43	160.13	87.4	42.8	147.2
19X-1, 68	162.58	89.0	46.8	206.0
19X-2, 67	164.07	44.2	27.3	68.7
19X-3, 84	165.74	44.7	25.2	107.9
19X-4, 55	166.95	46.8	26.2	78.5
21X-1, 83	181.93	47.8	29.5	112.8
21X-2, 83	183.43	67.4	38.4	171.7
21X-3, 83	184.93	55.0	34.6	161.9
21X-4, 83	186.43	63.8	37.2	196.2
22X-1, 85	191.65	47.3	28.6	98.1
22X-2, 85	193.15	48.3	29.5	147.2
22X-3, 68	194.48	79.2	42.9	220.7
22X-4, 107	196.37	50.4	28.6	157.0
22X-5, 105	197.85	53.0	31.3	132.4
22X-6, 35	198.65	58.1	34.3	176.6
23X-2, 63	202.16	70.5	39.8	210.9
23X-3, 50	203.53	65.3	37.7	176.6
23X-4, 51	205.04	81.3	44.6	166.8
23X-5, 48	206.51	61.2	37.3	196.2
23X-6, 38	207.91	65.8	37.0	171.7
23X-7, 35	209.38	85.4	36.9	313.9
24X-1, 72	210.72	36.5	23.8	117.7
24X-2, 85	212.35	45.3	30.6	176.6
24X-3, 72	213.72	44.2	28.1	147.2
24X-5, 51	216.51	45.3		210.9
25X-1, 67	220.37	35.5	24.0	250.2
26X-1, 80	230.10	40.6		117.7
26X-2, 89	231.50			78.5
26X-3, 80	233.10	51.9		215.8
26X-4, 49	234.30			107.9
26X-5, 60	235.90	47.8	29.7	206.0
27X-1, 100	240.00	67.2		191.3
27X-2, 85	241.35	70.7	44.6	210.9
27X-3, 59	242.59	91.1	56.4	250.2
27X-4, 78	244.28	73.4	43.3	240.3
27X-5, 70	245.70	86.6	49.9	240.3
27X-6, 68	247.10	96.4	71.6	196.2

Note: *Unconfined compressive strength (q_u) can be used to approximate undrained shear strength (S_u) by the relationship $q_u = 2S_u$.

CORE-SEISMIC INTEGRATION

Site 940 is located on the eastern flank of the Amazon Channel-levee System about 2 km upslope from the point of bifurcation from the Aqua Channel-levee System (Fig. 1). A *Conrad* water-gun seismic-reflection line was used for correlation with the drilling results (1716UTC, 15 December 1984, Leg C25-14; Fig. 28). Hole 940A penetrated sediment of the Aqua, Brown, and Amazon seismic-stratigraphic intervals (Fig. 29; Manley and Flood, 1988; Pirmez, 1994). The location of the site near the Aqua Channel bifurcation provided an opportunity to correlate seismic stratal patterns with sediment associated with different channel-growth phases.

Well-log velocity data measured between 75 and 214 mbsf show an approximately linear downhole increase (Fig. 30). Velocities between 0 and 75 mbsf were extrapolated from a linear fit to the upper portion of the logged interval; velocities below 214 mbsf were extrapolated from a linear fit throughout the entire logged interval (Fig. 30). The thickness of each seismic unit was obtained by integrating the velocity-depth curve.

Six seismic-facies units are recognized in the vicinity of the drill site (Fig. 29). Seismic-facies Unit 1 was classified from the 3.5-kHz profile acquired during the Leg 155 pre-site survey (Fig. 3) and seismic-facies Units 2–6 from the water-gun profile (Fig. 28). Prominent

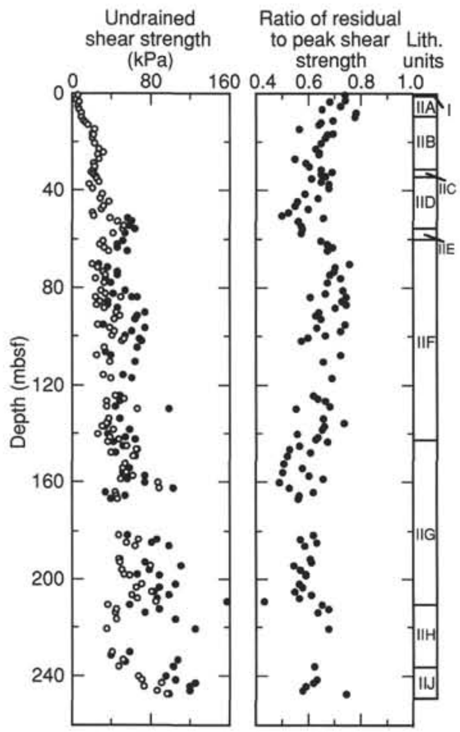

Figure 22. Undrained shear strength (open circles) and assumed undrained shear strength derived from unconfined compressive strength (solid circles), and ratio of residual to peak shear strength in Hole 940A.

reflections, interpreted from correlation of a regional grid of lines in the vicinity of the site (Pirmez, 1994), mark the boundaries of individual seismic-stratigraphic intervals associated with the development of the Aqua, Brown, and Amazon Channel-levee systems and occur at 40, 70, 110, 165, 240, and 315 ms.

Seismic-facies Unit 1 (0–40 ms; 0–31 mbsf) is acoustically transparent on the 3.5-kHz profile. A reflection at 40 ms on the water-gun profile marks the base of this seismic-facies unit and correlates with the contact between lithostratigraphic Subunits IIB and IIC, with an increase in silt-sand beds above a bioturbated mud.

Seismic-facies Unit 2 (40–70 ms; 31–55 mbsf) consists of low-amplitude, discontinuous, subparallel, irregular reflections. This unit correlates with lithostratigraphic Subunits IIC and IID, which consist of bioturbated muds at the top (Subunit IIC) and grade downhole to thin-bedded silty turbidites with scattered fine sand beds (Subunit IID). Seismic Units 1 and 2 are interpreted to correspond to the Amazon (including all channels younger than Brown; Pirmez, 1994) seismic-stratigraphic interval.

Seismic-facies Unit 3 (70–110 ms; 55–86.5 mbsf) consists of moderate-amplitude, discontinuous, slightly diverging reflections. This seismic unit is correlative with the upper portion of lithostratigraphic Subunit IIF, which consists of silt-laminated clays alternating with bioturbated muds. Seismic Unit 3 is interpreted from regional seismic data to correspond to the Brown seismic-stratigraphic interval.

Seismic-facies Unit 4 (110–165 ms; 86.5–132 mbsf) consists of low- to moderate-amplitude, discontinuous, divergent reflections. This unit is similar to seismic Unit 3, but differs in that reflections in Unit 4 form a package with different external geometry. This seismic unit correlates with the lower part of lithostratigraphic Subunit IIF, which grades from bioturbated silty clay beds at the top to sand and silty sand beds at the base. Within seismic Unit 4 the lithostratigraphy suggests the presence of two fining- and thinning-upward cycles (Fig. 29). This unit is interpreted to represent a phase of abandonment of the Aqua Channel-levee System during which time sedimentation may have occurred simultaneously within the Aqua and Brown Channel-levee systems.

Seismic-facies Unit 5 (165–240 ms; 132–196 mbsf) consists of mostly continuous, subparallel, irregular reflections. This seismic unit correlates with lithostratigraphic Subunit IIG, which consists of thin-bedded silty turbidites that vary in frequency downhole. This seismic unit forms a conformable package that gradually thins away from the channel and is interpreted to represent a phase dominated by aggradation of the Aqua Channel-levee System.

Seismic-facies Unit 6 (240–315 ms; 196–262 mbsf) consists of relatively low-amplitude, discontinuous, divergent reflections. The lower strata of this unit downlap onto a stratal surface that can be correlated regionally and represents the base of the Aqua Channel-levee overbank deposits. This surface was apparently not penetrated by Hole 940A. Seismic-facies Unit 6 correlates with an overall fining-upward sequence from mud with beds of medium sand at the base (Subunit IIH) to silt beds and laminae at the top (Subunit IIG), which overlies an interval of mud with silt laminae (Subunit IIJ). The seismic-reflection data show an irregular reflection at the base of seismic-facies Unit 6 that suggests local erosion, possibly by small channels. The abrupt contact between Subunits IIH and IIJ may represent the lateral migration of small channels over more distal levee deposits during early development of the Aqua Channel-levee System.

IN-SITU TEMPERATURE MEASUREMENTS

Temperature gradients and heat flow were determined using one downhole measurement and the bottom-water (mud-line) temperature. An ADARA measurement was made during Core 940A-6H (50.3 mbsf) using instrument number 12. The mud-line temperature of 2.73°C measured from this instrument was used as the reference bottom-seawater temperature at Site 940. A successful measurement resulted in an extrapolated equilibrium temperature of 4.2°C. A WSTP measurement was attempted before Core 14X, but was not obtained because an open circuit in the power supply did not allow the tool to record.

The equilibrium temperature, extrapolated from a synthetic curve constructed to fit transient temperature data, is plotted as a function of depth (mbsf) in Figure 31. Using the ADARA mud-line temperature and the sub-bottom temperature from the ADARA measurement downhole, the geothermal temperature gradient can be approximated by a linear mean of 29.2°C/km. We calculated heat flow by adopting the constant geothermal temperature gradient of 29.2°C/km and a linear increase in thermal conductivity, K, of 1.05 ± 0.15 W/(m·K), which is an average of regression estimates at 60 mbsf. This results in a calculated heat flow of 30.64 mW/m^2.

SYNTHESIS AND SIGNIFICANCE

Stratigraphic Synthesis

Surficial Foraminifer-nannofossil Clay (Unit I)

Unit I (0–0.24 mbsf) is a Holocene, bioturbated foraminifer-nannofossil clay (Fig. 32). Carbonate content is about 29% at 0.11 mbsf and decreases downhole.

Levee of the Amazon-Brown-Aqua Channel (Unit II)

The levee section cored in Unit II corresponds to the time period equivalent to the Aqua, Brown, and Amazon channels further downfan. Unit II (0.24–248.60 mbsf) consists of mud with interbedded laminae and beds of silt and very fine sand. The mud has about 3%

Table 14. Electrical resistivity at Site 940.

Core, section, interval (cm)	Depth (mbsf)	Longitudinal resistivity (Ωm)	Transverse resistivity (Ωm)
155-940A-			
1H-1, 69	0.69	0.205	0.216
1H-2, 90	2.40	0.200	0.199
2H-1, 60	3.40	0.193	0.204
2H-2, 80	5.10	0.204	0.184
2H-3, 95	6.75	0.211	0.202
2H-4, 78	8.08	0.193	0.212
2H-5, 111	9.91	0.224	0.220
2H-6, 80	11.10	0.239	0.228
2H-7, 10	11.90	0.259	0.234
3H-1, 72	13.02	0.242	0.236
3H-2, 118	14.98	0.236	0.238
3H-3, 143	16.73	0.249	0.242
3H-4, 21	17.01	0.259	0.246
3H-5, 16	18.46	0.247	0.246
3H-6, 68	20.48	0.271	0.245
4H-1, 117	22.97	0.290	0.288
4H-2, 88	24.18	0.333	0.302
4H-3, 39	25.19	0.332	0.306
4H-4, 68	26.98	0.343	0.328
4H-5, 77	28.57	0.364	0.349
4H-5, 138	29.18	0.373	0.363
4H-5, 8	27.88	0.359	0.339
4H-6, 23	29.53	0.321	0.352
4H-6, 85	30.15	0.320	0.301
4H-6, 144	30.74	0.366	0.361
4H-7, 44	31.24	0.336	0.314
5H-1, 97	32.27	0.300	0.301
5H-2, 88	33.48	0.293	0.272
5H-3, 20	34.30	0.304	0.273
5H-4, 10	35.24	0.316	0.280
5H-5, 59	36.53	0.293	0.276
5H-6, 48	37.21	0.303	0.293
5H-7, 81	39.01	0.278	0.290
6H-1, 68	41.48	0.314	0.301
6H-2, 73	43.03	0.314	0.314
6H-3, 70	44.50	0.316	0.333
6H-4, 88	46.18	0.322	0.311
6H-5, 83	47.63	0.328	0.328
6H-6, 83	49.13	0.327	0.323
6H-7, 54	50.34	0.312	0.303
7H-2, 19	51.26	0.330	0.325
7H-3, 18	52.59	0.340	0.336
7H-4, 40	54.31	0.332	0.330
7H-5, 64	55.98	0.326	0.319
7H-6, 77	57.61	0.346	0.326
8H-1, 97	60.77	0.335	0.334
8H-2, 95	62.25	0.349	0.344
8H-3, 92	63.72	0.343	0.331
8H-4, 50	64.80	0.338	0.331
9H-1, 120	70.50	0.328	0.309
9H-2, 94	71.74	0.343	0.341
9H-3, 94	73.24	0.348	0.337
9H-4, 94	74.74	0.345	0.324
9H-5, 94	76.24	0.313	0.317
10X-1, 97	77.97	0.351	0.323
10X-2, 97	79.47	0.336	0.323
10X-3, 97	80.97	0.328	0.324
10X-4, 97	82.47	0.330	0.328
10X-5, 97	83.97	0.330	0.339
11X-1, 86	85.56	0.341	0.344
11X-2, 86	87.06	0.336	0.336
11X-3, 84	88.51	0.344	0.338
11X-4, 82	89.99	0.360	0.359
11X-5, 84	91.51	0.394	0.378
11X-6, 88	93.05	0.366	0.355
12X-1, 65	94.95	0.357	0.346
12X-2, 65	96.45	0.379	0.356
12X-3, 65	97.95	0.372	0.365
12X-4, 65	99.45	0.381	0.381
12X-5, 45	100.75	0.398	0.367
12X-6, 8	101.82	0.370	0.370
13X-1, 85	104.75	0.403	0.386
13X-2, 101	106.37	0.356	0.369
13X-3, 100	107.78	0.374	0.362
13X-4, 60	108.88	0.333	0.342
13X-5, 60	110.38	0.349	0.351
14X-2, 81	115.91	0.374	0.365
14X-3, 83	117.43	0.389	0.188
15X-1, 104	124.34	0.398	0.375
15X-2, 105	125.85	0.404	0.358
15X-3, 35	126.65	0.365	0.349
15X-4, 125	129.05	0.340	0.339
15X-5, 50	129.80	0.385	0.354
16X-1, 93	133.93	0.364	0.332
16X-2, 109	135.59	0.354	0.323
16X-3, 118	137.18	0.318	0.298
16X-4, 90	138.40	0.328	0.319
16X-5, 110	140.10	0.304	0.314
16X-6, 106	141.56	0.329	0.314
16X-7, 46	142.46	0.363	0.338
17X-1, 73	143.33	0.375	0.356
17X-2, 97	145.07	0.380	0.381
17X-3, 98	146.58	0.401	0.375
17X-4, 101	148.11	0.364	0.377
17X-5, 56	149.16	0.374	0.363
18X-1, 26	152.46	0.396	0.375
18X-2, 76	154.46	0.389	0.364
18X-3, 103	156.23	0.381	0.369
18X-4, 49	157.19	0.380	0.368
18X-5, 66	158.86	0.414	0.402
18X-6, 43	160.13	0.380	0.380
19X-1, 68	162.58	0.387	0.400
19X-2, 67	164.07	0.378	0.367
19X-3, 84	165.74	0.359	0.364
19X-4, 55	166.95	0.355	0.350
21X-1, 83	181.93	0.403	0.382
21X-2, 83	183.43	0.415	0.363
21X-3, 83	184.93	0.353	0.378
21X-4, 83	186.43	0.373	0.357
22X-1, 85	191.65	0.365	0.355
22X-2, 85	193.15	0.366	0.359
22X-3, 68	194.48	0.436	0.393
22X-4, 107	196.37	0.351	0.354
22X-5, 105	197.85	0.370	0.365
22X-6, 35	198.65	0.384	0.410
23X-2, 63	202.16	0.396	0.403
23X-3, 50	203.53	0.413	0.403
23X-4, 51	205.04	0.404	0.431
23X-5, 48	206.51	0.389	0.398
23X-6, 38	207.91	0.399	0.387
23X-7, 35	209.38	0.450	0.415
24X-1, 72	210.72	0.380	0.362
24X-2, 85	212.35	0.383	0.369
24X-3, 72	213.72	0.393	0.381
24X-4, 44	214.94	0.410	0.409
24X-5, 51	216.51	0.382	0.383
25X-1, 67	220.37	0.362	0.352
26X-1, 80	230.10	0.418	0.410
26X-2, 89	231.69	0.370	0.366
26X-3, 80	233.10	0.403	0.407
26X-4, 49	234.29	0.367	0.369
26X-5, 60	235.90	0.383	0.381
27X-1, 100	240.00	0.462	0.427
27X-2, 85	241.35	0.420	0.414
27X-3, 59	242.59	0.424	0.411
27X-4, 78	244.28	0.421	0.404
27X-5, 70	245.70	0.410	0.400
27X-6, 68	247.10	0.427	0.427

carbonate content. Seismic-reflection profiles do not allow direct correlation between reflections at Site 940 and the reflections at the base of successive levee systems (Aqua, Brown, and Amazon) below the avulsion points down-fan, but correlations can be made on the basis of seismic character (Pirmez, 1994). Core-seismic correlation suggests that the hole was terminated just above the base of the Aqua levee. The Lake Mungo paleomagnetic excursion and *P. obliquiloculata* are absent in Unit II, confirming that the chronology from Sites 930, 935, and 938 is correct (i.e., that the Aqua Channel-levee System is younger than 30 ka).

Levee Section Equivalent to the Amazon Channel Down-fan (Subunits IIA–IID)

Core-seismic correlation suggests that the upper four subunits were deposited after the avulsion of the Amazon from the Brown Channel farther down-fan. Subunit IIA (0.24–9.50 mbsf) comprises color-banded and bioturbated mud. Subunit IIB (9.50–31.81 mbsf) is composed of mud with thin to thick beds of silt and fine sand, which increase in frequency and thickness toward the base of the subunit. Three thin intervals of contorted sediment are interpreted as slumps. Subunit IIC (31.81–34.39 mbsf) consists of slightly bioturbated, color-banded mud. Subunit IID (34.39–55.71 mbsf) consists of mud

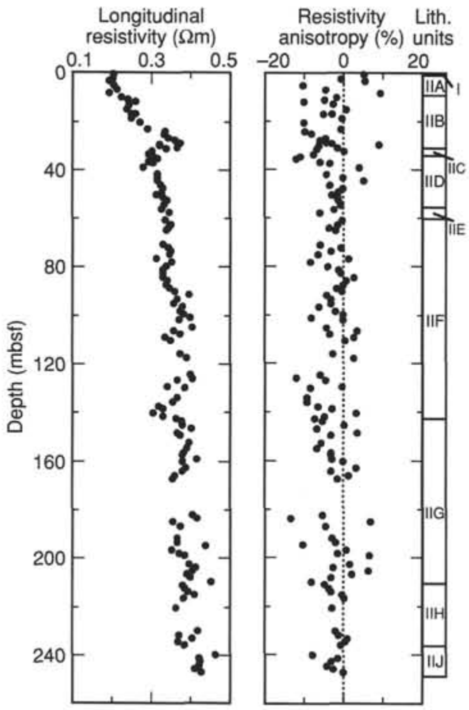

Figure 23. Longitudinal resistivity and resistivity anisotropy in Hole 940A.

with frequent laminae and beds of silt and fine sand, with the greatest abundance of sand at about 50 mbsf. This interval thus contains two overall fining-upward sequences, although in detail changes in abundance of silt beds may be quite abrupt.

Levee Section Equivalent to the Brown Channel Down-fan (Subunits IIE–IIF)

The section of the levee that was deposited when the Brown Channel was active down-fan is correlated with Subunit IIE and the upper part of Subunit IIF, to 86 mbsf. Subunit IIE (55.71–60.01 mbsf) consists of moderately bioturbated mud with silt laminae that have been tilted and deformed and is interpreted as a slump. Subunit IIF (60.01–142.6 mbsf) consists of mud with laminae and thin beds of silt. Intervals of upward-decreasing gamma-ray response from 72 to 76 mbsf and 77 to 85 mbsf reflect variations in silt bed thickness and frequency.

Levee Section Equivalent to the Aqua Channel Down-fan (Subunits IIF–IIJ)

Seismic profiles suggest that Unit II below 86 mbsf was deposited when the Aqua Channel was active. The interval 86–132 mbsf is interpreted as equivalent to a time when both the Aqua and Brown channels were active (Pirmez, 1994). The lower part of Subunit IIF (below 86 mbsf) consists of mud with laminae and thin beds of silt. The frequency of these beds fluctuates, but silt is more abundant near the base of the unit, and two fining-upward sequences are distinguished. An interval of upward-increasing gamma-ray response from 85 to 91 mbsf does not correlate with any prominent changes in sediment type, but upward increase in gamma ray from 92 to 115 mbsf corresponds to a fining-upward sequence in the middle part of Subunit IIF. Log data suggest abundant silt or sand in unrecovered intervals at 112–114 and 130–132 mbsf, the latter overlain by a 5-m-thick fining-upward sequence. Subunit IIG (142.6–210.57 mbsf) consists of mud with frequent laminae and beds of silt and sand. The top of the subunit is marked by a slump similar to that in Subunit IIE and is characterized by an abrupt increase in gamma ray and resistivity in log data. The slump overlies a fining-upward sequence from 147.5 to 161 mbsf. Recovery was poor through several intervals in this subunit. Subunit IIH (210.57–236.14 mbsf) comprises mud with laminae and beds of silt and frequent beds of sand up to 10 cm thick. Logs show substantial borehole washout at 218–230 mbsf. Subunit IIJ (236.14–248.60 mbsf) consists of mud with laminae of silt.

Implications

Nannofossils are rare or absent, whereas foraminifers are relatively abundant throughout the hole. The base of the Holocene was defined between 2.1 and 2.5 mbsf. *P. obliquiloculata* is absent below the Holocene section, indicating that the entire hole is younger than 40 ka. Cerrado-type vegetation is well represented in the palynomorph assemblage from Unit II, with *Byrsonima,* Compositae, and Gramineae.

No magnetic excursion was detected at this site. Magnetic remanence intensity can be tentatively correlated with Site 939 and suggests that 16 and 47 mbsf at Hole 940A correlate respectively with 7 and 42 mbsf at Hole 939B. Correlation with Site 939 is also possible using distinctive patterns in the magnetic susceptibility record, although by itself this correlation is ambiguous. These data, together with lithologic correlation, suggest that the Amazon levee system at Site 940 (Subunits IIA–IID) corresponds to Subunits IIA and IIB at Site 939; the bioturbated mud of the Brown levee system at Site 940 (upper part of Subunit IIF) corresponds to the bioturbated Subunit IIC at Site 939; and the thinning-upward sequence from 90 to 120 mbsf at Site 940 (middle of Subunit IIF) corresponds to the thinning-upward sequence from 67 to 100 mbsf in Hole 939B (Subunits IID and IIE).

Correlation to more distant sites may also be possible using paleomagnetic data. Peaks in remanence intensity at 16, 47, and 156 mbsf in Hole 940A may correlate with 4, 12, and 28 mbsf in Hole 935A, which is broadly consistent with the seismic stratigraphy.

Three depositional "packages" are recognized on the basis of lithologic description from Hole 940A. The oldest comprises Subunits IIJ, IIH, and IIG and is a thinning- and fining-upward sequence above the fine-grained deposits of Subunit IIJ. It is correlated with the similar Aqua levee sequence at Site 935. The second package comprises Subunit IIF, with two intervals of abundant silty turbidites al-

Table 15. Intervals logged and tools employed in Hole 940A.

		Open hole		In pipe		
String	Run	(mbsf)	(mbrf)	(mbsf)	(mbrf)	Tools
Quad	Down	91–233	3294–3436			NGT/LSS/CNT-G/HLDT/DITE/TLT
	Up 1	234–72	3437–3275	72–0	3275–3203	
	Up 2	157–72	3360–3275			
FMS	Up 1	227–80	3430–3283			NGT/GPIT/FMS
	Up 2	233–80	3436–3283			

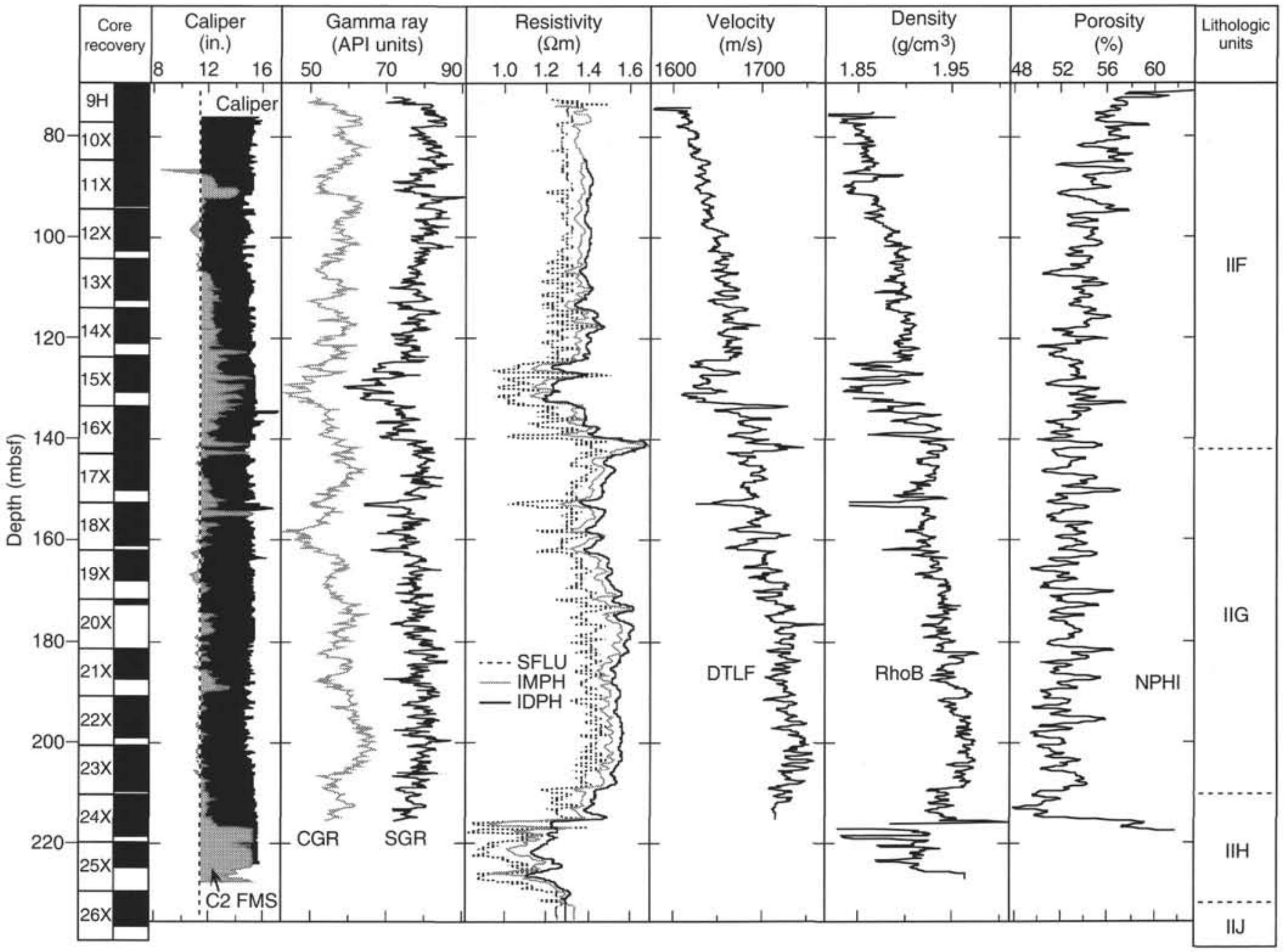

Figure 24. Summary of logging data obtained from the Quad-combination string in Hole 940A. Left to right: core numbers and recovery; spectral (SGR) and computed (CGR = Th + K) gamma ray; shallow spherically focused resistivity (SFLU); medium (IMPH) and deep (IDPH) phasor induction resistivity; long-spacing sonic velocity (DTLF); bulk density (RhoB); and neutron porosity (NPHI). On the right is the division of lithostratigraphic units.

ternating with intervals of bioturbated mud with fewer silts. The third package comprises Subunits IIB through IIE and has two intervals of abundant turbidite silts (more abundant than in Subunit IIF), together with long intervals of bioturbated and color-banded sediment. These siltier intervals in each package tend to show a thinning-upward and in some cases fining-upward sequence, except for the basal 5–10 m, which tends to be coarsening and thickening upward.

If the seismic correlation is correct, then the periods of deposition of siltier sediment correspond to times shortly after a major channel avulsion downstream. This may indicate that avulsion is triggered by more abundant large turbidity currents.

Comparison with Site 939 shows that Site 940 has a slightly higher overall sedimentation rate and a considerably higher number of silt beds. This is consistent with the channel-levee relief (50 m) at Site 940 compared with Site 939 (75 m).

Temperature anomalies detected with the TLT correspond to intervals where coarser sediment was recovered (although anomalies were also detected within the pipe), which may indicate advection of warmer fluid into the borehole.

Most physical and pore-water properties show distinctive changes between 24 and 35 mbsf (Fig. 21). Porosity is almost constant, yet resistivity is unusually high and shear strength is low. Unusually low salinities are recorded in this interval, but chlorinity is normal. A similar trend in physical properties is seen between 15 and 27 mbsf in Hole 939B. The interpretation of these observations is uncertain, although it may be due to the distribution of diagenetic hydrotroilite.

In Unit II, carbonate content ranges from 1% to 3%, and organic carbon from 0.8% to 1.2%. Pore-water samples show that sulfate reduction is not complete until 20–29 mbsf, the deepest encountered on Leg 155, and the peaks in phosphate (29 mbsf) and iron (91 mbsf) concentration are also deep. The greater depth of organic carbon remineralization compared with other sites of Leg 155 may be due to the high depositional rate.

In summary, Sites 940, 939, 935, and 936 provide a detailed stratigraphy near the crests of the youngest levees (Amazon, Brown, and Aqua) on the upper, middle, and lower fan. Site 940 has confirmed that the proportion of silt and sand to mud that are deposited fluctuate considerably within a single levee, but that each levee growth phase is represented by an overall fining-upward sequence. The relatively common foraminifers and the detailed paleomagnetic record at both Sites 939 and 940 indicate that shore-based study should allow the tentative correlation of the two sites to be refined. Site 940 has a higher sedimentation rate than Site 939 and has a higher frequency of silt beds.

REFERENCES*

Damuth, J.E., 1977. Late Quaternary sedimentation in the western equatorial Atlantic. *Geol. Soc. Am. Bull.,* 88:695–710.

Manley, P.L., and Flood, R.D., 1988. Cyclic sediment deposition within Amazon deep-sea fan. *AAPG Bull.,* 72:912–925.

Pirmez, C., 1994. Growth of a submarine meandering channel-levee system on the Amazon Fan [Ph.D. thesis]. Columbia Univ., New York.

*Abbreviations for names of organizations and publications in ODP reference lists follow the style given in *Chemical Abstracts Service Source Index* (published by American Chemical Society).

Ms 155IR-116

NOTE: For all sites drilled, core-description forms ("barrel sheets") and core photographs can be found in Section 4, beginning on page 703. Forms containing smear-slide data can be found in Section 5, beginning on page 1199. GRAPE, index property, magnetic susceptibility, and natural gamma data are presented on CD-ROM (back pocket).

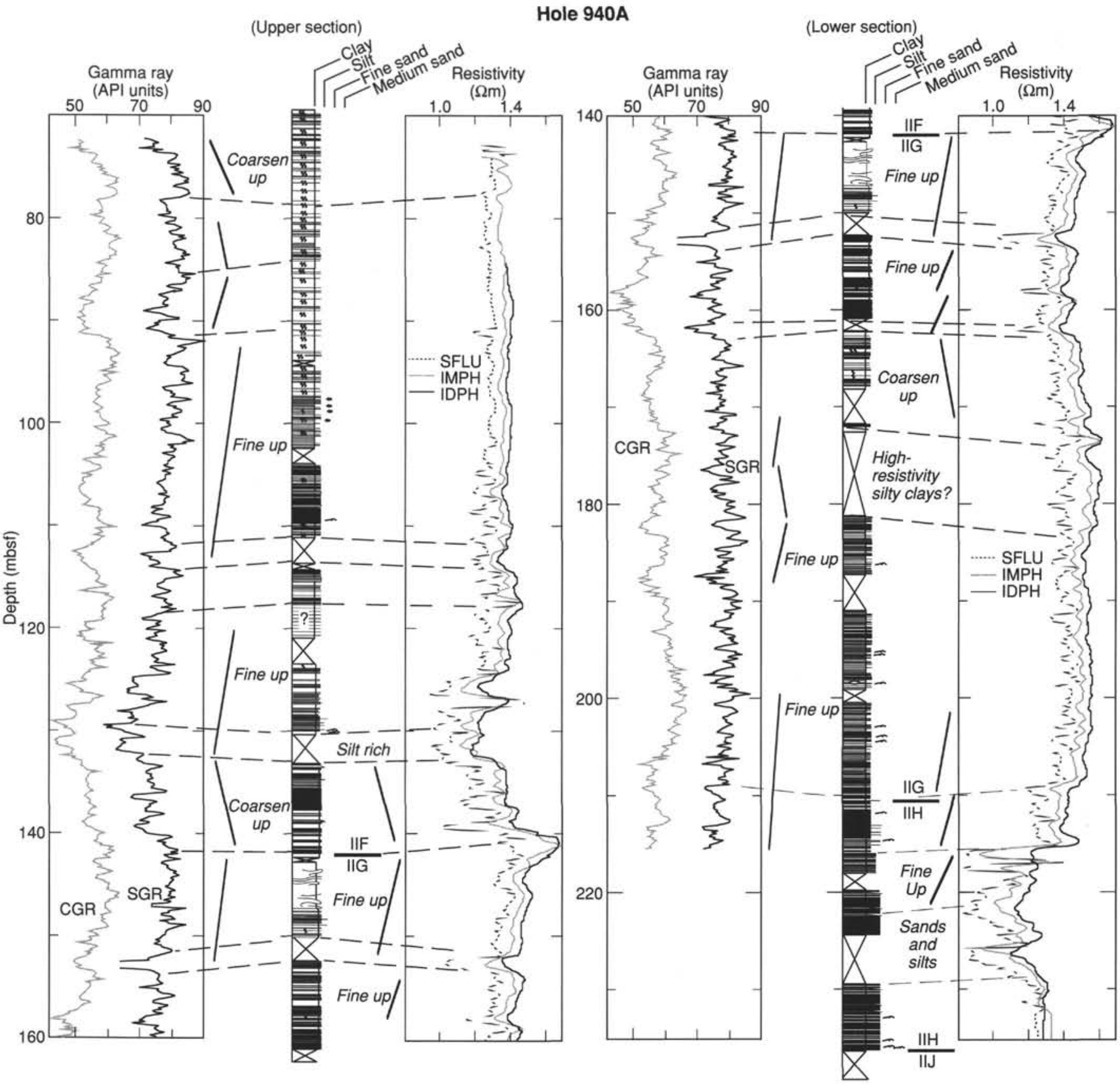

Figure 25. Comparison of gamma-ray and resistivity logs to visual core descriptions. The logged interval has been divided into two parts: 70–160 mbsf and 140–240 mbsf. "Fine up" and "coarsen up" are asymmetric trends inferred from the gamma-ray and resistivity logs. Lithology is inferred at intervals of poor recovery. Lithostratigraphic unit boundaries are indicated by thick lines.

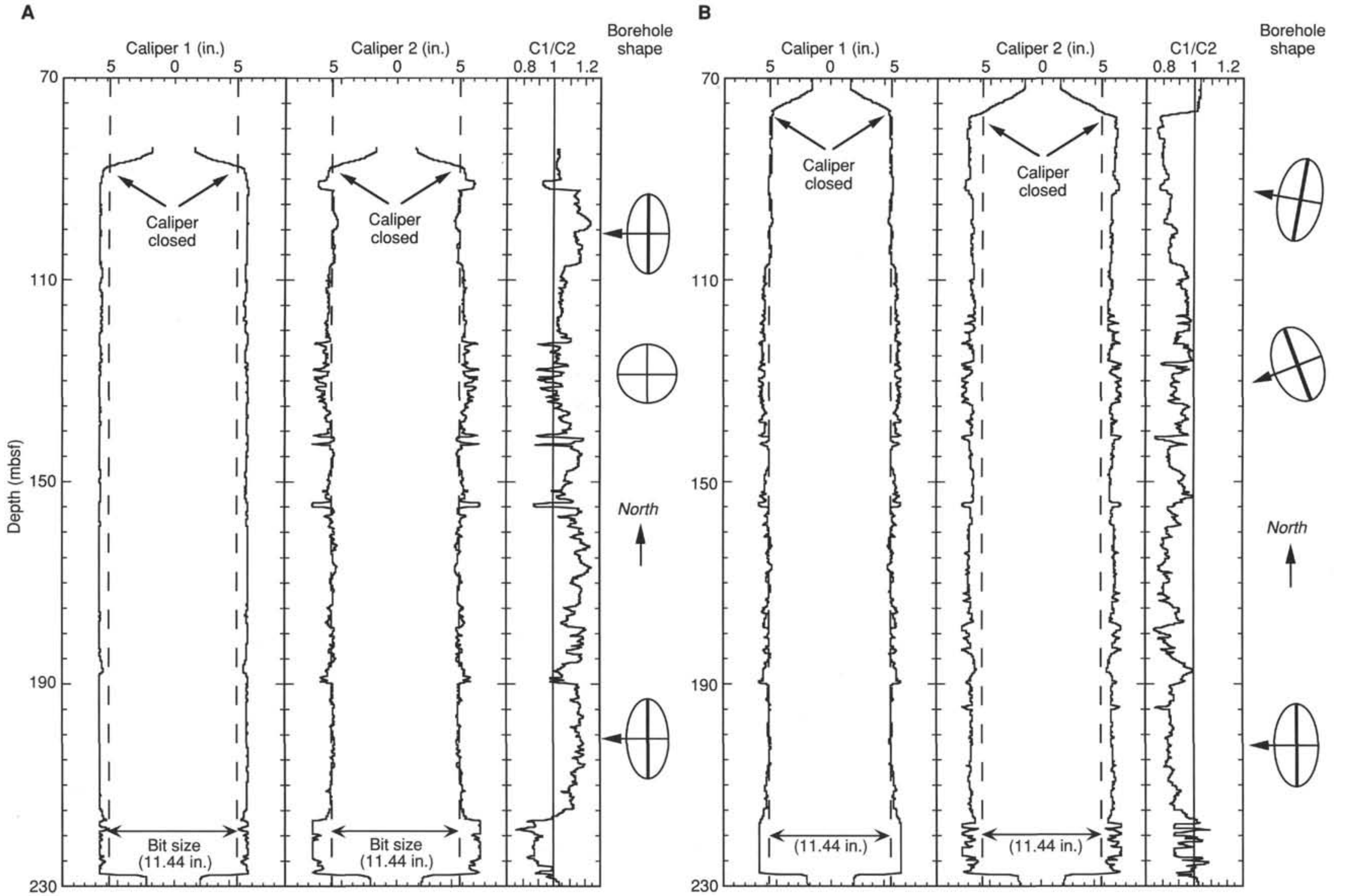

Figure 26. **A.** FMS caliper data (C1, C2) from run 1. **B.** FMS caliper data from run 2. Column on right summarizes the borehole shape and orientation based on the values of C1, C2, and azimuth of C1. The long axis of the borehole ellipse is oriented approximately parallel to the abandoned Aqua Channel, but is perpendicular to the surface bathymetric gradient. (Arrow on borehole shape shows orientation of Pad 1.)

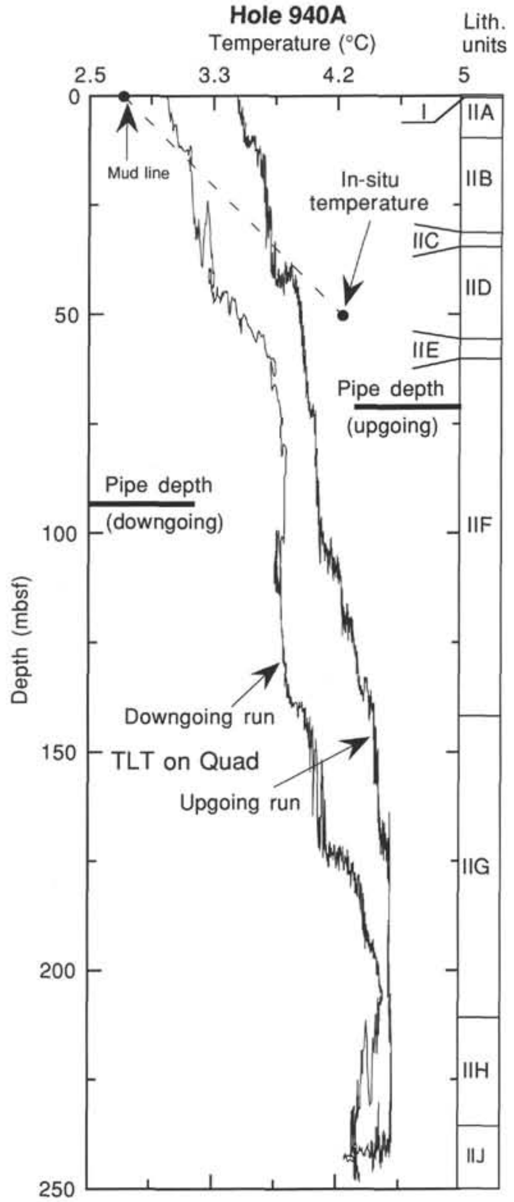

Figure 27. Borehole temperature log from the TLT and formation temperature from ADARA.

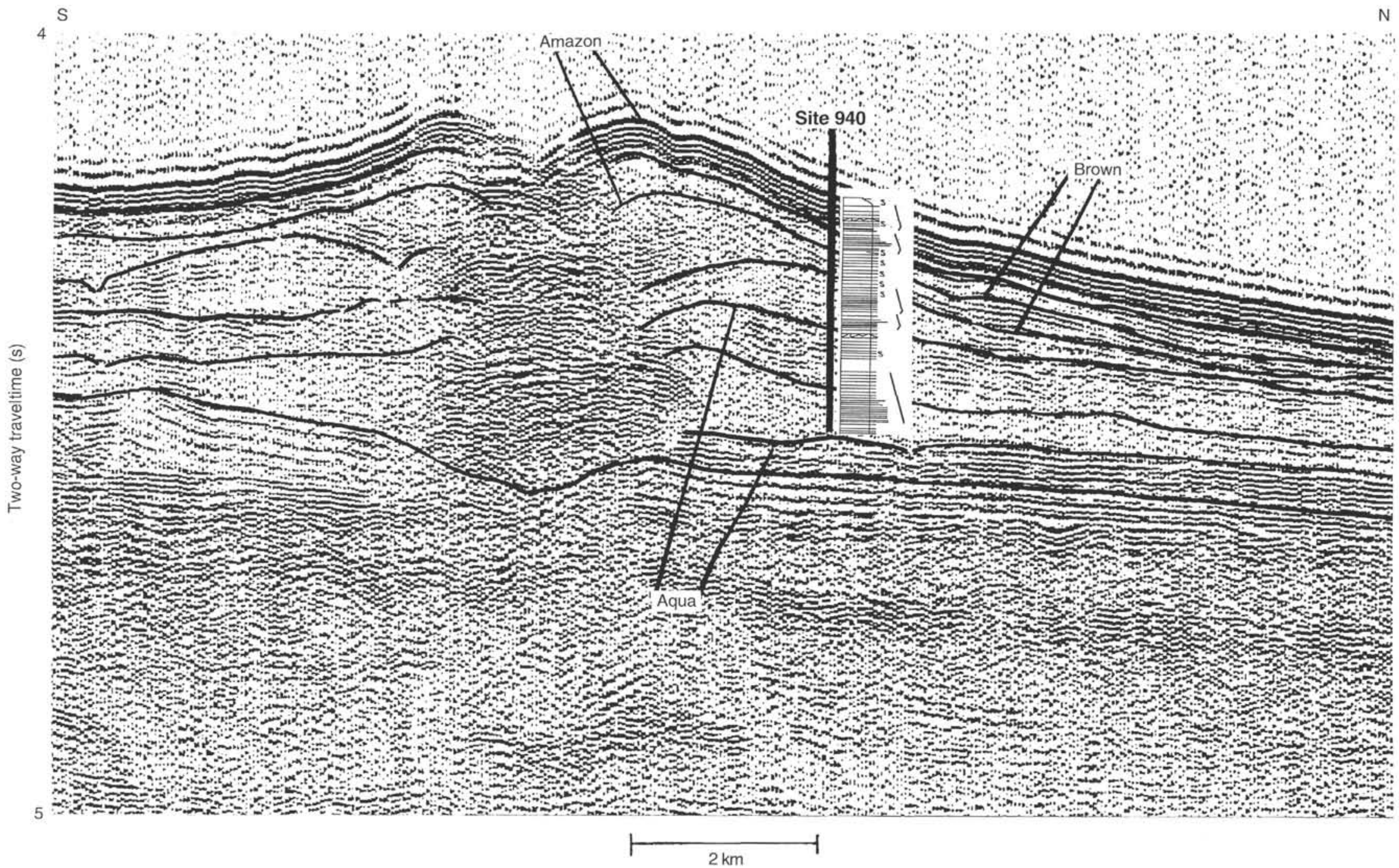

Figure 28. Interpreted seismic-reflection profile showing Site 940 with the corresponding lithostratigraphic section, prominent reflections, and seismic units.

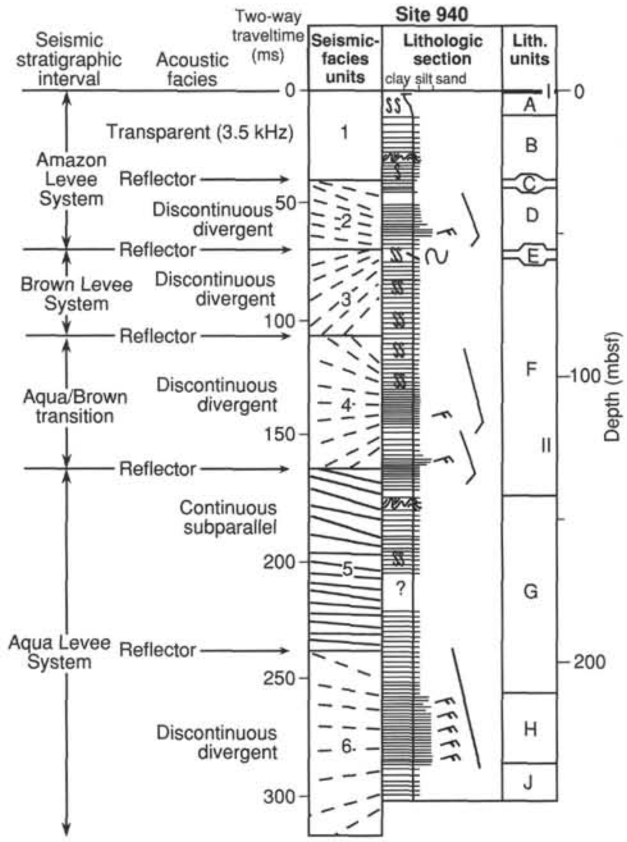

Figure 29. Correlation of lithostratigraphic observations with seismic-facies units and prominent reflections (arrows) on seismic profile at Site 940.

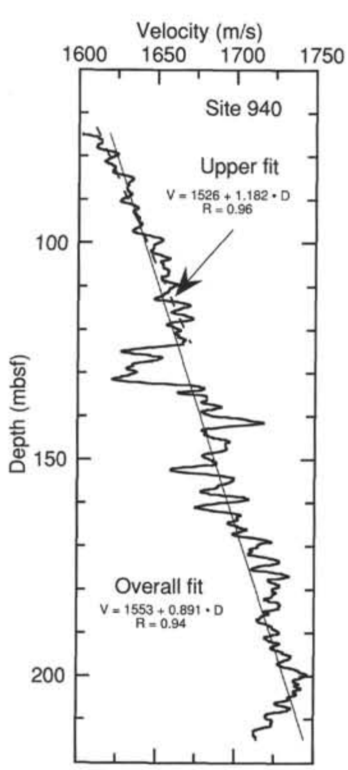

Figure 30. Sonic velocity from well logs and calculated best-fit linear regressions used to extrapolate velocity (V) from depth (D) for shallower portion of the site (upper fit) and for deeper interval (overall fit).

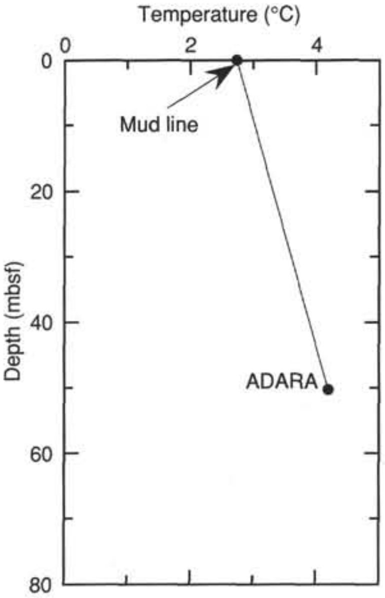

Figure 31. Estimated equilibrium temperatures in Hole 940A. A linear fit indicates a geothermal gradient of 29.185°C/km.

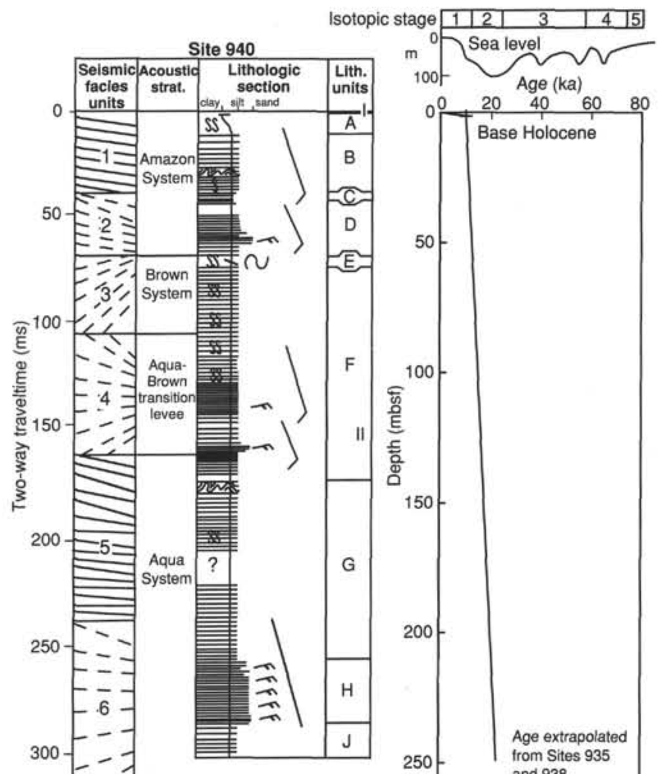

Figure 32. Summary of Site 940 showing (left to right) seismic-facies units, acoustic stratigraphy, schematic lithologic column, lithologic units, chronological picks, and interpreted age-depth curve (+ = datums; variations in slope between these points are interpreted, based on dated intervals of similar facies at other sites).

SHORE-BASED LOG PROCESSING

Hole 940A

Bottom felt: 3207.7 mbrf
Penetration: 248.6 mbsf
Total core recovered: 209.1 m (84.1%)

Logging Runs

Logging string 1: DIT/LSS/HLDT/CNTG/NGT
Logging string 2: FMS/GPIT/NGT (two passes)
Wireline heave compensator was used to counter ship heave.

Bottom-hole Assembly (BHA)

The following BHA depths are as they appear on the logs after differential depth shift (see **Depth shift** section below) and depth shift to the seafloor. As such, there may be a discrepancy with the original depths given by the drillers on board. Possible reasons for depth discrepancies are ship heave, use of wireline heave compensator, and drill string and/or wireline stretch.

DIT/HLDT/LSS/CNTG/NGT: BHA at 73.5 mbsf.
FMS/GPIT/NGT (main): Recorded open hole.
FMS/GPIT/NGT (repeat): BHA at 72 mbsf.

Processing

Depth shift: All original logs have been interactively depth shifted with reference to NGT from DIT/LSS/HLDT/CNTG/NGT run, and to the seafloor (–3201.3 m). This value does not correspond to the drillers' water depth ("bottom felt") but to the depth of the seafloor as seen on the logs. A list of the amount of differential depth shifts applied at this hole is available upon request.

Gamma-ray processing: NGT data have been processed to correct for borehole size and type of drilling fluid.

Acoustic data processing: No processing necessary due to the good quality of the logs.

Quality Control

During the processing, quality control of the data is mainly performed by cross-correlation of all logging data. Large (>12 in.) and/or irregular borehole adversely affects most recordings, particularly those that require eccentralization and a good contact with the borehole wall (CNTG, HLDT).

Hole diameter was recorded by the hydraulic caliper on the HLDT tool (CALI), and the caliper on the FMS string (C1 and C2).

Data recorded through the BHA, such as the NGT and CNTG above 73.5 mbsf, should be used only qualitatively because of the attenuation on the incoming signal. Invalid gamma-ray spikes were detected in the 47.5–51 mbsf interval.

Note: Details of standard shore-based processing procedures are found in the "Explanatory Notes" chapter, this volume. For further information about the logs, please contact:

Cristina Broglia
Phone: 914-365-8343
Fax: 914-365-3182
Email: chris@ldeo.columbia.edu

Elizabeth Pratson
Phone: 914-365-8313
Fax: 914-365-3182
Email: beth@ldeo.columbia.edu

940A Natural Gamma Ray-Density-Porosity Logging Data

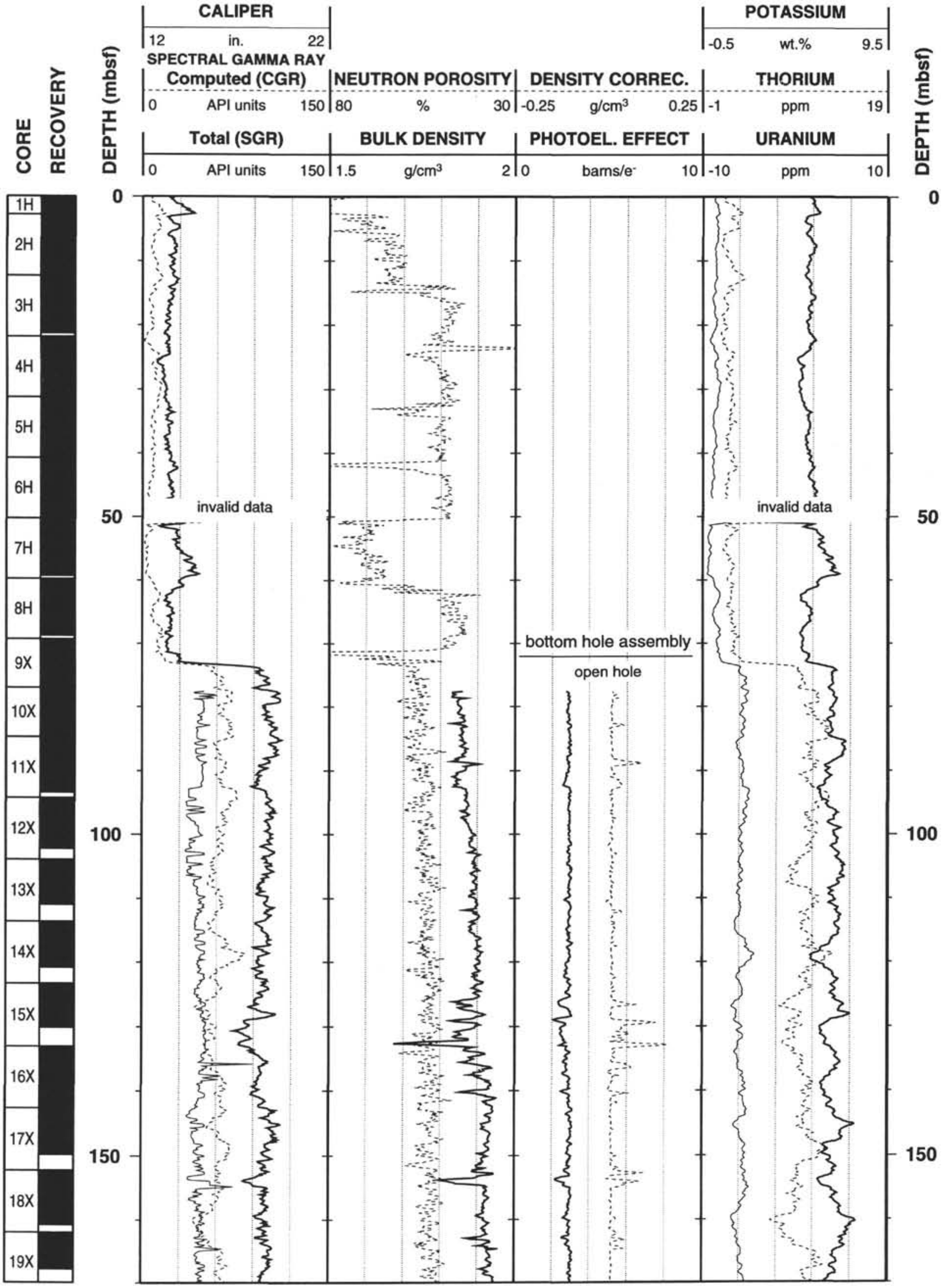

940A Natural Gamma Ray-Density-Porosity Logging Data (cont.)

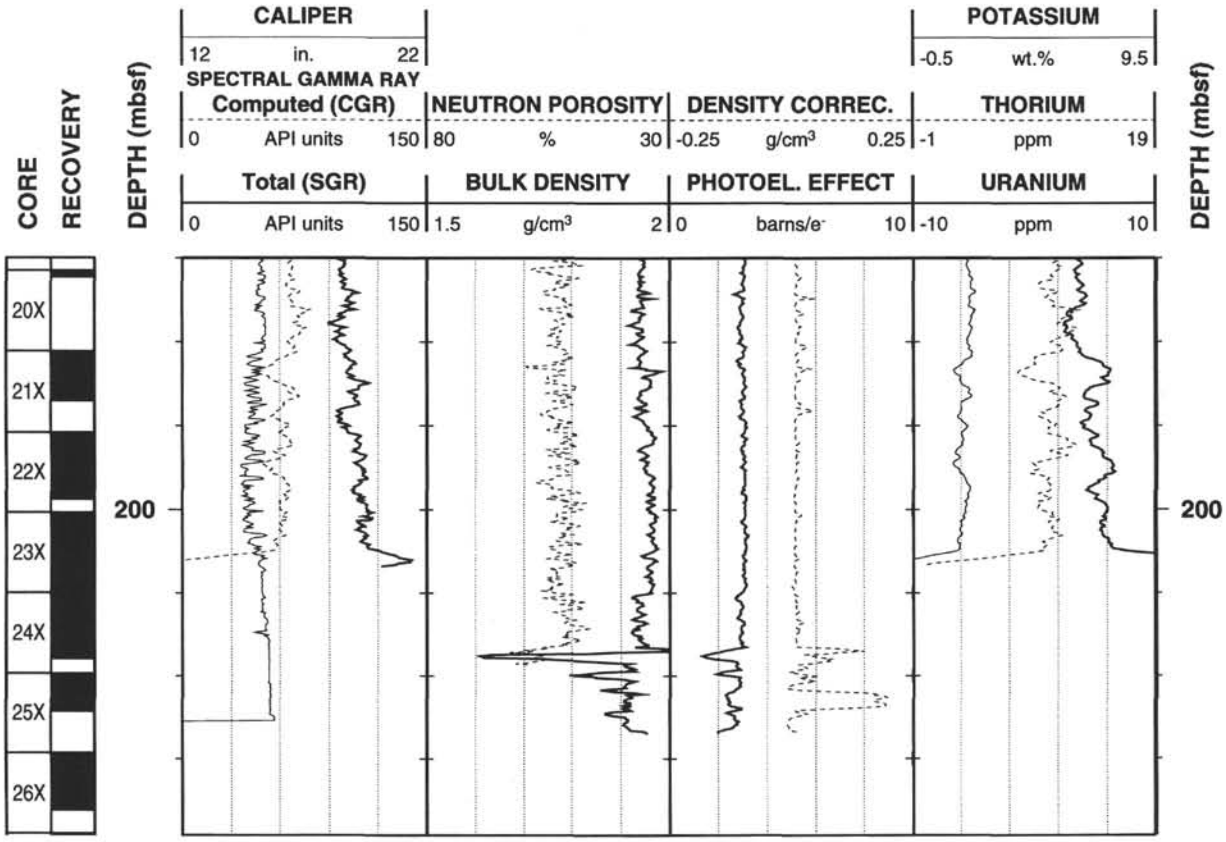

940A Natural Gamma Ray-Resistivity-Velocity Logging Data

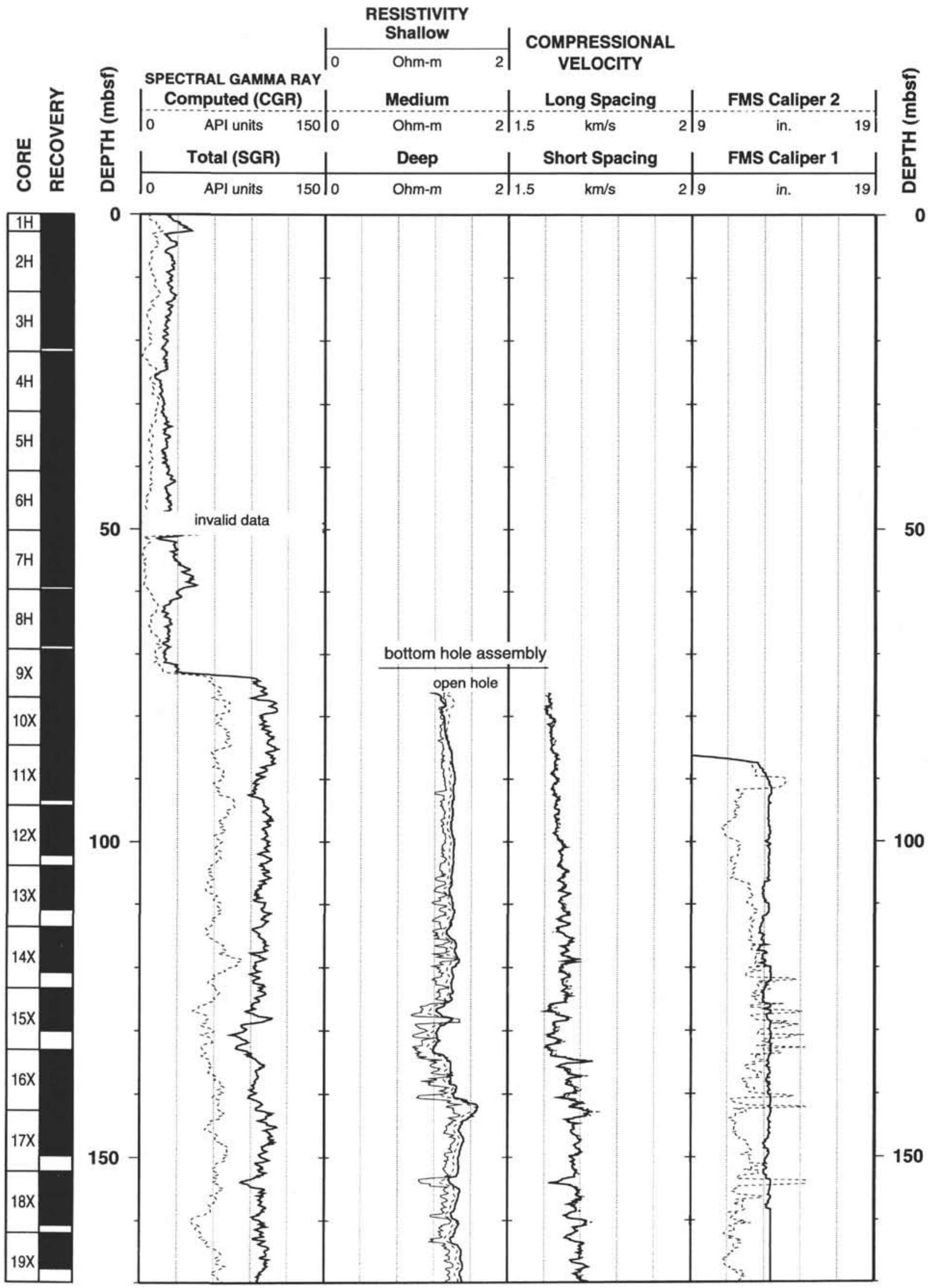

940A Natural Gamma Ray-Resistivity-Velocity Logging Data (cont.)